VNIVERSITAT DE VALÈNCIA

Departamento de física atómica, molecular y nuclear
Facultad de física

RADIATION PROTECTION OF PATIENTS UNDERGOING HIGH-DOSE-RATE BRACHYTHERAPY: PERIPHERAL DOSE ESTIMATION, REVIEW OF RADIATION RISKS AND IMPLANT SHIELDING DESIGN

Cristian Candela Juan

Valencia, 2015

RADIATION PROTECTION OF PATIENTS UNDERGOING HIGH-DOSE-RATE BRACHYTHERAPY: PERIPHERAL DOSE ESTIMATION, REVIEW OF RADIATION RISKS AND IMPLANT SHIELDING DESIGN

Thesis presented by

Cristian Candela Juan

to obtain the degree of Doctor of Philosophy in the subject of Physics

at *Universitat de València.*

Valencia, February 2015

Supervisor:

Facundo Ballester Pallarés

Co-supervisor:

José Pérez Calatayud

Co-supervisor:

Mark J. Rivard

DECLARATION

Dr. Facundo Ballester Pallarés, professor from the Atomic, Molecular and Nuclear Physics Department of the University of Valencia,

Dr. José Pérez Calatayud, head of the physics section of the Radiation Oncology Department of La Fe University and Polytechnic Hospital from Valencia, and

Dr. Mark J. Rivard, Professor of Radiation Oncology in the Department of Radiation Oncology of the Tufts University School of Medicine from Boston, Massachusetts,

CERTIFY:

That the thesis entitled "RADIATION PROTECTION OF PATIENTS UNDERGOING HIGH-DOSE-RATE BRACHYTHERAPY: PERIPHERAL DOSE ESTIMATION, REVIEW OF RADIATION RISKS AND IMPLANT SHIELDING DESIGN" has been developed under their direction by Cristian Candela Juan.

And for the record, in compliance with the current legislation of the University of Valencia, this memory is signed and presented to the Department of Atomic, Molecular and Nuclear Physics of the University of Valencia.

Signed:

Dr. Facundo Ballester Pallarés

Date: February 2015

Dr. José Pérez Calatayud

Date: February 2015

Dr. Mark J. Rivard

Date: February 2015

AGRADECIMIENTOS / ACKNOWLEDGEMENTS

En primer lugar, mis más sinceros agradecimientos a mis directores de tesis: el Dr. Facundo Ballester, el Dr. José Pérez-Calatayud y el Dr. Mark Rivard. Facundo, Pepe, muchísimas gracias por aceptarme en vuestro grupo como a uno más desde el primer día, por vuestra gran dedicación y ayuda durante estos tres años, y por ser como mi familia aquí en Valencia. Gracias también por la oportunidad de asistir con vosotros a todos los grandes congresos y a tantos comités científicos donde tanto he aprendido de los mejores, sin olvidar las excelentes comidas y catas de vino. Mark, muchas gracias a ti también por toda tu ayuda y tu apoyo incluso en la distancia. Sabes que me divertía mucho en esos intercambios rápidos de versiones que, como tú dijiste, hacía que la situación se asemejara a un partido de tenis. Serás muy bien recibido cuando quieras visitarnos de nuevo en Valencia y, por supuesto, habrá que repetir fiesta. Muchas gracias a los tres por vuestra gran humildad a pesar de ser los mejores. Seguro que me quedo corto de palabras para expresar estos agradecimientos.

Muchas gracias también a los otros miembros del grupo, los doctores Domingo Granero, Mª Carmen Pujades y Javier Vijande, por vuestra valiosa ayuda, ya sea en Monte Carlo o en medidas experimentales, y por esas maravillosas cenas esporádicas.

Quiero agradecer también a todas las personas que granito a granito tanto han contribuido a mi formación científica, por orden cronológico: el grupo del Dr. J. M. Benlloch Baviera (Valencia), el Dr. M. Aslaninejad (Londres) y M. Crispín (Valencia), el grupo de la Dra. M. Rafecas (Valencia) y el grupo del Dr. D. Ros y del Dr. J. Pavía (Barcelona). Quiero agradecer también a M. Karlsson, M. Lundell y A. Carlsson Tedgren (Suecia) por compartir con nosotros el proyecto de la dosimetría del radio que forma parte de esta tesis, y por su confianza a lo largo de todo ese estudio.

Muchas gracias también al Servicio de Protección Radiológica, al Servicio de Medicina Nuclear y al Servicio de Oncología Radioterápica del Hospital

Universitario y Politécnico La Fe, que tanto apoyo y ayuda me han dedicado en estos tres años de mi residencia para contribuir a mi formación como radiofísico hospitalario, como investigador y como persona. Gracias también al Dr. Luis Martí-Bonmatí (Valencia), a la Dra. Alegría Montoro (Valencia) y a sus grupos, por su confianza en mí, su apoyo y sus valiosos consejos. Aprovecho para agradecer también al Servicio de Docencia del hospital y al IIS La Fe por fomentar la investigación y el desarrollo de la tesis durante nuestra residencia.

Muchas gracias también a mis compañeros y buenos amigos de la facultad, con quienes tantas experiencias he compartido. En muchos casos el destino nos ha llevado por caminos diferentes, pero espero que nos podamos seguir reuniendo. Gracias también a mis nuevos y tan buenos amigos del ámbito hospitalario, por todas las fiestas y experiencias vividas y por vivir, y especialmente a mi amigo Juan por todas esas risas, cervezas, historias y aventuras ciclistas, y a Carolina, por animarme, quererme y hacerme reír tanto en estos últimos meses.

Gracias a todos mis amigos del pueblo, a esos que han estado ahí toda mi vida, casi desde que empecé a hablar. Ya sabéis quienes sois y todo lo que os aprecio.

Por último, muchas gracias a toda mi familia sin excepción, por ser la mejor y la más unida, y por apoyarme siempre en todas mis decisiones, aunque fueran arriesgadas o me llevaran lejos de vosotros. En especial me gustaría agradecer a mis padres y a mi hermano, sabéis que no hay palabras para expresar todo lo que me importáis.

First, my sincere thanks to my thesis supervisors: Dr. Facundo Ballester, Dr. José Pérez-Calatayud and Dr. Mark Rivard. Facundo, Pepe, thank you for accepting me in your group as one more since the first day, for your dedication and support during these three years, and to be like my family here in Valencia. Thanks also for the opportunity to attend with you at all major conferences and many scientific committees where I learned so much from the best, not to mention the excellent

food and wine tastings. Mark, you too thank you very much for all your help and your support even in the distance. I had a lot of fun in those fast exchanges of versions, like you said, it was like a tennis match. You will be very welcome anytime you visit us again in Valencia and, of course, we must repeat partying. Thank you very much to all you three for your great humility despite being the best. Sure I fall short of words to express these acknowledgments.

Thank you very much also to the other group members, doctors Domingo Granero, Mª Carmen Pujades and Javier Vijande, for your valuable support in either Monte Carlo simulations or experimental measures, and for those wonderful casual dinner.

I want to thank also everyone who has contributed to my scientific training, in chronological order: the group of Dr. JM Benlloch Baviera (Valencia), Dr. M. Aslaninejad (London) and M. Crispín (Valencia), the group of Dr. M. Rafecas (Valencia) and the group of Dr. D. Ros and Dr. J. Pavia (Barcelona). I would also like to thank M. Karlsson, M. Lundell and A. Carlsson Tedgren (Sweden) for sharing with us the dosimetric study of radium sources that has contributed to this, and their confidence throughout that study.

Thank you very much also to the Radiological Protection Service, the Department of Nuclear Medicine and the Department of Radiation Oncology from La Fe University and Polytechnic Hospital, which dedicated me support and help in these three years to allow me improving my skills as a medical physicist, as researcher and as a person. Thanks also to Dr. Luis Martí-Bonmatí (Valencia), Dr. Alegría Montoro (Valencia) and their groups for their confidence, their support and valuable advices. I take this opportunity to also thank the Teaching Department form La Fe Hospital and to the IIS La Fe for promoting research and development of the thesis during our residency program.

Thank you very much also to my colleagues and good friends of the faculty with whom I shared many experiences. Thanks also to my new and such good friends from the hospital, for all those parties and life experiences, and especially to my friend Juan for all those laughs, beers, stories and cycling adventures, and to

Carolina, for encouraging, loving and making me laugh so much during the last months.

Thanks to all my friends from the town, those who have been there for all my life, almost since I started talking. You know who you are and all that I appreciate you.

Finally, thanks very much to all my family without exception, being the best and most united, and for always supporting me in all my decisions, even if they were risky or took me away from you. I would especially like to thank my parents and my brother, you know there are no words to express all I love you.

TABLE OF CONTENTS

LIST OF TABLES

LIST OF FIGURES

LIST OF ABBREVIATIONS AND ACRONYMS

AAPM	American Association of Physicists in Medicine
ABS	American Brachytherapy Society
ALARA	As Low As Reasonably Achievable
APBI	Accelerated Partial Breast Irradiation
ASTRO	American Society for Radiation Oncology
BEIR	Biological Effects of Ionizing Radiation
BT	Brachytherapy
CGE	Cobalt Gray Equivalent
CRT	Conformal RadioTherapy
CT	Computed Tomography
DDREF	Dose and Dose-Rate REduction Factor
EBRT	External Beam RadioTherapy
ERR	Excess Relative Risk
ESTRO	European Society for Therapeutic Radiology and Oncology
GEC	Groupe Européen de Curiethérapie
HDR	High-Dose-Rate
HEBD	High Energy Brachytherapy Source Dosimetry
ICRP	International Commission on Radiological Protection
ICRU	International Commission on Radiation Units and measurements
IMRT	Intensity Modulated Radiation Therapy
IORT	IntraOperative Radiation Therapy
LAR	Lifetime Attributable Risks
LDR	Low-Dose-Rate
LNT	Linear No-Threshold
MC	Monte Carlo
MDR	Medium-Dose-Rate
NCRP	National Council on Radiation Protection and Measurements

OAR	Organ At Risk
PD	Peripheral Dose
PDR	Pulsed-Dose-Rate
RBE	RadioBiological Effectiveness
TLD	ThermoLuminiscent Dosimeter
UNSCEAR	United Nations Scientific Committee on the Effects of Atomic Radiation
VMAT	Volumetric Modulated Arc Therapy
WBI	Whole Breast Irradiation

Chapter 1. INTRODUCTION

1.1 High-dose-rate brachytherapy

Brachytherapy (BT) is a radiation treatment modality in which a sealed radioactive source is placed near, in contact or inside the tumor volume. The disintegration of this source produces the emission of energy, which may give place to cell death. A very high dose (absorbed dose is defined as energy absorbed per unit mass) is delivered in a short time period and a small number of fractions. It requires the treatment volume to be accessible and well limited in size and shape. BT is commonly used as an effective treatment modality for cancers of cervix, prostate, breast, and skin. It has been also shown to be effective to treat tumors of the brain, head and neck region (*e.g.* lip, tongue or floor of mouth), eye, trachea and bronchi, the digestive and urinary tract (*e.g.* bladder, rectum, anus, urethra, penis), female reproductive tract (uterus, vagina and vulva), and other soft tissues (Gerbaulet *et al.*, 2002). BT plays today a fundamental therapeutic tool. For example, for prostate carcinomas the cancer cure rates are either comparable to those of external beam radiotherapy (EBRT) and surgery, or even improved when used in combination with them (Viswanathan *et al.*, 2007; Pickles *et al.*, 2009; Haie-Meder *et al.*, 2009; Pieters *et al.*, 2009).

Compared to EBRT, in which collimated photon beams produced by a linear accelerator are generated outside the patient, BT has the advantages of a rapid fall off of dose around the sources due to the inverse distance square law. This implies less adverse side effects, and shorter overall treatment duration, thus reducing the risk of tumor repopulation. However, the dose distribution is not homogeneous and accuracy in source positioning is critical (Gerbaulet *et al.*, 2002). The use of BT has increased substantially since the 1990s and it is expected to grow even more in the near future (Guedea, 2014).

Depending on the dose rate D of the radioactive BT source employed, either high-dose-rate (HDR) (D>12 Gy/h), medium-dose-rate (MDR) (D=2 to 12 Gy/h), pulsed-dose-rate (PDR) (short pulses of radiation, usually once an hour) or low-dose-rate (LDR) (D<2 Gy/h) can be distinguished. In detriment of LDR, HDR is

becoming nowadays the most extended BT modality worldwide (Guedea, 2014). Advantages of HDR over LDR BT include reduced radiation exposure to personnel, reduced overall treatment time, treatment delivery in the outpatient setting, and potential cost savings (Bastin *et al.*, 1993). In addition, for the particular case of prostate brachytherapy, common problems related to permanent seeds implants such as inability to correct seeds position, inability to optimize the dose delivered once the seeds are in place, and discrepancy between planned and actual seeds distribution are relatively infrequent in HDR brachytherapy (Demanes *et al.*, 2014). Nevertheless, with HDR BT an increased risk of late tissue effects has been estimated (Dale, 1985), and so more efforts are needed in this field. For these reasons, HDR therapy is the BT technique considered in this study.

In HDR BT one single source is placed at several dwell positions in order to cover the whole extension of the tumor, staying in each position a planned dwell time. The delivery of the treatment is performed by an afterloader system controlled from outside the treatment room. The overall treatment time is just a few minutes. A high specific activity (radioactivity per unit mass) of a radionuclide is necessary to produce miniaturized sources of just a few mm as those used in HDR BT. ^{60}Co and ^{192}Ir sources are nowadays the only commercially-available radionuclides for HDR BT. The characteristics of these sources are presented in detail in **Chapter 2**. The reasons why ^{60}Co is an alternative option to the traditional ^{192}Ir sources have already been reported (Righter *et al.*, 2008; Strohmaier *et al.*, 2011; Andrássy *et al.*, 2012; Palmer *et al.*, 2012). Relative dosimetric differences around ^{60}Co and ^{192}Ir sources are less significant than prescription technique and the optimization parameters, given that they have a similar radial dose distribution governed by the inverse distance square law, $1/r^2$. This results in no clinically significant differences. Advantage of ^{60}Co over ^{192}Ir is the significant cost savings, due to the fact that this source has to be replaced every 4 to 5 years, whereas ^{192}Ir sources need to be changed every 3 to 4 months. Thus, in comparison to ^{192}Ir, with ^{60}Co equipment down-time and physics support time is also reduced by around 40%. However the irradiation time is on average a factor 1.7 longer with ^{60}Co. The ^{60}Co source activity

required to produce the same absorbed dose rate in air is a factor 2.8 lower. In addition, due to its higher mean energy, ^{60}Co needs a higher room shielding.

1.2 Peripheral dose and secondary radiation risks

During radiation therapy not only does the tumor volume absorbs dose, but also all the remaining tissues of the body, even though they are out of the beam path in the case of EBRT or far from a brachytherapy source. The latter is known as peripheral dose (PD). This may result in some cases in acute, sub-acute and/or long-term side-effects, which depend on the location of the target volume, the type of BT that is used and also the amount of absorbed dose. Due to improved long term survival rates, long-term side-effects are becoming increasingly important. Thus, reducing the PD helps to improve the treatment success.

The hazard effects of ionizing radiation in the human health can be classified in deterministic and stochastic. Deterministic effects are those for which a threshold dose exists, below which the hazard effect is not produced. If the dose to healthy organs at risk (OAR) is reduced, then the possibility to overcome that threshold decreases. On the other hand, stochastic effects are those in which the probability of having the effect generally increases with absorbed dose, with no threshold dose. The severity of these effects is independent on dose.

Among the stochastic effects is the induction of a secondary tumor not related to the initial one. The scientific community tries to establish a relationship between organ equivalent dose and the probability that a specific tumor is induced. If the relationship were known, the secondary cancer induction from a typical brachytherapy treatment could be obtained and compared with the probability from other radiation therapies. However, this requires the knowledge of both the dose-response relationship and the peripheral dose. A deep review of the literature is necessary to evaluate the knowledge on this dose curve. In addition, the PD is necessary. This can be already estimated in EBRT using the software program

Peridose (Van der Giessen, 2001). However, according to a summary on second cancer induction done by Xu *et al.* (2008), the American Association of Physicists in Medicine (AAPM) Task Group 158 and the National Council on Radiation Protection and Measurements (NCRP) Scientific Committee have excluded brachytherapy from their studies due to lack of data, which confirms the necessity to make a complete study regarding equivalent doses to all organs when applying brachytherapy (NCRP, 2001). Furthermore, a major European collaboration involving 13 organizations across Europe, the ALLEGRO project (http://www.allegroproject.org), whose aim is to address many issues of damage produced to normal healthy tissues after treatment with conventional and emerging radiotherapy techniques, has not yet considered brachytherapy, which again confirms the need for greater knowledge in this treatment technique.

1.3 Review of Monte Carlo methods

Most part of the research work of this study is based on the results of Monte Carlo (MC) simulation techniques. MC simulations have become an essential tool to improve the calculation of absorbed doses in brachytherapy. The basic principle of the MC method is the use of random numbers and probability density distributions programmed into computers to find the solution to a physical or mathematical problem.

For BT with its pertinent laws of radiological physics, the MC method enables accurate calculation of absorbed doses in regions with a high dose gradient. This allows enhancing and complementing the dose calculations obtained experimentally since the latter has a large uncertainty due to small errors in the position of the detector. In addition, with MC there are no experimental problems such as energy and sensitivity dependence of the detectors. Another advantage of the MC method compared to experimental measurements is the possibility to separate the different components of absorbed dose: the primary radiation, scattered

radiation and multiple scattering components. This is useful in modeling dose deposition. Also, the MC method can provide additional information of interest such as the energy spectra from radioactive sources at any distance in any medium.

In MC simulations, absorbed dose can be calculated directly or from collision kerma. In the direct method, the absorbed dose in a given cell is computed as the sum of the energies deposited in the cell divided by the cell mass. When there is electronic equilibrium, then absorbed dose equals collision kerma, which is given by the sum of the initial kinetic energies of charged particles released in the cell by non-charged particles. The calculation of absorbed dose from kerma significantly reduces the variance (Williamson, 1987), *i.e.*, the simulation time necessary to achieve a given statistical noise. This is achieved by using the linear track-length estimator, which is based on the equivalence between particle fluence and the total length of the photon path per unit volume (Carlsson, 1985). The variance is significantly reduced because all the paths of the photons passing through a given cell contribute to the calculation of the linear track-length estimator.

Currently there are multiple MC codes available for medical physics applications. The main ones are: MCNP (X-5 Monte Carlo Team, 2003; Goorley *et al.*, 2012), EGS (Nelson *et al.*, 1985), PENELOPE (Salvat *et al.*, 2011), FLUKA (Ferrari *et al.*, 2005) and GEANT4 (Agostinelli *et al.*, 2003; Allison *et al.*, 2006).

For the development of this study, I specialized in the MC code GEANT4, a general purpose code written in C++ that allows simulating the passage of particles through matter. GEANT4 allows creating complex geometries using predefined shapes or importing CAD geometries and voxelized phantoms. In addition, all kind of “particles” (including leptons, hadrons, ions or even new particles created by the user) can be initiated. GEANT4 provides the user with a large set of physical processes including electromagnetic, hadronic and optical physics. In addition, the user can "communicate" with the code by choosing various interfaces and visualize the geometry and particle tracking using multiple display systems. The code functions are designed in a compact and reusable way such that the user can extend

or modify the services provided by these to be used in their own applications. GEANT4 has been widely validated for its use in brachytherapy dosimetry (Rivard *et al.*, 2010; Granero *et al.*, 2011; Vijande *et al.*, 2012).

1.4 Objectives and outline of this thesis

The goal of this thesis was threefold. Firstly, to evaluate the peripheral dose in a typical brachytherapy scenario and discern which HDR radioactive source is more advantageous from a patient radiation protection point of view, *i.e.*, which source deposits less dose to the nearest and the furthest tissues. Secondly, the risk of secondary malignancies induced by the BT treatment was reviewed. Because old epidemiological studies are needed with higher accuracy in dose calculation, we provide a more accurate dosimetry based on the current formalism for old radium brachytherapy sources, for which a lot of patient follow-up exists, allowing performing retrospective studies. Thirdly, we aimed to reduce the peripheral dose received by organs and tissues near the implant using specifically designed implant shielding.

Chapter 1 has covered the principles behind HDR brachytherapy and secondary risks associated with this treatment modality. It also presents the objectives and outline of the present thesis. **Chapter 2** to **Chapter 6** are based on papers which have been published in international peer-reviewed journals. **Chapter 2** evaluates through MC simulations the peripheral dose in the treatment of a prostate carcinoma when using ^{60}Co and ^{192}Ir sources. Results of this study are compared with the peripheral dose in other radiotherapy modalities such as EBRT and proton therapy. **Chapter 3** assesses the probability that the radiation doses absorbed by the healthy organs can induce a secondary tumor. Following a thorough literature review of current knowledge in this field, a critical analysis is presented. **Chapter 4** aids epidemiologists with accurate dose estimations, which can be linked to secondary risks for a BT treatment. For this purpose, a radium

(^{226}Ra) tube and needle, widely used from 1920s to the 1970s, and for which there exists a wide medical record with clinical follow-up, are dosimetrically characterized using MC simulations and the formalism employed in clinical practice. **Chapter 5** is the first chapter aimed to reduce the peripheral dose. The use of lead shielding in certain surface treatments is considered, and the optimum shielding thickness is evaluated. Because the shield may increase the dose near the patient surface that is in contact with the shield, the use of a layer of material equivalent to water (bolus) placed between the shield and the patient surface is proposed, and its effect is evaluated, as well as the required bolus thickness as a function of the radionuclide used. Results of this study are applied in **Chapter 6** to a case of great interest: dose reduction to the fetus of a pregnant patient having breast cancer. For this particular case, a novel breast shield is designed and absorbed dose to the fetus is measured, with and without shielding. These data are compared to the fetal dose delivered by other radiotherapy techniques. Finally, **Chapter 7** presents a general discussion of all previous studies.

Chapter 2. PERIPHERAL DOSE IN HDR BRACHYHTERAPY

Most of the content of this chapter was published in the original research paper:

Candela-Juan C, Perez-Calatayud J, Ballester F, Rivard MJ. *Calculated organ doses using Monte Carlo simulations in a reference male phantom undergoing HDR brachytherapy applied to localized prostate carcinoma*. Medical Physics. 40: 033901 (2013).

Kind permission was granted by the journal to reprint this article as a chapter of this dissertation.

2.1 Introduction

Prostate carcinoma is the second most frequently diagnosed tumor among men in economically developed countries (14% of cancer cases in 2008), being the sixth leading cause of cancer death (6% of cancer deaths in males in 2008) (Jemal *et al.*, 2011), although there are variations amongst countries (IARC, 2001). If increasing life expectancy is also considered, an even higher death rate due to prostate cancer is expected and it is thus worth directing efforts to improve treatment options for this disease.

The American Brachytherapy Society (ABS) has shown the success of HDR brachytherapy applied to localized prostate cancer (Yamada *et al.*, 2012). In addition to low toxicities (<5% for Grade 3 or higher), biochemical control rates of 85% to 100%, 81% to 100%, and 43% to 93% have been reported for low-, intermediate-, and high-risk prostate tumors, respectively. In addition, it has been shown that HDR brachytherapy achieves complete prostate target coverage and doses to urethra, bladder and rectum below the dose constraints for these OARs (White *et al.*, 2013). From a population-based analysis, it is also shown that mortality rates are reduced when applying brachytherapy alone or in combination with EBRT, even for high-risk cancers. In fact, besides HDR monotherapy being a treatment technique for this disease, it also plays a fundamental tool as a boost (9 Gy or 15 Gy) after 60 Gy or 46 Gy intensity modulated radiation therapy (IMRT), respectively.

Several manufacturers have traditionally offered HDR ^{192}Ir as a brachytherapy source. The new Eckert & Ziegler BEBIG GmbH MultiSource remote afterloader permits HDR ^{60}Co brachytherapy.

Tumor control is the main concern in a radiotherapy treatment plan. However, production of secondary cancers becomes a criterion that can be used to establish the treatment choice when target coverage and dose sparing are comparable for different radiotherapy modalities. As stated by Schneider *et al.* (2006), new radiation treatment techniques such as IMRT or hadron therapy may

increase cancer cure rates, although it is expected they can also increase secondary tumor incidence. This is because of the relatively high equivalent dose deposition in OARs that are within the primary beam trajectory. In addition, a considerable increase in beam-on time for IMRT gives to organs out of field a higher absorbed dose, mainly from leakage radiation, since contribution from scatter is equal or less than in 3D-conformal radiotherapy (3D-CRT) if proper collimation is used. In the case of proton therapy or radiation therapy with high energy photons, neutrons are created in the accelerator which, due to their higher radiobiological effectiveness than photons, may also lead to an increase of secondary cancers.

Given the successful clinical results when using brachytherapy, IMRT, or proton therapy (Schneider *et al.*, 2006; Shen *et al.*, 2012), it is of interest to discern the treatment modalities and compare probabilities for secondary cancer occurrence. The peripheral dose has been obtained for 3D-CRT, IMRT, and proton therapy (Schneider *et al.*, 2006; Stathakis *et al.*, 2007; Fontenot *et al.*, 2009; Bednarz *et al.*, 2009; Bednarz *et al.*, 2010). This has also been done for brachytherapy applied to the breast, using HDR ^{192}Ir and electronic sources (Mille *et al.*, 2010). However, it does not appear to have been done for HDR brachytherapy with ^{60}Co and ^{192}Ir sources applied to prostate cancer, nor with comparison to EBRT techniques. As previously stated, according to a summary on the topic done by Xu *et al.* (2008), the AAPM Task Group 158 and the NCRP Scientific Committee excluded brachytherapy from their studies due to lack of data. This exclusion supports the study of equivalent doses in a similar context to include brachytherapy.

Consequently, the aim of this study was to obtain equivalent doses to a variety of organs when applying HDR brachytherapy to the prostate using ^{60}Co or ^{192}Ir sources, and to provide EBRT comparisons. Given that absorbed doses to the bladder and rectum are dependent on patient-specific treatment plans and are already estimated during the planning process, the focus is on farther organs. Due to the intrinsic difficulties and limitations of absorbed dose measurements to organs,

MC simulated radiation transport has been selected as the calculation method to estimate the needed data.

2.2 Materials and methods

2.2.1 Geometry definition

In order to reproduce a prostate brachytherapy treatment, a representative adult male phantom is needed. Since the 1960s, more than one hundred phantoms have been reported in the literature (Caon, 2004; Zaidi *et al.*, 2007; Zhang *et al.*, 2009; Xu *et al.*, 2010), going from stylized phantoms formed by mathematical shapes, to voxelized phantoms, and finally to mesh phantoms, where their postures can be adjusted and the body organs deformed. A recent and complete analysis of all these body phantoms was presented by Xu *et al.* (2010).

In its Publication 110 (ICRP, 2009), the International Commission on Radiological Protection (ICRP), jointly with the International Commission on Radiation Units and Measurements (ICRU), defines an official voxelized phantom that reproduces reference organ and tissue values given in ICRP Publication 89 (ICRP, 2002). For design of the ICRP/ICRU 110 phantom, tomographic datasets from a real individual with physical characteristics close to those from the reference phantom (176 cm tall and 73 kg mass) were selected, and voxel scaling was applied to adjust the body height and the skeletal mass. Individual organs were then segmented and adjusted to reproduce reference masses within 0.01 g. The final phantom consists of over 140 organs and tissues, formed by almost 1.95 million voxels (7.16 million voxels if exterior air is considered). For the male phantom, the voxel height is 8 mm, whereas the voxel in-plane resolution is 2.137 mm with a voxel volume of 36.54 mm^3. Since the physical posture of a patient with prostate carcinoma who is being treated with HDR brachytherapy is not very different from the ICRP/ICRU 110 phantom, this voxelized phantom was used in this work.

Some tissues/organs such as lymphatic nodes, blood, and bone marrow, among others, could not be perfectly segmented due to the limited voxel resolution (ICRP, 2009). Lymphatic nodes were included manually at specific locations, whereas a blood portion was incorporated in the elemental tissue composition of each organ. In addition, the mass percentage of bone marrow in the spongiosa part of skeletal targets is given in ICRP Publication 110 (ICRP, 2009), which allows an estimation of absorbed dose to red bone marrow and endosteum tissue (bone surface), which are part of the radiosensitive organs needed to obtain effective dose. This is, however, an overestimation of absorbed dose in these two tissues given that secondary equilibrium between the mineral bone and soft tissue components of the spongiosa does not exist (ICRP, 2009). Despite this, the voxelized phantom is considered adequate for the purpose of this study given that variation of absorbed doses due to exact organs resolutions is expected to be small compared to variations between different patients. In addition, dealing with relatively high energy photons, this voxel resolution should not be a concern.

In order to assess the adequacy of a homogeneous phantom for HDR absorbed dose calculations, and to permit model validation against measurements by others, simulations were repeated with the entire phantom composition replaced as liquid water. In addition, an extra simulation with the heterogeneous voxelized phantom immersed in water was later performed in order to explain the behavior of organ doses as a function of distance when compared to an 'infinite' medium. Additional simulations were performed in 1 m radii spheres of water (ρ = 1.00 g/cm^3) and muscle (ρ = 1.05 g/cm^3).

2.2.2 Brachytherapy sources

Energy spectra used in the MC simulations and their probabilities are the ones obtained by our group in previous studies (Ballester *et al.*, 2009; Rivard *et al.*, 2010), which provide spectra exiting real encapsulated HDR ^{60}Co and ^{192}Ir sources. The photons were generated at the prostate center of the voxelized phantom (*i.e.*, point sources) emitting photons isotropically. Source capsule effects have been

included in the simulations using those spectra. These spectra were also used for simulations at the center of the spheres of water and muscle as explained above.

2.2.3 MC simulation setup and organ equivalent dose calculation

The simulation toolkit GEANT4 version 9.4 (Agostinelli *et al.*, 2003) was used to read ASCII data provided in ICRP/ICRU 110 (ICRP, 2009) and to simulate the human phantom and the HDR brachytherapy treatment. The low-energy electromagnetic models of the Livermore physics package, which use detailed handling, were employed. Standard multiple scattering cross-sections were also utilized, with specialized processes for each particle type. Detailed information about these models can be found in the GEANT4 User Documentation webpage (http://geant4.cern.ch/supports/userdocuments.shtml). This code has been widely validated for its use in brachytherapy dosimetry (Rivard *et al.*, 2010; Granero *et al.*, 2011; Vijande *et al.*, 2012). Secondary electrons were also tracked. For electrons and photons, the cutoff range was set to 0.1 mm, so secondary particles having a smaller range were not generated.

In order to hasten simulation time without extra memory requirement, the G4RegulatorNavigation algorithm was used, as implemented in the DICOM example of GEANT4. It is based on removing voxel frontiers when two voxels share the same material. An iterative algorithm is later applied to determine absorbed dose in each individual voxel of a cluster. More details about this technique, which has already been validated, can be found on the cited example of GEANT4.

A text file with absorbed dose in each voxel was obtained as an output of the simulation. In-house developed software was then used to convert this output to absorbed dose D_T in each organ or tissue T, by summing all voxel absorbed doses in an organ and dividing by the number of voxels that form it. This is a mass weighted average considering that all voxels of the same tissue have the same mass. D_T was

then converted to mean absorbed dose per released photon by dividing by the number of events per simulation, N. Finally, equivalent dose per photon, H_T/N, was obtained from absorbed dose through a radiation weighting factor w_R:

$$\frac{H_T}{N} = \sum_R w_R \frac{D_{T,R}}{N} \qquad \textbf{(2-1)}$$

According to ICRP Publication 103 (ICRP, 2007), w_R equals 1 for photons and electrons. Since these are the only particle types in the simulation environment, the equivalent dose H_T in an organ was numerically equal to absorbed dose in that organ. Effective dose E was also obtained through a tissue weighting factor w_T:

$$\frac{E}{N} = \sum_T w_T \frac{H_T}{N} \qquad \textbf{(2-2)}$$

The point source was located at the prostate center. For each source and phantom composition (heterogeneities or water), 10^9 initial photons were used, which provided statistical (Type A) uncertainties < 1% for most of the organs considered. As recommended in the joint AAPM Task Group No. 138 report (DeWerd *et al.*, 2011), a coverage factor of k=2 (confidence level of 95%) was used to express uncertainties in brachytherapy dose.

The procedure by Pujades *et al*. (2011) was used to correlate the MC simulations of the source at a single position at the prostate center with a realistic therapeutic absorbed dose to the prostate for the source at various locations and with different dwell times. They derived the relationship between prostate volume V, therapeutic absorbed dose D_P, air-kerma strength S_K, and total irradiation time t for 127 clinical cases. The correlation was presented as a nomogram fitted to a linear function and allowed estimation of t for the source at the center of the prostate to deliver the required absorbed dose:

$$t \times S_K = D_P(a \times V + b) \qquad \textbf{(2-3)}$$

where *a* and *b* are fitting parameters obtained experimentally (Pujades *et al.*, 2011). From previous Monte Carlo studies (Ballester *et al.*, 2009; Rivard *et al.*, 2010; Granero *et al.*, 2011; Vijande *et al.*, 2012), the air-kerma strength per Bq, S_K/A, was derived for both HDR ^{60}Co and ^{192}Ir sources. From all these clinical data, the number of events $N_{1\,\mathrm{Gy}}$ necessary to provide a therapeutic absorbed dose of $D_P = 1$ Gy to the prostate, as a function of *V* was obtained:

$$\frac{N_{1\,\mathrm{Gy}}}{D_P} = \frac{(a \times V + b)}{S_K / A} \qquad \textbf{(2-4)}$$

Using $N_{1\,\mathrm{Gy}}$ with Eq. (2-1), equivalent dose per therapeutic absorbed dose to the prostate, H_T/D_P, was determined. Data correspond to those from a typical prostate volume of V=30 cm^3, although variations with *V* were also analyzed.

2.3 Results

2.3.1 Organ equivalent dose

$N_{1\,\mathrm{Gy}} = 8.4\times10^{12}$ and $N_{1\,\mathrm{Gy}} = 3.0\times10^{13}$ photon histories for ^{60}Co and ^{192}Ir, respectively, were needed to deliver 1 Gy of therapeutic absorbed dose to a 30 cm^3 prostate. If the method by Pujades *et al.* (2011) had not been used, for that number of initial events, absorbed dose in the prostate would be 3.9 Sv/Gy and 4.9 Sv/Gy instead of 1 Sv/Gy for ^{60}Co and ^{192}Ir, respectively. They are larger than 1 Sv/Gy, which was expected given that $N_{1\,\mathrm{Gy}}$ is used to account for a real case where the source is located at various points inside the prostate. This source distribution reduces overall absorbed dose in the prostate in exchange for uniform dose deposition in the target volume. This methodology might underestimate absorbed

doses to the nearest organs (mainly the ones which are in contact with the prostate), due to proximity of a specific source position. For the rest of the organs, the variations were expected to be negligible.

Table 2-1 shows mean equivalent doses (per therapeutic absorbed dose to a 30 cm^3 prostate), H_T/D_P, in several radiosensitive organs in the heterogeneous phantom, for both the ^{60}Co and ^{192}Ir sources, all together with the Type A statistical uncertainties. Effective dose is also included. In addition, the relative variation of organ absorbed doses for the water phantom in comparison to the heterogeneous phantom is shown. For completeness, organ masses and distances, *r*, from their center of mass to the center of mass of the prostate are also given.

Figure 2-1 shows organ absorbed doses as a function of *r*. The depth dose distribution in the 1 m radius water sphere and fitted curves obtained by Venselaar *et al.* (1996) from measurements of point sources (^{60}Co and ^{192}Ir) in water are plotted (see **Figure 2-1a** and **Figure 2-1b**, respectively) for comparison. Similarity of the curves validates the simulations and physics package used.

There is reasonable agreement between organ data and the fitted curves. There are three organs that received an absorbed dose higher than predicted by simulations in water: spinal cord, small intestine wall, and the colon. The latter two are close to the prostate, and all three subtend volumes over a large range of distances from the prostate. For organs with $d > 30$ cm, organ absorbed dose is smaller than expected in water by 50% to 125% for ^{192}Ir, and by 17% to 60% for ^{60}Co. These discrepancies are also present for organ absorbed doses in the homogeneous water phantom. There are two known radiological effects that contribute to these differences. First, there is dosimetric difference between water and soft tissue for $d > 30$ cm, as shown later. Second, there is lack of backscatter at the phantom skin compared to an infinite medium. This was demonstrated by immersing the heterogeneous voxelized phantom in water. With this configuration, organ absorbed doses increased up to ~25% with variations between different organs.

Table 2-1. *Organ equivalent dose per therapeutic absorbed dose to the prostate, (H_T/D_P), given to the heterogeneous voxelized phantom by the ^{60}Co source and by the ^{192}Ir source. Distances correspond to those between the prostate and the organ center of masses. The statistical uncertainty (Type A) percentage (k=2), ε, is also shown (but for those with ε < 0.05%), as well as the effective dose. The last column corresponds to the relative variation of absorbed dose between the water and the heterogeneous phantom, Δ, being positive if absorbed dose in water is higher than in a tissue.*

Organ name	Mass	Distance	H_T / D_P (Sv/Gy)				Δ (%)	
			^{60}Co		^{192}Ir			
	(g)	(cm)	Mean	ε (%)	Mean	ε (%)	^{60}Co	^{192}Ir
Urinary bladder wall	50.0	5.0	$1.30x10^{-1}$	0.1	$1.60x10^{-1}$	0.1	0.6	-0.4
Rectum wall	30.0	5.3	$1.51x10^{-1}$	0.1	$1.83x10^{-1}$	0.1	0.6	0.5
Testis, right	17.5	11.2	$2.51x10^{-2}$	0.3	$2.94x10^{-2}$	0.3	-0.1	0.2
Testis, left	17.5	11.3	$2.42x10^{-2}$	0.2	$2.82x10^{-2}$	0.2	0.2	0.2
Small intestine wall	650.0	20.3	$9.24x10^{-3}$	0.1	$1.05x10^{-2}$	0.1	1.2	2.7
Colon	340.0	24.0	$6.21x10^{-3}$	0.1	$6.78x10^{-3}$	0.1	0.9	2.7
Kidney, right	157.0	29.9	$1.75x10^{-3}$	0.3	$1.40x10^{-3}$	0.3	5.1	11.5
Kidney, left	153.0	31.1	$1.56x10^{-3}$	0.5	$1.20x10^{-3}$	0.3	4.9	10.8
Pancreas	140.0	31.2	$1.53x10^{-3}$	0.3	$1.21x10^{-3}$	0.4	4.9	9.5
Gall bladder wall	13.9	32.9	$1.26x10^{-3}$	1.2	$9.33x10^{-4}$	1.3	4.2	7.5
Adrenal, right	7.0	33.6	$1.11x10^{-3}$	1.9	$7.63x10^{-4}$	1.4	10.5	19.5
Adrenal, left	7.0	34.8	$9.79x10^{-4}$	1.7	$6.50x10^{-4}$	2.3	9.4	17.6
Stomach wall	150.0	35.8	$9.50x10^{-4}$	0.5	$6.40x10^{-4}$	0.4	2.4	6.9
Liver	1800.0	36.2	$8.88x10^{-4}$	0.1	$5.88x10^{-4}$	0.2	4.2	9.3
Spleen	150.0	38.1	$7.15x10^{-4}$	0.6	$4.32x10^{-4}$	0.3	6.2	13.1
Heart contents	510.0	44.3	$4.03x10^{-4}$	0.3	$2.09x10^{-4}$	0.7	9.3	17.9
Heart wall	330.0	44.7	$3.97x10^{-4}$	0.2	$2.08x10^{-4}$	0.3	9.0	15.1
Lung, right	471.7	47.3	$3.37x10^{-4}$	0.4	$1.60x10^{-4}$	0.4	1.0	8.8
Lung, left	376.8	47.9	$3.27x10^{-4}$	0.3	$1.56x10^{-4}$	0.6	0.1	5.7
Esophagus	40.0	50.0	$3.01x10^{-4}$	1.8	$1.55x10^{-4}$	1.9	14.7	23.3
Spinal cord	36.6	50.9	$4.35x10^{-4}$	1.3	$2.51x10^{-4}$	1.7	13.1	34.4
Thymus	25.0	54.6	$1.53x10^{-4}$	2.5	$6.16x10^{-5}$	4.5	13.6	6.3
Trachea	10.0	57.0	$1.28x10^{-4}$	4.1	$4.74x10^{-5}$	6.1	11.4	18.5
Thyroid	20.0	59.1	$1.04x10^{-4}$	3.7	$3.46x10^{-5}$	4.6	5.9	6.2
Tongue (inner part)	42.3	70.0	$5.62x10^{-5}$	1.8	$1.50x10^{-5}$	6.7	0.6	0.8
Salivary gland, right	42.5	70.3	$5.88x10^{-5}$	2.3	$1.45x10^{-5}$	6.7	-16.7	-14.1
Salivary gland, left	42.5	70.3	$4.71x10^{-5}$	2.5	$1.20x10^{-5}$	6.3	-0.9	-4.0
Brain	1450.0	79.5	$2.08x10^{-5}$	1.1	$4.17x10^{-6}$	2.0	2.6	4.3
Active bone marrow	-	-	$1.26x10^{-2}$	-	$1.62x10^{-2}$	-	0.4	-6.2
Skin	-	-	$3.21x10^{-3}$	-	$3.23x10^{-3}$	0.1	2.5	4.7
Lymphatic nodes	-	-	$2.69x10^{-2}$	0.1	$3.13x10^{-2}$	0.1	1.5	1.3
Effective dose	**-**	**-**	**$1.11x10^{-2}$**	**-**	**$1.32x10^{-2}$**	**-**	-	-

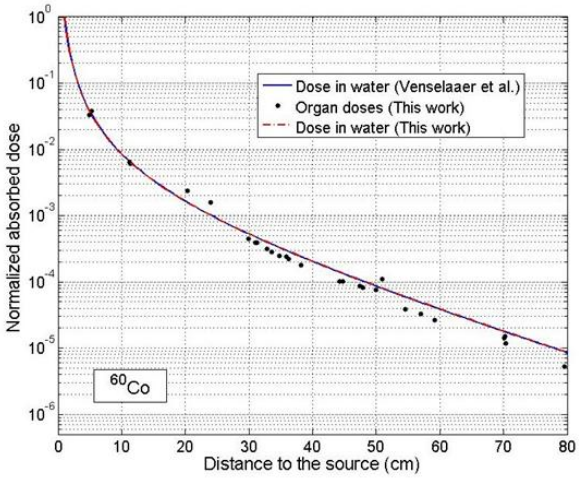

a)

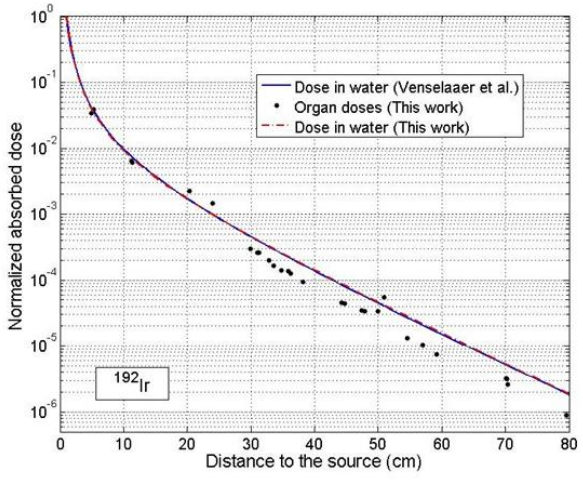

b)

Figure 2-1. *Organ absorbed doses obtained in this work as a function of distance to the prostate for: a) ^{60}Co source and b) ^{192}Ir source. Distances are between the prostate and the organ center of masses. Absorbed doses are normalized such that D(1 cm)=1 (arbitrary units). The fitting curve obtained from Venselaar et al. (1996) is also shown and compared with depth dose distribution in the 1 m radius water sphere simulated in this work, with real spectra exiting the source capsules.*

2.3.2 Influence of prostate size

Mean equivalent dose in each organ is proportional to the number of photons emitted by the source, $N_{1\,Gy}$. In addition, according to Eq. (2-4), $N_{1\,Gy}$ is linear with V. Hence, if D_0 is the absorbed dose in a specific organ when the prostate volume is V_0=30 cm^3, when $V=V_0\,(1+X)$, *i.e.*, when the volume is X % higher or lower, then the relative variation of organ absorbed dose is:

$$\frac{D_X - D_0}{D_0} = X\,\frac{a\times V_0}{a\times V_0 + b} \qquad \textbf{(2-5)}$$

Using real clinical values obtained by Pujades *et al.* (2011) (a=0.0605 cm^{-1}, b=1.7 cm^2), then the relative variation is 0.52 times X. Therefore, if prostate volume increases (decreases) 10% respect to the reference volume, equivalent dose in each organ increases (decreases) by ~5.2%.

2.3.3 ^{60}Co vs. ^{192}Ir

Figure 2-2 represents the ^{60}Co to ^{192}Ir absorbed dose ratio for each organ, for the heterogeneous and the water phantom. Presented error bars are statistical (Type A) uncertainties from MC simulations. Absorbed doses have been normalized such that the prostate receives the same absorbed dose from both sources. It can be observed that absorbed doses in those organs near the treated prostate, such as the bladder, rectum, testes, small intestine, and colon are roughly 10% smaller when using ^{60}Co. This can be rationalized considering that in a real treatment, as shown above, to give the same absorbed dose at 1 cm from the source, the required activity of ^{60}Co is smaller and so is the number of emitted photons. This is not the case for distant organs. As the distance between the prostate and the organ increases, so does the relative contribution of ^{60}Co absorbed dose in comparison to ^{192}Ir. This can be understood from the mean energy of emitted photons for each radionuclide, which is higher for ^{60}Co and has greater penetration within the body. This trend can be

also observed in **Figure 2-3**, where it is plotted the dose distribution in a coronal plane containing the sources.

Given that the same therapeutic absorbed dose is prescribed with both radionuclides, and that estimated effective doses were 11.1 mSv/Gy for ^{60}Co and 13.2 mSv/Gy for ^{192}Ir, an overall advantage of ^{60}Co seems to exist when organ doses are considered.

2.3.4 Heterogeneous vs. water phantom

Currently, brachytherapy treatment planning systems consider the body to be composed of water. In this section, validity of this assumption when obtaining organ absorbed dose in the whole body is analyzed. **Figure 2-4** shows the organ absorbed dose ratio of heterogeneous media to water for the two sources. For the closest organs considered, absorbed dose was the same for all organs having near-unity mass density.

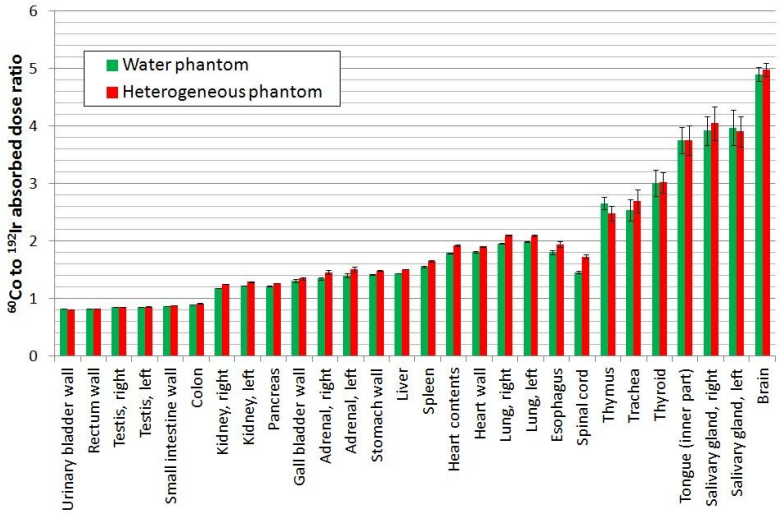

***Figure 2-2** .^{60}Co to ^{192}Ir absorbed dose ratio for different body organs, using a heterogeneous and a water phantom.*

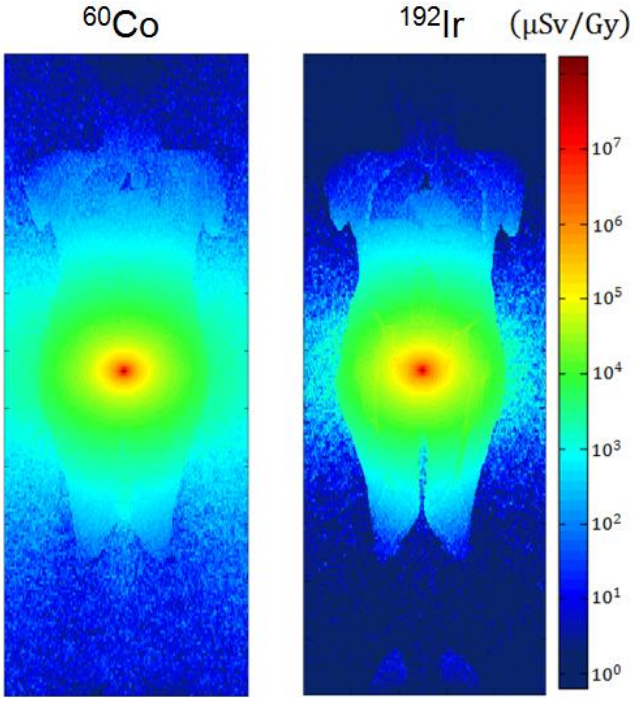

Figure 2-3*. Equivalent dose per therapeutic absorbed dose in a coronal plane containing the [60]Co source (left) and the [192]Ir source (right).*

However, as the distance increases the absorbed dose ratio decreases, reaching differences of almost 25% (but for the spinal cord, which is surrounded by bone and so the absorbed dose ratio is even lower), being lower for ^{192}Ir than for ^{60}Co (but for the thymus and the left salivary gland, where uncertainties are relatively high and so no conclusions can be extracted). The reason for the absorbed dose rate reduction is in the material composition. In order to prove this, absorbed dose as a function of distance was obtained in water and muscle spheres with the sources placed at the centers. The absorbed dose ratios when using both ^{60}Co and ^{192}Ir, with their real spectra exiting the sources, are shown in **Figure 2-5**.

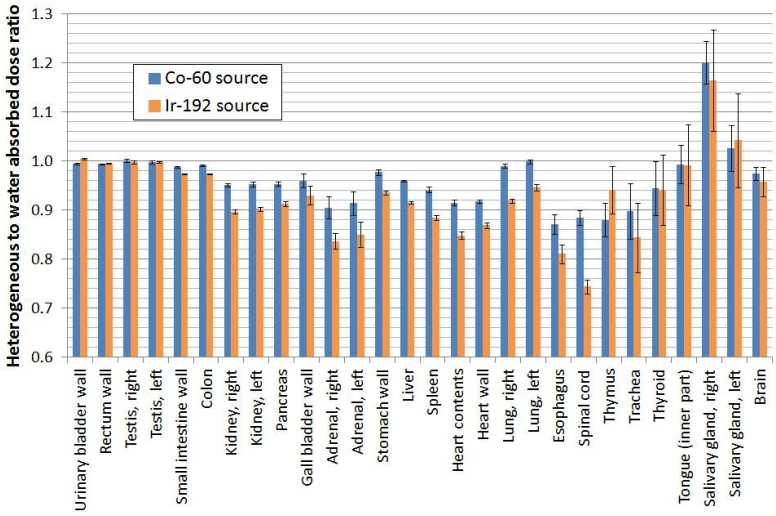

***Figure 2-4**. Heterogeneous to water absorbed dose ratio, using ^{60}Co and ^{192}Ir sources.*

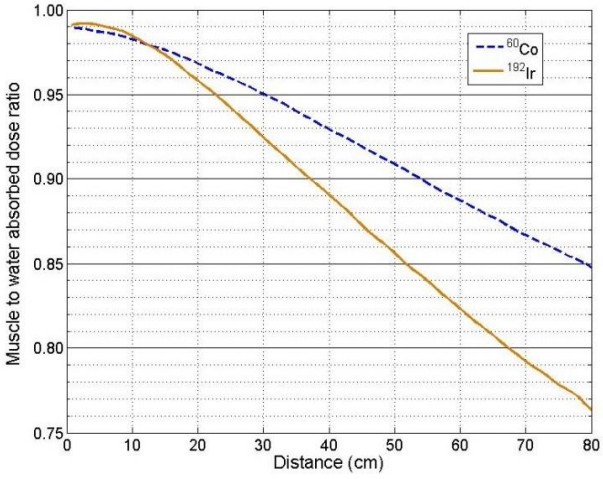

***Figure 2-5**. Muscle to water absorbed dose ratio for ^{60}Co and ^{192}Ir encapsulated sources at the center of 1 m radius spheres. Absorbed doses are averaged over shells of 5 mm width.*

As an example, at 30 cm from the source, the muscle to water absorbed dose ratio for ^{192}Ir is 0.92, being the difference between the kidneys and its corresponding water volume of around 10%, in agreement. Hence, the general decrease of the heterogeneous to water absorbed dose ratio can be explained considering the differences between real tissue and water, which are negligible for distances below 10 cm, but not after that. With ^{60}Co, which has higher mean photon energy, photoelectric effect is not dominant and so the difference between water and soft tissue is smaller than for ^{192}Ir. The other factor which influences the curve from **Figure 2-4** is the presence of different materials like air inside some organs, bone, or the lungs. An interesting case is the salivary glands, where the heterogeneous to water absorbed dose ratio between the left and the right gland might seem consistent for the ^{192}Ir source considering their uncertainties, but not for the ^{60}Co source. This difference can be explained taking into account that the prostate center of mass of the voxelized phantom is almost 1 cm at right from our geometrical center, and so it traverses more lung to reach the right salivary gland than to reach the left one. In addition, the right lung is more superior than the left one due to the presence of the heart, and so the effect is even larger.

2.4 Discussion

It is interesting to compare organ equivalent doses that result from different radiation modalities (brachytherapy, 3D-conformal radiotherapy, IMRT, and proton therapy). There are some studies regarding organ equivalent doses from proton therapy applied to prostate. Fontenot *et al.* (2008) estimated equivalent doses from stray radiation, *i.e.*, neutrons and photons generated (either inside or outside the body) in a passively scattered proton treatment to radiosensitive organs. The prescribed equivalent dose was 75.6 CGE (Cobalt Gray Equivalent), *i.e.*, 68.7 Gy×1.1 RBE (radiobiological effectiveness of protons), to the clinical treatment volume. Simulations were run in the MCNPX code, using an anatomically realistic male phantom developed by Billings and Yucker (1973). In their first work, they

did not consider absorbed dose from the therapeutic beam, which mainly concerns additional absorbed dose to the bladder and rectum. In a follow-up paper (Fontenot *et al.*, 2010) they considered primary absorbed dose calculated using a commercial treatment planning system applied to three patients. Summing the contributions from secondary particles, they obtained total equivalent dose and estimated the probability of secondary tumor induction using recommendations by the Biological Effects of Ionising Radiation (BEIR) committee (BEIR, 2006). Given that some data were not explicitly written in the paper (Fontenot *et al.*, 2010*)*, the authors were contacted and kindly provided the needed details. The three patients were of different sizes (small, medium, and large). Their medium sized data are compared in the current study. In their work, equivalent dose to the colon was obtained as a mass-weighted average of the equivalent doses to the colon and rectum:

$$D_{total-colon} = w_{colon} D_{colon} + w_{rectum} D_{rectum} \qquad \textbf{(2-6)}$$

where the colon w_{colon} and rectum w_{rectum} mass weights were 20% and 80%, respectively, according to ICRP 89 (2002).

On the other hand, Bednarz *et al.* (2009, 2010) estimated organ equivalent doses and risk probabilities from two 3D-CRT (a 4-field box and a 4-field box + 6-field boost), and a 7-field IMRT treatment applied to the prostate. Absorbed doses were estimated through MCNPX using a voxelized male phantom also in agreement with the male reference phantom from ICRP Publication 89, and a previously validated Varian Clinac 2100C linear accelerator (Bednarz *et al.*, 2009). Their results are within an order of magnitude of those obtained by Kry *et al.* (2005) and Howell *et al.* (2006*)*. Study discrepancies are due in part to the different organ locations and methods used to obtain absorbed doses. Organs within the therapeutic beam (testes, bladder, skin, and prostate) were not yet considered in those papers (Bednarz *et al.*, 2009; Bednarz *et al.*, 2010). However, this was evaluated by Fontenot *et al.* (2009), who considered primary radiation for IMRT to colon,

bladder, and testes. Eq. (2-6) was also used to obtain equivalent dose to colon from the IMRT treatment.

Figure 2-6 shows organ equivalent doses per therapeutic absorbed dose for three radiation modalities: brachytherapy, IMRT, and proton therapy, whereas numerical data in **Table 2-2** also include 3D-CRT. First, H_T/D_P in organs near the prostate (*e.g.* testes, urinary bladder, and colon) are about a factor of two larger when using IMRT than when using proton therapy. A higher amount of beam time is needed for IMRT to conform absorbed dose to the prostate. In fact, besides results from Fontenot *et al.* for protons, which are based on a passive scanning system, there are other studies by Schneider *et al*. (2006, 2007) that have shown that the probability of secondary cancers could be decreased by a factor of two when using spot-scanned proton therapy instead of IMRT. A spot-scanned system requires fewer beam conformal elements and results in a lower secondary neutron flux than in a passive system.

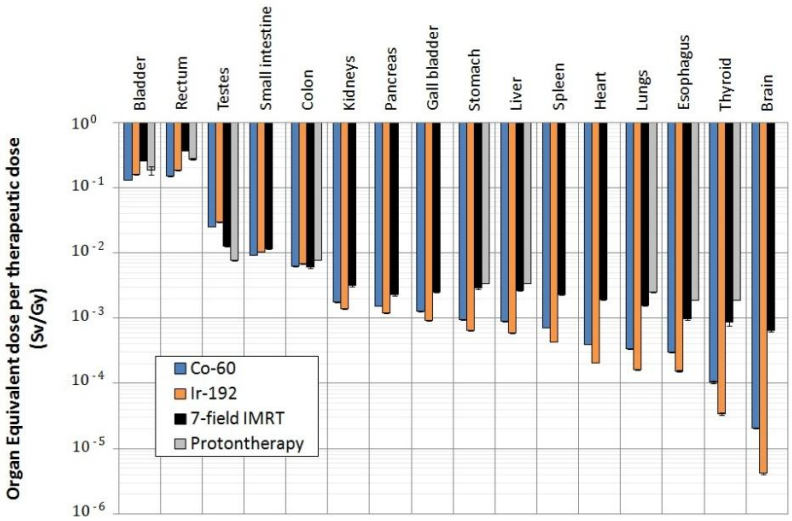

***Figure 2-6**. Organ equivalent dose per therapeutic absorbed dose for different radiation treatments applied to the prostate: brachytherapy (from this work, with ^{60}Co and ^{192}Ir), IMRT (Bednarz et al., 2009; Fontenot et al., 2008), and proton therapy (Fontenot et al., 2008; Fontenot et al., 2009).*

Table 2-2. Equivalent dose per therapeutic absorbed dose (H_T/D_P) for some body organs, comparing brachytherapy results from this work in a heterogeneous phantom and previously reported data for 3D-CRT (ref. (Bednarz et al., 2009; Bednarz et al., 2010)), IMRT (ref. (Fontenot et al., 2008; Bednarz et al., 2009)) and protontherapy (Fontenot et al., 2008; Fontenot et al., 2009). Relative uncertainties ε (type A for brachytherapy (but for those with ε < 0.05%) and the ones published for EBRT) are given in brackets (%) with one decimal unit.

	H_T/D_P (Sv/Gy)									
Organ name	**^{60}Co**		**^{192}Ir**		**Box+boost**		**IMRT**		**Protons**	
Bladder	$1.30x10^{-1}$	(0.1)	$1.60x10^{-1}$	(0.1)	-		$2.57x10^{-1}$		$1.87x10^{-1}$	(14.5)
Rectum	$1.51x10^{-1}$	(0.1)	$1.83x10^{-1}$	(0.1)	-		$3.65x10^{-1}$		$2.75x10^{-1}$	(3.4)
Testes	$2.51x10^{-2}$	(0.3)	$2.94x10^{-2}$	(0.3)	-		$1.26x10^{-2}$		$7.60x10^{-3}$	
Small intestine	$9.24x10^{-3}$	(0.1)	$1.05x10^{-2}$	(0.1)	$2.36x10^{-2}$	(0.4)	$1.16x10^{-2}$	(0.8)	-	
Colon	$6.21x10^{-3}$	(0.1)	$6.78x10^{-3}$	(0.1)	$9.07x10^{-3}$	(1.4)	$6.01x10^{-3}$	(3.2)	$7.80x10^{-3}$	
Kidneys	$1.75x10^{-3}$	(0.3)	$1.40x10^{-3}$	(0.3)	$5.88x10^{-3}$	(2.3)	$3.14x10^{-3}$	(3.7)	-	
Pancreas	$1.53x10^{-3}$	(0.3)	$1.21x10^{-3}$	(0.4)	$3.43x10^{-3}$	(3.8)	$2.27x10^{-3}$	(3.5)	-	
Gall bladder	$1.26x10^{-3}$	(1.0)	$9.33x10^{-4}$	(1.3)	$3.02x10^{-3}$	(3.4)	$2.55x10^{-3}$	(2.5)	-	
Stomach	$9.50x10^{-4}$	(0.5)	$6.40x10^{-4}$	(0.4)	$3.50x10^{-3}$	(1.5)	$2.87x10^{-3}$	(2.9)	$3.40x10^{-3}$	
Liver	$8.88x10^{-4}$	(0.1)	$5.88x10^{-4}$	(0.2)	$3.68x10^{-3}$	(1.1)	$2.65x10^{-3}$	(2.0)	$3.40x10^{-3}$	
Spleen	$7.15x10^{-4}$	(0.6)	$4.32x10^{-4}$	(0.3)	$4.15x10^{-3}$	(2.3)	$2.33x10^{-3}$	(3.6)	-	
Heart	$3.97x10^{-4}$	(0.2)	$2.08x10^{-4}$	(0.3)	$2.14x10^{-3}$	(2.0)	$1.95x10^{-3}$	(3.6)	-	
Lungs	$3.37x10^{-4}$	(0.4)	$1.60x10^{-4}$	(0.4)	$2.76x10^{-3}$	(1.5)	$1.57x10^{-3}$	(2.0)	$2.50x10^{-3}$	
Oesophagus	$3.01x10^{-4}$	(1.8)	$1.55x10^{-4}$	(1.9)	$1.60x10^{-3}$	(10.4)	$9.75x10^{-4}$	(3.2)	$1.90x10^{-3}$	
Thyroid	$1.04x10^{-4}$	(3.7)	$3.46x10^{-5}$	(4.6)	$2.12x10^{-3}$	(17.5)	$8.67x10^{-4}$	(10.8)	$1.90x10^{-3}$	
Brain	$2.08x10^{-5}$	(1.1)	$4.17x10^{-6}$	(2.0)	$1.21x10^{-3}$	(2.4)	$6.50x10^{-4}$	(3.6)	-	
Active bone marrow	$1.26x10^{-2}$	-	$1.62x10^{-2}$	-	$2.28x10^{-3}$	(1.9)	$2.00x10^{-3}$	(4.3)	$6.40x10^{-3}$	
Skin	$3.21x10^{-3}$	-	$3.23x10^{-3}$	(0.1)	-		-		$6.40x10^{-3}$	

When considering HDR brachytherapy with ^{60}Co and ^{192}Ir, equivalent doses (per prescribed absorbed dose) to organs up to the stomach (around 35 cm from the prostate) are the same within an order of magnitude when compared to IMRT and proton therapy. This is consistent with results published more recently by Georg *et al.* (2014), who considered the dose distribution in OARs near the prostate for ten patients planned with: volumetric modulated arc therapy, intensity-modulated proton therapy, intensity-modulated carbon-ion therapy, and LDR and HDR brachytherapy. This study showed that, despite the different EBRT prescription and

fractionation schemes, the high-dose regions of bladder wall and rectal wall were on the same order of magnitude for all radiation modalities, and that BT were clearly superior in terms of bladder wall, rectal wall, and normal tissue sparing, with better values for HDR-BT.

The high doses to organs near the prostate dominate in the calculation of effective doses from the different radiation modalities. Results from **Table 2-2** provide an effective dose of 12 mSv/CGE for proton therapy and 13 mSv/Gy for IMRT, similar to 11.1 mSv/Gy and 13.2 mSv/Gy obtained for both brachytherapy sources. Nevertheless, in the previous figure, only stray radiation is considered for the testes when using IMRT, and so real equivalent dose there is expected to be higher. For all these near organs, there might be variations between patients within an order of magnitude. As an example, Fontenot *et al.* (2009) estimates an H_T/D_P=0.07 Sv/Gy for the colon when using IMRT, a factor ten higher from what it is shown here. In addition, estimation done by Fontenot *et al.* of equivalent doses to skin and bone marrow, which contributes considerably to effective dose, are average values from equivalent dose in the other organs they considered. Furthermore, in our study equivalent dose to bone marrow was overestimated, as explained above, although equivalent doses to rectum and bladder might be under estimated. As a result, effective doses per therapeutic absorbed dose might be similar between all radiation modalities considered in this comparison. These results are estimations for the considered cases and exact conclusions for the nearest organs are patient and equipment dependent.

For the furthest organs, this study has shown that equivalent doses were approximately the same (within an order of magnitude) throughout the whole body (see **Figure 2-6**) for 3D-CRT, proton therapy, and IMRT. For these three modalities, although equivalent doses were smaller for larger distances, given a smaller contribution from scattering radiation, they were within the same order of magnitude. This was not the case when using brachytherapy. As the distance increased, equivalent dose decreased rapidly, going from approximately 1 mSv/Gy in the stomach to 10 μSv/Gy in the brain. For the furthest organs, equivalent doses

given by brachytherapy are between one and two orders of magnitude smaller to those delivered by other radiation modalities. This gives brachytherapy a clear advantage if, for a given prostate absorbed dose, equivalent dose for distant organs needs to be minimized.

HDR monotherapy has been shown to be an excellent treatment modality for prostate carcinoma, although there seems to be no consensus on the optimal dose and fractionation schedule for this radiation technique (Demanes *et al.*, 2014). The longest follow-up for outcomes is with moderate-hypofractionation (4 to 9 fractions), although excellent results are also being reported with ultra-hypofractionation (1 to 3 fractions). Based on a recent literature review performed by Demanes and Ghilezan (2014), one of the most extended protocols for HDR monotherapy is based on 4 fractions, with 9.5 Gy per fraction, thus totaling 38 Gy. Considering this prescribed dose, beyond roughly 25 cm, *i.e.*, beyond the colon, all organs absorb doses below 100 mSv after the complete BT treatment. Therefore, most of the organs of the patients are exposed to low radiation doses.

In this work, probabilities for secondary cancer induction have not been estimated given the low equivalent doses received by organs far from the prostate and given the dose-risk model uncertainties in this dose range (Hall *et al.*, 2004; Candela-Juan *et al.*, 2014). This will be discussed in more detail in **Chapter 3**.

Although this work provides results concerning radiation protection applications in radiotherapy, the presented conclusions are based on certain assumptions. First, the point source was placed in the prostate center. Although it was corrected from empirical clinical data (nomogram) to account for a clinical source with varying dwell positions within the prostate, the source would be closer to an OAR at some positions and would cause some discrepancies with results presented herein for the nearest organs. This variation, however, is lower than an order of magnitude and would only apply to the nearest organs, being negligible for the rest, beyond roughly 10 cm. The aim of this work was to provide a general organ equivalent dose database for this particular treatment, comparing ^{60}Co and

^{192}Ir sources in the same circumstances, bearing in mind that equivalent dose to the closest organs is patient and facility dependent, and so general values for these tissues cannot be established. Hence, the first assumption was not a limitation of the proposed aim. Second, the different radiation treatments have been compared according to equivalent dose per therapeutic absorbed dose. It has not been taken into account that the therapeutic course is generally given in several fractions to take advantage of biological effects like cell repair. The hypothesis made is that cell damage is proportional to overall absorbed dose, without considering some biological effects which are dependent on parameters that could be modality dependent. If this hypothesis is correct, then this work shows an advantage of brachytherapy in comparison to IMRT and proton therapy when considering equivalent doses to the farthest organs. If not, a biological model should be included. However, given that several possible fractionating plans can be applied for the different radiation treatments, with different total prostate absorbed dose in each case, no general conclusions can be extracted. As stated above, comparison herein between the different radiation modalities cannot be considered as representative of all particular cases. Next, when comparing ^{60}Co and ^{192}Ir sources, the same amount of absorbed dose was assumed in both cases to produce the same biological effects, *i.e.*, dependence of biological effects was assumed to be independent of source energy. A more precise estimation would account for radiobiological effectiveness (it was considered as unity in this work) as a function of energy (Reniers *et al.*, 2008). However, this is expected to be a proportionately small correction for these high energy sources that would not change the overall findings. Therefore, after all these considerations, data presented in **Table 2-1** can be considered as representative equivalent doses received by a patient with a body height similar to the reference male phantom, considering however a 30 cm^3 prostate instead of 16.5 cm^3, the latter corresponding to the prostate size of the reference male phantom, which has many variations among people and age.

2.5 Conclusions

A database of organ equivalent doses when applying HDR brachytherapy to the prostate with either ^{60}Co or ^{192}Ir is provided. Making only physical considerations, ^{192}Ir seems to be a better choice than ^{60}Co when considering damage to distant organs, which have to be also considered because of their radiosensitivity, but not to the farthest ones, which are the ones which receive a considerably higher equivalent dose.

Up to around 30 cm, organ variations due to differences between water and soft tissue are negligible. However, for larger distances this is not the case. More variations with an infinite water medium are due to the lack of back-scattering after the skin, which depends on organ positions. Both effects together make that an infinite water volume can be used to obtain organ absorbed doses all over the body considering, however, a higher uncertainty. The latter will be discussed in more detail in **Chapter 4**. Finally, the radiation treatment (considering HDR brachytherapy, IMRT, and proton therapy) to be used if considering organ equivalent doses are patient, treatment, and facility dependent. In any case, as the distance increases, brachytherapy shows a radiation protection advantage over all EBRT techniques.

Chapter 3. TUMOR INDUCTION BY RADIATION DOSES

Most of the content of this chapter was published in the review paper:

Candela-Juan C, Montoro A, Ruiz-Martínez E, Villaescusa JI, Martí-Bonmatí L. *Current knowledge on tumour induction by Computed Tomography should be used carefully*. European Radiology. 24: 649-656 (2014).

Kind permission was granted by the journal to reprint this article as a chapter of this dissertation.

3.1 Introduction

Data on population radiation exposure and advances in the field of radiobiology showed that ionizing radiation could be associated to secondary risks for an individual subject (ICRP, 2007). In particular, cell damage may give place to genetic mutations and even the induction of a tumor.

The dose–effect curve represents the likelihood of inducing a tumor as a function of organ-equivalent dose or effective dose. Graphically, three main areas can be identified in this dose–effect curve (Hall *et al.*, 2004). In the central zone (between around 0.1 Sv and 2.5 Sv) there seems to be a clear linear relationship in which, as the effective dose increases so does the probability of tumor induction, which has been confirmed by numerous studies (Xu *et al.*, 2008). In particular, the Life Span Study of the Japanese atomic bomb survivors of Hiroshima and Nagasaki was the first large enough group used to conduct an epidemiological dose relationship, being the clearest evidence of the linear relationship at intermediate doses. Part of the Japanese population was exposed to this dose range, generally uniform throughout the body and involving different types of radiation particles such as neutrons, alpha particles, and gamma rays.

However, uncertainties in the dose–effect curve do exist at the high and low extreme doses. At high organ equivalent doses (>2.5 Sv), radiation induced cell sterilization, cell repopulation, and proliferation may cause a deviation from a linear dose response (Nguyen *et al.*, 2015). Several studies show that the higher probability of cell death decreases the possibility of inducing a tumor in comparison with the linear extrapolation, although the rate of decline appears to vary between different published data (Hall *et al.*, 2004). Most of the second cancers from radiation therapy appear within the volume irradiated by the primary radiation field (Nguyen *et al.*, 2015), *i.e.*, at high radiation doses. While Boice *et al.* (1985) estimated that 43% of second cancers are developed near the primary field, Dorr and Herrmann (2002) increased this percentage to between 60% and 90%. This

chapter reviews recent estimates of cancer induction from high radiation doses, and their associated uncertainties.

On the other part, at low radiation doses (less than 0.1 Sv) different models have been proposed and observed, as summarized in **Figure 3-1**. One of them is the adaptive response (curve a), in which there is a threshold dose below which no extra risk exists (NCRP, 2001; UNSCEAR, 1994). Uncertainties in past epidemiological data of irradiation exposures within the diagnostic dose range did not rule out a possible threshold dose, which might be within the range of 10 to 60 mSv (Pierce *et al.*, 2000; Hall *et al.*, 2004; Pauwels *et al.*, 2011). Even more, some researchers have indicated that very low doses may produce hormesis (Cuttler *et al.*, 2009), *i.e.* they stimulate our immunological system such that they inhibit effects of higher doses later received (curve b). This effect has also been questioned (Wall *et al.*, 2006). Other experiments have shown the so-called bystander effect, in which not only the irradiated cells are affected but also others near them, hence increasing the probability of cancer induction (curve c). Based on theoretical studies, the bystander effect is also predicted to be present at higher doses (Nikjoo *et al.*, 2003; Rzeszowska-Wolny *et al.*, 2009). Finally, because of its simplicity, reasonability, and conservative approach, international committees such as the ICRP and the NCRP, among others, recommended extrapolating the linear relationship to the lowest dose range (curve d in **Figure 3-1**). The latter term is known as the linear no-threshold (LNT) model and its assumption implies that even the least amount of absorbed dose can lead to an induced tumor or, put in another way, a radiation-induced tumor may develop from a single hit to a single cell (microdosimetric argument (Rossi *et al.*, 1972; Brenner *et al.*, 2006). Brenner and Sachs (2006) argued that, if the action in a single cell dominates over intercellular effects, then the linear model is appropriate. However, the microdosimetric argument has also been criticized (Tubiana, 2005; Tubiana *et al.*, 2006).

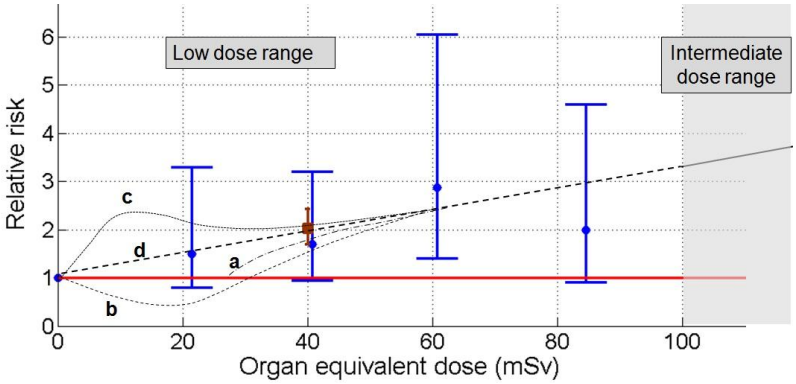

Figure 3-1. *Schematic representation of different possible models of radiation-induced cancers at low radiation doses: a) adaptive response with threshold dose, b) hormesis, c) bystander effect and d) linear-no threshold. The horizontal line expresses no over or under risk. Data points and their 95% confidence intervals correspond to the relative risks of brain tumour induction as a function of brain dose, taken from recent epidemiological studies with paediatric CTs performed in the UK (Pearce et al., 2012) (in blue) and Australia (*Mathews *et al.*, 2013) *(in red), considering a 5-year exclusion period.*

Chapter 2 has shown that most of the organs exposed during a brachytherapy treatment receive low radiation doses (< 0.1 Sv). For this reason, and because diagnostic medical exposures, which contribute significantly to the overall collective dose, give doses to patients within this low dose range, we will focus a notable part of this chapter to risks due to radiation exposures which imply less than 0.1 Sv. Current knowledge on the probability that such absorbed doses can induce tumor is under discussion among the scientific community. This chapter reviews the methods used in the literature to estimate the likelihood that low radiation doses induce cancer and summarizes the current quantitative estimates. It is also intended to highlight their main sources of uncertainty. Based on all information reported, it is discussed whether the linear model that relates probability of cancer induction

and dose can be considered to be validated. Finally, some recommendations about the appropriate use of current knowledge on this topic are stated.

3.2 Factors that affect the probability of cancer induction

Although the probability that ionizing radiation may induce a tumor has been shown to be dose-dependent (see **Figure 3-1**), there are some other factors that also affect the "intensity" of the dose–effect curve:

1) Different biological effects appear when the same amount of energy is either deposited in several fractions or continuously during a long or short period of time. In order to take this into account, the dose and dose–rate reduction factor (DDREF) were defined. International committees recommended extrapolation of known data at intermediate doses (and with a high-dose-rate irradiation) to the low-dose range by dividing the linear estimations by a DDREF within the range of 1.1–2.3 (BEIR, 2006).

2) Different organs/tissues have different sensitivity to ionizing radiation. Hence, the probability of inducing a tumor is dependent on the organs that are irradiated. As a quantitative example, for a male patient receiving a single dose of 0.1 Sv to the colon and the liver, the lifetime attributable risk (LAR) of cancer incidence (probability that an individual develops a cancer because of the exposure) is 0.125% and 0.022%, respectively (BEIR, 2006). It is reasonable to think that this organ-dependency can be extrapolated to an even lower dose.

3) The gender of the irradiated person has also been observed to influence the "intensity" of the dose–effect curve. The male to female LAR ratio depends on each specific organ and ranges between around 0.2 (female more sensitive in the case of the thyroid) and 2.2 (male more sensitive in the case of the liver) (BEIR, 2006).

4) Significant variations are also associated with age at exposure. Particularly, children have been a group considered to be of greatest concern. First, they are

more radiosensitive than adults (Pierce *et al.*, 1996; Brenner, 2002) as they have a higher fraction of cells in full division processes where genetic changes may lead to tumor induction. Second, they will have more time to express any stochastic effect in relation to older persons. The excess relative risk (ERR) of cancer incidence (rate of disease in an exposed population divided by the rate of disease in an unexposed population minus 1) after 40 years of a 1 Sv exposure is around a factor of 3 higher when the age at exposure is 10 compared with a person older than 30 years-old (BEIR, 2006). The ERR ratio progressively increases as the age at exposure decreases. A variation of cancer induction with age at exposure is also expected in the low dose range used in medical imaging.

5) As in a brachytherapy treatment, medical imaging examinations involve a heterogeneous dose distribution. Differences of a factor of 2 between the mean and maximum dose received by the lung in chest computed tomography (CT) examination have been reported using Monte Carlo methods (Samei *et al.*, 2013). This underscores the need for a systematic study with a risk model that takes into account dose heterogeneities in the excess relative risk and whether the mean or maximum dose value should be used.

6) Finally, given that many cancers have different baseline risks in different countries, it might be possible that the ERR is also dependent on environmental or sociological factors, and so data from the Japanese population cannot be extrapolated worldwide (BEIR, 2006).

3.3 Estimation of cancer risk at high radiation doses

In general, two different procedures are being used nowadays to estimate the probability that a given radiation exposure in excess of 2.5 Gy may induce a tumor: phenomenological risk models and epidemiological studies.

Phenomenological risk models based on fitting parameters have been applied to estimate the risk of inducing a tumor in organs inside the primary radiation field,

i.e., at doses in excess of 2.5 Gy. Recent studies have applied a model developed by Schneider (2009), which is based on the linear-quadratic formula, to estimate the outcome of different treatment modalities (Nguyen *et al.*, 2015). Linear, linear-exponential and plateau models have been also used (Abo-Madyan *et al.*, 2014). As an example, Paganetti *et al.* (2012) evaluated the dose distribution to OARs located inside the primary radiation field, for pediatric phantoms planned to be irradiated with IMRT and proton therapy. LARs were then evaluated using risk models, and it was found to be up to 2.7% for a 4 year old optic glioma patient treated with IMRT, decreasing a factor of 2 for a 14 year old patient. In all cases considered in that study, the estimated risk from proton therapy was up to a factor of 10 lower. Similar results have been published in other studies (Moteabbed *et al.*, 2014). A review study by Xu *et al.* (2008) showed that the cumulative risk for the development of second cancers has been estimated as ranging from 5% to 12% over a 25 year follow-up interval, although there exists a high dispersion of data.

The model parameters have been determined with limited data and, therefore, uncertainties will limit the model predictions. Nguyen *et al.* (2015) have recently estimated that the uncertainties associated with model predictions are higher than 100%. This is a lower limit to the overall uncertainty because the uncertainty introduced by different fractionations was not considered, neither the uncertainty in dose delivered to OAR. As concluded in this uncertainty study, the large magnitude of the uncertainty implies that, currently, it might not be feasible to reliably predict cancer risks based on treatment plan information and phenomenological risk models.

On the other hand, many epidemiological studies have been also performed on second cancer induction after radiation therapy. However, they focused on a typically narrow dose range, making the transfer of the reported risk to other doses difficult (Nguyen *et al.*, 2015).

In relation with **Chapter 2**, Murray *et al.* (2014) have recently performed a literature review on second primary cancers after radiation for prostate cancer. It

was concluded that the risk was below 0.5% over all durations of follow-up when considering older radiation techniques. About more modern RT techniques such as HDR BT, it was faced that there are not enough clinical data to extract firm conclusions. Limited evidence is encouraging as no excess risks have been found, although it may be likely that long follow-up might show a small increase.

3.4 Estimation of cancer risk at low radiation doses

Two methodological procedures are being used nowadays to estimate the probability that a given radiation exposure may induce a tumor: a) risk coefficients that linearly relate equivalent dose to probability of tumor induction, and b) epidemiological data assessing the ratio of tumor incidence between population exposed and unexposed to ionizing radiation.

3.4.1 Risk coefficients

Radiation risk models have been developed in the last decade by international bodies such as the BEIR VII committee (BEIR, 2006). They are extrapolations of the LNT model for all doses lower than 2.5 Sv, based on data from the atomic bomb survivors and other medical studies in animals and in vitro. This committee provides for several organs the risk coefficients for estimating lifetime risks of cancer incidence and mortality, which depend on the dose rate, gender and age of the exposed person. If multiplied by the organ-equivalent dose, these coefficients provide the probability of cancer induction. Of relevance, risk estimations based on effective doses are clearly obsolete (Brenner *et al.*, 2008; HPA, 2011; Calandrino *et al.*, 2012; Ivanov *et al.*, 2012; Ivanov *et al.*, 2013). Effective dose is the sum of organ equivalent doses weighted by tissue-specific factors (ICRP, 2007). These age-independent factors are based on a subjective mix of different endpoints of cancer mortality and incidence, life shortening, and hereditary risk. In addition, those endpoints have different significant age

dependencies not considered by the weighting factors and, thus, effective dose has high associated uncertainties when applied to a specific patient different than the reference male or female phantoms (Martin, 2007).

Other international organizations that review radiation risks are the United Nations Scientific Committee on the Effects of Atomic Radiation (UNSCEAR), the NCRP, and the ICRP (ICRP, 2007). Risks from CTs were already estimated in children through risk coefficients more than a decade ago (Brenner *et al.*, 2001), and are still used nowadays with the same aim (Berrington *et al.*, 2012; Perisinakis *et al.*, 2012; Miglioretti *et al.*, 2013). The BEIR VII model has been also applied to estimate cancer risks from radiotherapy. Bednarz *et al.* (2010) used the linear relationship to estimate the risk of second primary cancer in out-of-field organs receiving less than 0.1 Sv after 3D-CRT and IMRT applied to the prostate. They concluded that the probabilities for secondary cancer induction for the considered organs were about an order of magnitude lower than the baseline risks for those organs. On another study, Mazonaquis *et al.* (2014) evaluated through MC simulations the radiation dose to all organs that were out of the primary beam of a testicular seminoma treatment, and used gender- and organ-specific risk coefficients to estimate the risk of second primary cancer induction. It was concluded that the lifetime intrinsic risk of developing thyroid, lung, bladder, prostate, and esophageal cancer was increased by (0.1-1.4)%, (0.4-1.1)%, (2.5-5.4)%, (0.2-0.4)%, and (6.4-9.2)%, respectively, depending upon the patient age at exposure and the field size employed. For the other organs considered the increased risk was nearly negligible. Similar studies were performed by Berris *et al.* (2014) and by Kourinou *et al.* (2013) considering the treatment of heterotopic ossification and head and neck lesions, respectively.

As noted by Fletcher *et al.* (2013), it can be concluded from the BEIR VII report that the available evidence for the use of the LNT model at low radiation doses has not been statistically significantly better for predicting cancer than other methods based on a threshold dose owing to high background incidence cases (ICRP, 2007; Wall *et al.*, 2006). Even international committees were critical with

their own coefficients and pointed out several sources of uncertainty related to: limitations in the epidemiological data; extrapolating the data to low doses and dose rates (appropriate choice of DDREF); and transporting results from Japanese survivors to any other country (BEIR, 2006). Of importance, there are large and clear differences between atomic bomb survivors and people exposed to radiotherapy treatments. The first ones were exposed to a uniform radiation dosage throughout the whole body, with several types of radiation particles (including neutrons), whereas patients exposed to brachytherapy receive a heterogeneous and lower dose throughout most of his body. Thus, current methods used to estimate probabilities within the low dose range may be scientifically questionable *(*Pauwels *et al.*, 2011). This is why the Health Physics Society recommended that, below effective doses of 50 mSv, no quantitative estimations of health risks should be made with risk coefficients (HPS, 2004; Fletcher *et al.*, 2013).

3.4.2 Recent epidemiological data

Computed tomography (CT), which was invented in 1972, makes nowadays the biggest contribution to the collective dose (being from 46% up to 80% (Aroua *et al.*, 2013)) of a population exposed to x-rays imaging techniques. Typical median effective doses from CT examinations are 1.2 mSv for a head CT, 4.1 mSv for a chest CT and 7.7 mSv for an abdominal CT (Teeuwisse *et al.*, 2007), although variations within the same order of magnitude might be found between different x-ray acquisition techniques and equipment models. Thus, CT exposure provides the most complete database that can be used to relate cancer induction and organ equivalent dose at low radiation doses, and so it was been analyzed in detail in this chapter.

Two independent epidemiological studies that used data from a large sample of children exposed to CT have recently been published. The first one was conducted in the United Kingdom by Pearce and colleagues (Pearce *et al.*, 2012; Kim *et al.*, 2012), taking data from nearly 180,000 teenagers under age 22 at the time of the examination (between 1985 and 2002). Doses to brain and red bone

marrow were roughly estimated with typical x-ray acquisition techniques combined with MC simulations. In addition, given that up to 2001 protocols used for children were usually the same than for adults, the authors of the study considered that before that year the dose children received was approximately 2–3 times higher. Exclusion periods of 2 years for leukemia and 5 years for brain tumor were considered, meaning that cancers diagnosed up to that exclusion period since the CT was undertaken were considered not to be due to the CT. Results suggest a LNT relationship between the absorbed dose in the brain (see **Figure 3-1**) or bone marrow, and the probability of inducing a brain tumor or leukemia, respectively. These are the two types of tumors that are expected to appear earlier in irradiated children, given the higher sensitivity of bone marrow and brain (UNSCEAR, 2010).

From the previous epidemiological study, it was concluded that for children in their first decade of life one brain tumor and one case of leukemia would be induced every 10,000 CTs with a dose close to 10 mSv per CT in the first decade after the study (Pearce *et al.*, 2012). Even more, 10 years after the CT exposure, 30% and 90% of final cases of leukemia and brain tumor, respectively, have yet not appeared (Ron *et al.*, 1988; Preston *et al.*, 1994). Therefore, the risk of inducing leukemia over a lifetime is 1 in every 7500 CTs in children explored in their first decade of life, and to infer a brain tumor is 1 per 1,000 CTs (Brenner *et al.*, 2012b). These values, from epidemiological studies, are roughly similar in magnitude to those inferred (Brenner *et al.*, 2001) from a linear extrapolation of the LNT model.

On the other hand, the most recent and massive study conducted in Australia by Mathews and colleagues (Mathews *et al.*, 2013) evaluated the cancer incidence in over 680,000 young people (0 to 19 years) exposed to CT and compared with the baseline risk for the same age range of a cohort of over 10 million unexposed persons. Radiation exposures were carried out between 1985 and 2005, and exposed children were followed for at least 10 years, up to 2007. In this case, not only leukemia and brain tumors were considered, but also all other solid tumors. Average effective doses and average organ absorbed doses were estimated for each CT category, each site and year of CT, and each age. As in the previous study by

Pearce et al, doses before 2001 were rescaled. The Australian epidemiological study detected an increase in cancer incidence of 24% in young people exposed to a single CT, considering a 1-year exclusion period. If the exclusion period is considered to be 5 years, the increase would be 21%. Average effective doses of around 4.5 mSv were considered. If, instead, 2 mSv are given (as usually happens with current equipment and imaging techniques), 1 excess cancer per 4000 head CTs would be radiation-induced (Sodickson, 2013). This study "generally" supports the linear-no-threshold dose-response model, and roughly matches attributable risks predicted by the BEIR report (BEIR, 2006) and by the epidemiological study by Pearce *et al.* (2012) (see **Figure 3-1**).

3.4.3 Analysis of the situation

Epidemiological data taken by Pearce and colleagues in the United Kingdom and, more recently, by Mathews and colleagues in Australia, constitute important steps in the difficult path of modeling the development of radiation-induced tumors at low doses. It is important to note that results from cancer risk coefficients (with high uncertainties already discussed earlier) and from both studies roughly agree for pediatric patients. Can we then consider the linear model at low radiation doses to be validated with no threshold dose? Some authors have answered yes (Brenner *et al.*, 2012b), but precautions should be taken given the following arguments:

1) Acquisition protocols and, consequently, doses assigned to individual exposures were estimations based on national surveys, but did not consider the exact techniques used in different hospitals from which data were taken, neither physical constitution of each patient. The Smith–Bindman group (2009) found a mean 13-fold variation between the highest and lowest dose given by different hospitals that performed the same study. In addition, no registries of repeated exposures exist for the people considered in the recent epidemiological studies (Mathews *et al.*, 2013), which also increase uncertainty in dose estimation. The low

magnitude of cancer induction makes necessary a more accurate evaluation of organ doses, which is still lacked. Guidance for developing a harmonized system that allows intercomparability has been provided (ECRP, 2008) and the capture of patient-specific dosimetry in future epidemiological studies will surely improve the validation of the model (Sodickson, 2013; Smith-Bindman *et al.*, 2009). With this aim, the IAEA launched in 2006 a Smart Card project, which would allow personal recording of all expositions to ionizing radiation in medical imaging (Rehani *et al.*, 2009; 2011).

2) It is difficult to know whether a tumor has been radiation-induced or, on the contrary, the CT was performed because there already was a suspicion of its presence. If the second option applies, at least partially, risk estimations from epidemiological studies would be reduced (Pearce *et al.*, 2012; Mathews *et al.*, 2013), although reverse causation cannot explain all the cancer excess observed (Sodickson, 2013). The appropriate choice of the exclusion period might be considered as an intrinsic uncertainty of epidemiological studies on this difficult task.

3) Relative uncertainties in the risks derived from the epidemiological studies are still large (statistical uncertainty) (see **Figure 3-1**), making feasible other adjustments of the values aside from the linear fitting (AAPM, 2013).

Thus, there are several biases that make us to be cautious before definitely accepting the LNT model within the CT dose-range. Independently of the last two arguments, the linear fit has been shown to be preferable according to a statistical analysis of the epidemiological data (Mathews *et al.*, 2013). However, as far as we know, it has not been studied how the high dose uncertainty in each individual patient may influence this analysis.

Also, a deep literature review of studies concerning radiation therapy and cancer risks for organs receiving low radiation doses was published by Xu *et al.* (2008). It was concluded that many of the past dosimetry studies were based on inconsistent and sometimes confusing dose quantities. Thus, a systematic dosimetry

methodology for quantifying secondary organ absorbed doses needs to be developed in the future based on MC simulations.

If current estimations of radiation-induced tumors by medical imaging exposures are correct, should they really be a concern? The probability of inducing a brain tumor after a single 10 mSv exposure has been estimated to be ~0.1%, which is clearly within the background level produced by environmental and physiological aspects (Fletcher *et al.*, 2013). As an example, in some situations the increase in cancer risk due to a higher concentration of radioactive radon is estimated to be 0.3%. If all cancer types and CT protocols were considered, a single CT in children would increase their baseline risk probability (~0.2% in children up to 14 years old (Stiller, 2007)) by around 20% according to the latest epidemiological study. This relative number may seem large, but it has to be noted that the baseline incidence of cancer in children and teenagers is very small, and so this increase just makes it slightly less small (Sodickson, 2013). In addition, doses are continuously reduced and they can now be up to 2–5 times lower than those considered in the epidemiological studies (AAPM, 2012). In adults, who represent the largest proportion of patients with CT examinations, the probability of inducing a tumor is even smaller. Thus, data provided in this work corresponds to the worst scenario in medical imaging.

Based on the reviewed information of this work, some recommendations may be useful for CT examinations (some of these may be applied to brachytherapy treatments as well), as stated by different authors:

1) Prediction of the absolute number of tumors that will be induced in a large amount of the population exposed to ionizing radiation should be avoided as it would have a great and unknown absolute uncertainty (UNSCEAR, 2012). In addition, it has been estimated that about 10% of the total effective dose given in medical imaging is received by cancer patients (Brix *et al.*, 2009), who have a reduced life expectancy. Therefore, a considerable fraction of the dose is ineffective from a radiobiological point of view (Eschner *et al.*, 2010).

2) Always reemphasize the great benefits that a CT examination or a brachytherapy treatment may provide to an individual patient in personalized medicine (AAPM, 2012). In a quite timely fashion, the International Organization for Medical Physics states that predictions of radiation-induced cancers should be accompanied by estimates of reductions in mortality and patient morbidity (Hendee, 2013).

3) For CTs, because the estimated cancer risks are near the background level, no attempts at reducing the radiation dose should be made if image quality is likely to be reduced to a point where accurate diagnosis is compromised or not performing a CT examination if its information may be relevant for the patient's condition (Eisenberg *et al.*, 2012).

4) The scientific and popular press has to avoid exploiting the sensational nature of this topic without a critical analysis (Hendee *et al.*, 2012), and medical specialists should be careful and not worry patients at the time of the exposure. Appropriate information should be given to patients to improve autonomy (Recchia *et al.*, 2013).

5) Despite the extremely low magnitude of the risk, the increased incidence could be real according to the latest epidemiological studies. Pediatric CT protocols should be always standardized and acquired with dose reduction algorithms. The As Low As Reasonably Achievable (ALARA) principle must be considered when performing a CT examination and radiologists should understand dosimetric magnitudes (Durand *et al.*, 2012) and be consistent when approving a CT examination (Pandharipande *et al.*, 2013). It has been shown that around 30% of all CT examinations conducted on patients younger than 35 years were not properly justified, being unnecessary or replaceable by other imaging procedures like magnetic resonance imaging (Oikarinen *et al.*, 2009). In another study of Brenner, it was estimated that 20 to 40% of CT scans could have been avoided if decision guidelines for mild traumatic brain injury were followed (Brenner *et al.*, 2012a).

3.5 Conclusions

Several estimations of the probability that high and low radiation doses induce cancer have been made in the past, either through risk models and fitting parameters or through epidemiological studies. The uncertainties associated with model predictions at radiation doses above 2.5 Sv are higher than 100%, and it might not be feasible to reliably predict cancer risks based on treatment plan information. For the low dose range (<0.1 Sv), recent epidemiological studies undergone in United Kingdom and Australia are roughly consistent with each other and with risk coefficients. Some authors have considered this to be the ultimate prove of the validity of the LNT model at low radiation doses. However, because of some dosimetric uncertainties and the proximity of the risk estimates to the background level, we should still be cautious and wait for possible incoming new results, with even higher and more accurate data. The latter is addressed in more detail in **Chapter 4**. Estimated risks of a low radiation exposure, if existent, are very low even for pediatric patients.

Therefore, based on many reviewed papers on this topic, several recommendations may be synthesized. Prediction of the number of tumors that will be induced in population exposed to ionizing radiation should be avoided or, if given, it should be accompanied by a realistic evaluation of its uncertainty and of the advantages of the medical exposures. Otherwise they may be used inappropriately and have a negative impact. For the particular case of CTs, it is not justified that society panics, neither the medical or scientific community has to obsess on reducing doses even more if that compromises clinical image quality, as long as we are all consistent with ALARA's principle.

Chapter 4. DOSIMETRIC CHARACTERIZATION OF ^{226}RA SOURCES

Most of the content of this chapter is included in the original research paper:

Candela-Juan C, Karlsson M, Lundell M, Ballester F, Carlsson Tedgren A. *Dosimetric characterization of two radium sources for retrospective dosimetry studies*. (Under review by Medical Physics)

Kind permission was granted by the journal to reprint this article (if accepted) as a chapter of this dissertation.

4.1 Introduction

From the discovery of radium in the late 19th century and well into the 20th century, ^{226}Ra was the most used radionuclide for brachytherapy (Gerbaulet *et al.*, 1998; Williamson, 2006). Radium pioneers investigated the therapeutic use of this radionuclide in numerous diseases, with various clinical outcomes and sometimes leading to tissue necrosis or infections due to overdosage (Dutreix *et al.*, 1998). The source filtration with gold or platinum improved radium therapy by effectively stopping the β-rays and low-energy photons, preventing tissue complications (Aronowitz, 2002). When radium became more accessible, methodologies were developed that propagated the spread of radium therapy. Radium sources for brachytherapy have been reported in many different models, often as tubes or needles, containing 0.5 to 20 mg of radium and filtrated with 0.5 to 2.0 mm of Pt (with possible addition of silver or gold) (Fitzwilliams, 1930; Smocovitis, 1966). In general, the tubes were wider and longer than needles.

The use of radium was associated with radiation protection problems due to the relative high-energy photons emitted (mean energy approximately 800 keV). In addition, helium and ^{222}Rn produced by α-decay increased the pressure in the sealed sources, eventually leading to gaseous ^{222}Rn-leaks (Villforth, 1964; Hilaris, 1975), causing a wide contamination. These drawbacks made the use of radium to gradually be replaced with artificially produced radionuclides, such as ^{60}Co and ^{137}Cs (Myers, 1948; Brucer, 1952). ^{226}Ra remained the most used radionuclide for brachytherapy into the late 20th century (Hilaris, 1975; Boice *et al.*, 1988). Experiences from radium therapy have left a legacy which has effectively influenced methods of modern brachytherapy.

Radium was used extensively in intracavitary, gynecological applications and was also commonly applied to treat many other types of cancer. Other fields of application include treatment of skin hemangioma in early childhood, using tubes and needles of ^{226}Ra, which was performed between 1920 and 1959 at Radiumhemmet (Stockholm, Sweden) (Lundell *et al.*, 1994; 1995; 1999), between

1930 and 1965 at Sahlgrenska University Hospital (Gothenburg, Sweden) (Lindberg *et al.*, 1995) and between 1940 and 1973 at Institut Gustave-Roussy (Paris, France) (Dondon *et al.*, 2004). As recently noted by the UNSCEAR (2013) committee, the hemangioma cohort is of current interest in the search for improved knowledge on dose-response relationships for cancer induction and other late effects due to exposure to ionizing radiation in early childhood. Sweden has long held a complete registry on cancer incidence coupled to unique citizen ID numbers. Together with detailed knowledge about the children that underwent ^{226}Ra treatment, these data are of interest to use in research on late effects due to radiation exposure in early childhood.

Retrospective risk assessments of ionizing radiation demand, among other information, high-quality dosimetry data. Previous dose estimations for the hemangioma cohort at Karolinska University Hospital were based on measurements with thermoluminescent dosimeters (TLD) in an anthropomorphic phantom using the original sources, and by Sidos (Operating Instructions SIDOS/EVADOS/SOMADOS, SIDOS-BRACHY, Siemens, 1984) (Visser, 1989; Feroldi *et al.*, 1992), an early computerized dose planning system (Lundell *et al.*, 1990; 1994). Today, the original sources have been decommissioned, leaving only drawings and specifications of the sources. Having the dosimetry data in a modern format would enable its use with modern planning systems and open up for further individualization of patient doses and improved uncertainty estimations.

The aim of this study was to facilitate and investigate ways to allow flexible and as accurate as possible recalculation of absorbed doses from old, decommissioned radiation sources for retrospective studies. Having data in the format recommended by AAPM Task group 43 (TG-43) (Nath *et al.*, 1995; Rivard *et al.*, 2004) opens for implementation in modern planning systems and hence for effective recalculation and further individualization of absorbed doses for various scenarios of interest. The absorbed dose distribution around two of the most used radium sources at Radiumhemmet was characterized using MC simulations. The accuracy of TG-43 dosimetry parameters for surface brachytherapy with several

needles is evaluated, as well as compared with previously reported dose measurements with TLDs. Finally, because absorbed doses to organs far from the treatment volume are also required by epidemiologists, and because TG-43 parameters are calculated up to about 15 cm from the implant, the fitting parameters of an analytical function valid up to about 60 cm, which was previously used for ^{60}Co, ^{192}Ir and ^{137}Cs sources (Venselaar *et al.*, 1996), are provided here for a ^{226}Ra source.

4.2 Materials and methods

4.2.1 Description of sources

The radium sources used at the Radiumhemmet were constructed in 1925. The sources were of two types, the tube and the needle, containing 8 mg and 10 mg of ^{226}Ra, respectively. Both source types consisted of an active volume of radium sulphate and barium sulphate, surrounded by an internal capsule of gold and an external capsule of platinum. The radioactivity is assumed to have been homogeneously distributed in the radium compound. Both sources were cylindrically symmetric and the needle had a conical tip. Cross-sectional drawings of the radium tube and the needle are shown in **Figure 4-1**. Values for the elemental compositions denoted in this figure are presented in **Table 4-1**. Geometries and material compositions were based on preserved drawings and commissioning protocols of the sources from 1925. For liquid water and air, elemental compositions were taken from the updated recommendations by the AAPM Task Group 43 (Rivard *et al.*, 2004).

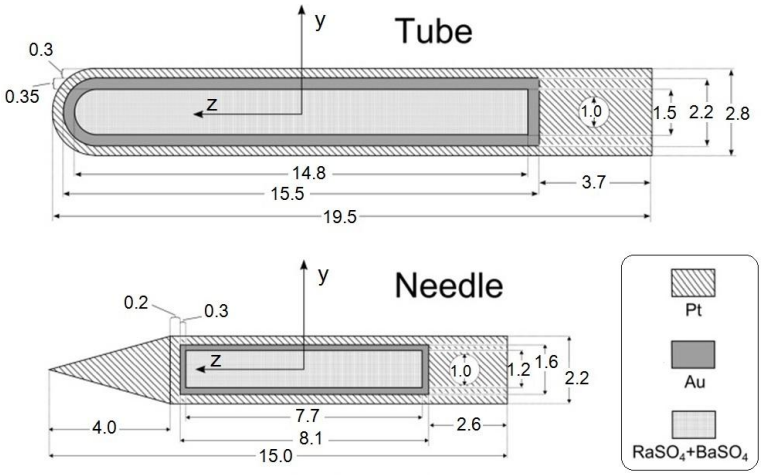

***Figure 4-1**. Cross-sectional drawing of the 8 mg radium tube and the 10 mg radium needle. The white circle at the right side of both sources is a cylindrical air cavity. All distances are given in mm.*

***Table 4-1**. Elemental compositions and mass densities for the materials used.*

Material	Element	% by weight	Mass density (g/cm^3)
Gold	Au	100	19.32
Platinum	Pt	100	21.45
$RaSO_4$+$BaSO_4$	S	10.03	5.74
	O	20.02	
	Ba	1.18	
	Ra	68.77	
Dry air (0% humidity)	C	0.01	0.00119
	N	75.53	
	O	23.18	
	Ar	1.28	
Liquid water	H	11.19	0.998
	O	88.81	
Pyrex glass	B	4.01	2.230
	O	53.96	
	Na	2.82	
	Al	1.16	
	Si	37.72	
	K	0.33	

4.2.2 Decay scheme of the radioactive source

The sources contain ^{226}Ra and its radioactive daughter nuclides, as observed in the decay scheme shown in **Figure 4-2**. ^{226}Ra is the sixth member of the uranium series. With its decay, a chain of daughter radionuclides will follow to the stable ^{206}Pb. In total, the decay chain comprises emission of α-, β- and γ-rays, internal conversion electrons, Auger electrons and characteristic x-rays.

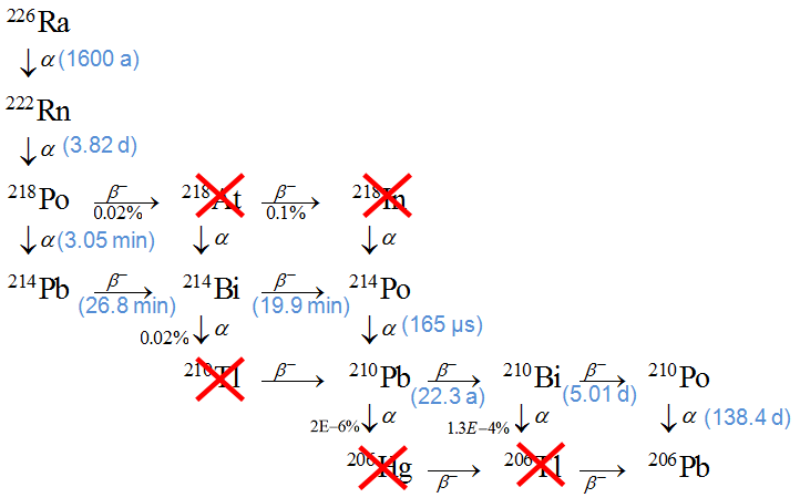

***Figure 4-2**. Decay scheme of a ^{226}Ra source, adapted from a document by Laboratoire National Henri Becquerel, Le radium 226 et ses descendents: Tables et commentaries. The crossed radionuclides can be neglected due to their low yield (< 0.1%). Only the half-lives of those transitions considered in this study are included in the figure.*

The contribution of ^{218}At, ^{218}Rn, ^{210}Tl, ^{206}Hg and ^{206}Tl to the overall absorbed dose can be neglected due to their very low yield (< 0.1%). Thus, the considered decay scheme includes nine radionuclides, with their half-lives differing in orders of magnitude. In order to determine the overall absorbed dose, it is necessary to

know the activity of each radionuclide at the treatment time. Bateman equations (Bateman, 1910) provide the solution to this problem. These were programmed in MATLAB 7.10.0 (R2010a) (The MathWorks Inc., Massachusetts, US) such that the number of radionuclides present in the source and the activity of each one was known as a function of elapsed time.

4.2.3 AAPM Task group 43 dosimetry formalism

The absorbed dose calculation formalism recommended in the updated report of AAPM Task Group 43 (TG-43U1) (Rivard *et al.*, 2004) is based on the parameters air-kerma strength S_K, dose-rate constant Λ, radial dose function $g_L(r)$, geometry function $G_L(r,\theta)$ and anisotropy function $F(r,\theta)$. In the general 2D TG-43 formalism, using the line source approximation, the absorbed dose rate in a point at the radial distance r and polar angle θ relative to the longitudinal axis of the source, can be expressed as:

$$\dot{D}(r,\theta) = S_k \Lambda \frac{G_L(r,\theta)}{G_L(r_0,\theta_0)} g_L(r) F(r,\theta) \qquad \textbf{(4-1)}$$

where the reference distance is $r_0 = 1$ cm and reference polar angle is $\theta_0 = \pi/2$. The TG-43 formalism models the dose distribution in water around a single source. Further discussion on the formalism can be found in the reports of AAPM Task Group 43 (Nath *et al.*, 1995; Rivard *et al.*, 2004).

4.2.4 Monte Carlo methodology for the derivation of TG-43 parameters

The tube and the needle were modeled with GEANT4 (Agostinelli *et al.*, 2003) and MCNP5 (Briesmeister *et al.*, 2004). This study adheres to the latest

recommendations from the High Energy Brachytherapy Source Dosimetry (HEBD) working group (Perez-Calatayud *et al.*, 2012). The relatively high mean energy of photons involved in the decay scheme of ^{226}Ra made it necessary to consider in detail the secondary electrons that exit the source (Ballester *et al.*, 2009).

Absorbed dose in water was obtained with the sources immersed in the center of a water sphere R=50 cm in radius, with the origin of coordinates at the center of the radioactive pellet, with the z-axis being the longitudinal axis of the source and the y-axis the transversal one (see **Figure 4-1**). It was scored in $D(y,z)$ and $D(r,\theta)$ coordinates, $\theta = 0$ corresponding to the needle tip. This scoring allowed obtaining the radial dose and the anisotropy functions, as required in TG-43 formalism. Doses were scored in histograms, with a bin width of 0.5 mm for coordinates y, z, and r, and 1° for θ.

The air-kerma strength per unit activity, $S_K / A \equiv s_K$, was estimated with the sources positioned in vacuum scoring collisional kerma over a cylindrical cell filled with air of height and thickness 0.10 cm at a distance of r=10 cm in a plane perpendicular to the source axis passing by the origin of coordinates. The recommended air composition for dry air from the HEBD report was used (Perez-Calatayud *et al.*, 2012).

The default cutoff energy of 1 keV was used for both photons and electrons in all simulations except for S_K estimation, where the cutoff was 10 keV for both of them (Perez-Calatayud *et al.*, 2012).

4.2.4.1 GEANT4

The low energy package PENELOPE included in GEANT4 v.9.4.p02 was used to track electromagnetic processes. All radioactive ions can be simulated in GEANT4 using the G4Physics package G4RadioactiveDecay v.0.b.4. By default, once a ^{226}Ra nuclide is released, it decays until ^{206}Pb. Hence, for each ^{226}Ra atom,

approximately one radioactive daughter of each of the considered types would be created. However, given the different half-lives, each daughter product has a different number of disintegrations per unit of time, at different time periods. Therefore, each radioactive nuclide was decided to be simulated separately. For example, when a ^{226}Ra nuclide was created, it automatically disintegrated via alpha emission to ^{222}Rn. When the daughter nuclide (in this example, the ^{222}Rn) had zero excitation energy, it was halted. Then, another independent simulation starting with ^{222}Rn was performed, saving the results in a different file. This was done for each of the nine radionuclides considered in the decay chain of ^{226}Ra, and after that, results were weighted and summed according to the activities given by Bateman equations, which are time dependent, *i.e.*:

$$\dot{D}(r,\theta,t) = \sum_{i=1}^{9} A_i(t)\, \dot{D}_i(r,\theta) \qquad \textbf{(4-2)}$$

where $i=1$ corresponds to ^{226}Ra, $i=2$ to ^{222}Rn, $i=3$ to ^{218}Po, $i=4$ to ^{214}Pb, $i=5$ to ^{214}Bi, $i=6$ to ^{214}Po, $i=7$ to ^{210}Pb, $i=8$ to ^{210}Bi, and $i=9$ to ^{210}Po. This enabled that dosimetric data could be obtained either in secular equilibrium or at any previous state.

All secondary particles generated by the G4RadioactiveDecay package (recoil nuclei, gammas, electrons, and alphas) were tracked, except neutrinos coming from beta decays, which were removed at their generating point. Energy spectra of generated alphas, betas, and gammas were saved, as well as spectra of particles leaving the platinum shield.

Given the photon energies involved in the decay scheme, a build-up region of a few mm in water around the source was expected. Thus, absorbed dose was scored as energy deposited per unit mass and disintegration. For each radioactive nuclide of the decay chain, 5×10^9 initial radioactive atoms were released and their disintegration was simulated until the next daughter product. Collision kerma was

also scored. Since collision kerma equals absorbed dose where electronic equilibrium exists, data from absorbed dose was used where there is not such equilibrium, whereas data from collision kerma was used in the rest of the space. 10^8 atoms of each radioactive nuclide of the decay chain were released to estimate S_K/A. Track-length kerma estimator was used in both water and air.

4.2.4.2 MCNP5

To validate results from GEANT4, independent simulations were performed with "Monte Carlo N-particle transport code, version 5" (MCNP5 v.1.51) (Briesmeister *et al.*, 2004), to derive S_K/A, Λ and $g_L(r)$. The daughter nuclei were considered to be in secular equilibrium with ^{226}Ra. Default MCNP5 photon cross-section library MCPLIB04 was used, based upon "Evaluated Nuclear Data File/B Version VI" (ENDF/B-VI) release 8, which in turn is derived from "Evaluated Photon Data Library '97" (EPDL97). In this case, decay data were taken from ICRP Publication 107 (Cullen *et al.*, 1997) to validate energy spectra generated by GEANT4.

Since MCNP5 does not allow photons and electrons to be started in the same run, two separate runs were needed to estimate each parameter. First, the contribution from primary photons were scored and then the contribution from β-particles, internal conversion electrons and Auger electrons (including bremsstrahlung). Simulations of absorbed dose to water were run using tally *F8, starting 2×10^9 particles in each run and detailed electron transport (mode PE). S_K was estimated with the track length collision kerma estimator tally F6, starting 5×10^8 particles in each run.

4.2.5 Monte Carlo simulation of a superficial mould mesh

One of the limitations in accuracy of the TG-43 formalism arises when scattering properties are altered from that of an extended phantom, such as when sources are positioned close to patient surfaces and at low photon energies (<50 keV) where differences between water and soft tissues are large due to high influence of photoelectric effect (Beaulieu *et al.*, 2012). In the presence of several sources, source-to-source attenuation may also produce dose variations.

In order to test the influence of these effects in surface treatments with ^{226}Ra sources, a typical clinical case consisting of a superficial mould mesh with 5 radium needles of 10 mg·Ra each was studied. During treatment, each needle was inside a rectangular glass casing that held the sources. Each glass casing was 4.5 mm wide, 9 mm in height and 17 mm in length, with a glass density of 2.23 g·cm^{-3} (see composition in **Table 4-1**). Each needle fitted perfectly the inner hole of the glass casing. Each casing was next to each other, with the longitudinal axes of the sources (*z*-axis) in parallel. This clinical setup was used to prevent the sources to be in direct contact with the skin, which resulted in severe skin damage. In addition, the glass kept a fixed geometry, which allowed determining treatment times from tabulated curves valid for this particular configuration (Strandqvist, 1939a; 1939b).

The superficial mould was placed on top of a 20 cm cubic liquid water phantom that mimics the patient. The centers of the needles were at the mid-plane of the casing, *i.e.* 4.5 mm above the water surface (along the *y*-axis). Center-to-center distance between the needles was 4.5 mm (along the *x*-axis). The geometrical setup described in this section is illustrated in the results section. With GEANT4, absorbed dose was scored in the water phantom and results were compared with those of the TG-43 formalism applying the principle of dose superposition. Independent simulations were performed for each radionuclide, totaling an equivalent of 2×10^{9} radium atoms per needle.

4.2.6 Absorbed dose at large distances

Another set of simulations was run with GEANT4 in order to evaluate the absorbed dose at large distances (>10 cm) from a ^{226}Ra source. Due to the reduced dimensions of the sources, beyond 10 cm these can be considered to be point sources. Thus, a point-like source emitting photons with the energy spectrum of the photons exiting the needle previously simulated was placed in the center of a 100 cm radius water sphere. 2.4×10^{9} photons were released and absorbed dose was scored in spherical shells of 1 mm thickness.

Absorbed dose rate $\dot{D}$ [cGy·h^{-1}] as a function of radial distance r [cm] was then fitted using the following expression:

$$\dot{D}(r)=\frac{S_K\times\left(\mu_{en}/\rho\right)_a^w\times\left[1+\mathrm{a}\times\left(\mu\times r\right)^{\mathrm{b}}\right]\times\exp(-\mu\times r)}{r^2} \qquad \textbf{(4-3)}$$

where the average mass energy absorption coefficient $\left(\mu_{en}/\rho\right)_a^w=1.112$ was used (Venselaar *et al.*, 1996). The coefficients *a*, *b* and μ are the fitting parameters to be obtained. The activity of radium sources *A* was generally given in terms of the quantity mg·Ra. The S_K [U] value of the source can be calculated from *A* [mg·Ra] and the air-kerma strength per unit activity S_K/A [U·Bq^{-1}] calculated in this study, considering that 1 mg·Ra equals 37 MBq, *i.e.*:

$$S_K=3.7\times10^{7}\times A\times\left(\frac{S_K}{A}\right) \qquad \textbf{(4-4)}$$

Expression (4-3) was used by Kornelsen and Young (1981) for ^{226}Ra sources in the range up to 18 cm. Venselaar *et al.* (1996) showed that the same expression could be used with ^{60}Co, ^{192}Ir and ^{137}Cs sources for distances up to 60 cm, so this study aims to provide the required fitting parameters needed to use expression (4-3) between 10 cm and 60 cm for a ^{226}Ra source.

4.3 Results

4.3.1 Contribution from each radionuclide to the overall absorbed dose

Figure 4-3 shows collision kerma along the transversal axis of the ^{226}Ra needle immersed in water. Contribution from the decay of each radionuclide to the overall collision kerma is plotted. ^{218}Po, ^{210}Pb and ^{210}Po have not been included in **Figure 4-3** because of their negligible contribution (< 0.001%) and high statistical noise in the curves. As observed, only the decay of ^{214}Pb and, mainly, ^{214}Bi contribute; the collision kerma contribution by the others is < 0.2%.

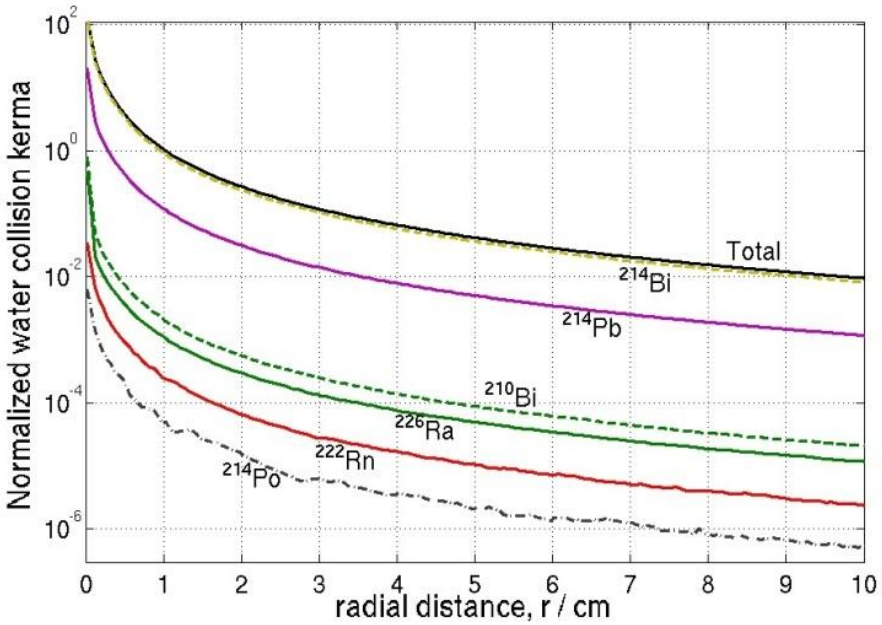

***Figure 4-3**. Collision kerma along $\theta = 90^{o}$ and normalized at $r_0 = 1$ cm for the ^{226}Ra needle in secular equilibrium and immersed in water. The contribution to the collision kerma from the decay of each radionuclide is plotted, neglecting energy released by ^{218}Po, ^{210}Pb and ^{210}Po.*

Simulations with GEANT4 were performed to assess the influence of high-energetic α- and β-rays emitted in the decay chain to absorbed dose and collision kerma. It was found that α-rays were completely stopped in the source encapsulation. However, some high energetic β-rays and mono energetic electrons, with associated bremsstrahlung, contributed to approximately 1% of absorbed dose to water. Therefore, the electrons generated during the decay should be also considered for any MC simulation with ^{226}Ra sources.

4.3.2 Time dependence of absorbed dose

Figure 4-4 shows the activity of each daughter product considered in the decay chain of ^{226}Ra as a function of elapsed time, normalized by the activity of ^{226}Ra. These curves are given by the Bateman equations.

Some of the radionuclides reached secular equilibrium after about 50 days. However, ^{210}Pb, with a half-life higher than 22 years, and its daughter products ^{210}Bi and ^{210}Po reached transient equilibrium after about 200 years since the ^{226}Ra source was sealed. Therefore, this is the time required for the source to be considered in secular equilibrium.

Given that calculations with GEANT4 provided the independent contribution of each radionuclide to the overall absorbed dose (as a function of the activity of the radionuclides), the absorbed dose at each point around the source was known as a function of time. For the reference point given by r_0 = 1 cm and $\theta_0 = \pi/2$, the variation in absorbed dose (in comparison with the complete equilibrium) was undetectable (variation < 0.01%) after 120 years. However, after 55 days the dose variation was below 0.2%, and after 27 days it was below 1%, which is considered to be negligible. Therefore, even though secular equilibrium was not reached until 200 years after the source was made, after 1 month the absorbed dose around the source could be considered to decrease only due to the radioactive decay of ^{226}Ra. If the sources were used before one month, some corrections to the overall absorbed

dose should be done. For example, if the source was used after 11 days, the dose was 14% smaller than in the secular equilibrium, whereas after 7 days it was 27% smaller.

From now on, all results presented correspond to the secular equilibrium state, which from a practical point of view, was considered to be reached after 1 month since the source was sealed.

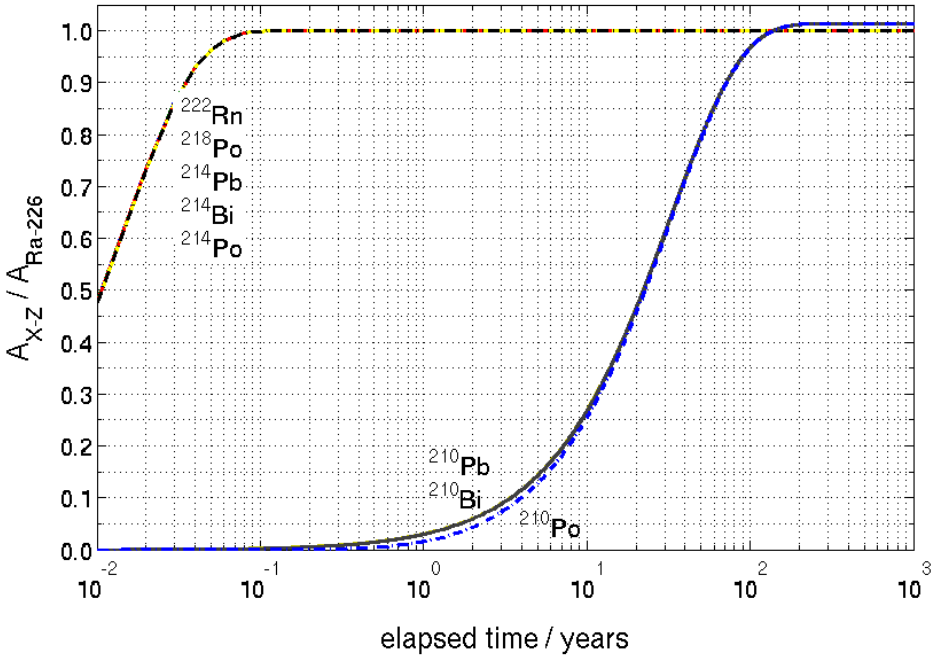

***Figure 4-4**. Ratio of the activity of the daughter product with symbol X (and atomic number Z) and the activity of the parent ^{226}Ra, as a function of time, according to Bateman equations (Bateman, 1910).*

4.3.3 Absorbed dose distributions

Absorbed dose and collision kerma distributions in water were obtained in (y,z) and (r,θ) coordinates. The left part of **Figure 4-5** shows the absorbed dose to collision kerma ratio around the ^{226}Ra tube, which illustrates the area around the source where there is not electronic equilibrium (ratio different than 1). In the right part, the absorbed dose distribution is plotted, showing a build-up region of 2 to 3 mm. For this reason $D(y,z)$ and $D(r,\theta)$ were derived taking collision kerma results for distances where there is electronic equilibrium (beyond 1.1 cm from the source approximately) and absorbed dose results (*i.e.* tracking electrons) for shorter distances. The procedure to choose the limit between collision kerma and absorbed dose was as follows: a table was calculated with the ratio of absorbed dose and collision kerma, and collision kerma was used when ratios became smaller than 1.01 (see the left part of **Figure 4-5**).

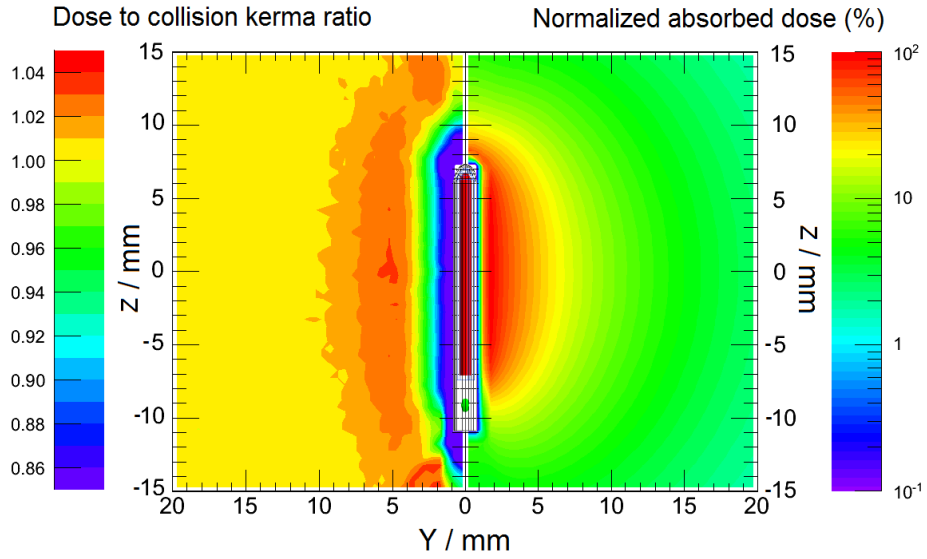

***Figure 4-5**. Absorbed dose to collision kerma ratio (left-half part of the figure), and normalized dose distribution (right-half part of the figure) around the ^{226}Ra tube. The tube location is also represented.*

Differences between GEANT4 and MCNP5 results beyond 5 mm were below 1% along the transversal axis ($\theta = 90^{o}$) of the source. Roughly 1 to 2% differences exist for other θ values, except at the longitudinal axis, where there exist differences up to 4%. Furthermore, the energy spectra of photons and electrons generated within the source with both MC codes were compared. Relative differences in intensity were at most 3% for a few energy lines, but below 1% for most of them. Higher discrepancies appear for very low energies (<10 keV). However, those low energy photons are stopped in the source shielding and so they do not contribute to the absorbed dose.

4.3.4 TG-43U1 parameters

The absorbed dose rate distributions $D(r,\theta)$ derived with GEANT4 were used to derive the TG-43 dosimetry parameters for both, the tube and the needle. For each source being in secular equilibrium, the radial dose function, the anisotropy function, the air-kerma strength per unit activity, the dose rate constant and an along-and-away table for QA purposes (extracted from $D(y,z)$) were obtained. All these data have been uploaded in an Excel spreadsheet as additional material together with published paper.

$g_L(r)$ and $F(r,\theta)$ were obtained using collision kerma for $r \geq 1.1$ cm approximately (except for angles θ near the longitudinal axis of the source, where a higher r value was used), whereas absorbed dose was used for shorter distances (see section 3.C.).

GEANT4 yielded an air-kerma strength per unit activity S_K/A value of 1.892×10^{-7} U Bq^{-1} for the tube, and 1.948×10^{-7} U Bq^{-1} for the needle. Results from both MC codes for S_K/A agreed within 0.2%. For comparison purposes, the exposure rate constant stated in previous works for a ^{226}Ra source filtrated by 0.5

mm Pt was $\Gamma(^{226}\mathrm{Ra}) = 8.25$ R cm^2 h^{-1} mCi^{-1} (Attix *et al.*, 1957; Williamson *et al.*, 1983; ICRP, 2008), which corresponds to 1.955×10^{-7} U Bq^{-1} in dry air.

The dose rate constant, Λ, obtained with GEANT4 was 0.952 cGy h^{-1} U^{-1} for the tube and 1.062 cGy h^{-1} U^{-1} for the needle. Both values have roughly 1.7% uncertainty with k=1 coverage factor (see uncertainty analysis in section 3.G.). The relative deviations of these values compared to those of MCNP5 were 0.7% and 0.08% for the tube and the needle, respectively.

4.3.5 Superficial mould mesh

The validity of the TG-43 parameters for surface treatments was evaluated by comparing the dose distribution obtained from TG-43 tables and the principle of dose superposition, with results from a MC simulation with 5 needles immersed in glass casing, and placed over a water phantom. **Figure 4-6a** shows geometry of the mould mesh described in section 2.E., whereas **Figure 4-6b** shows the ratio of these two dose distributions in a coronal plane that crosses the active center of the radioactive needles (left) and a tangential plane parallel to the mould, corresponding to a depth in water of 2 mm (right). Because of the symmetry of the dose ratio (the central needle is placed at x=0, whereas the others are placed at x=±4.5 mm and ±9.0 mm), only the right part of the plane has been shown. Results agree within 5% inside the volume covered by the implant, and within 10% up to at least 6 cm from the implant center, except within y=1 cm from the surface, where large differences appear mainly due to the higher attenuation in the glass casing and the lack of backscattering. These results are consistent with those obtained by Granero *et al.* (2014) for ^{60}Co, ^{192}Ir and ^{169}Yb sources.

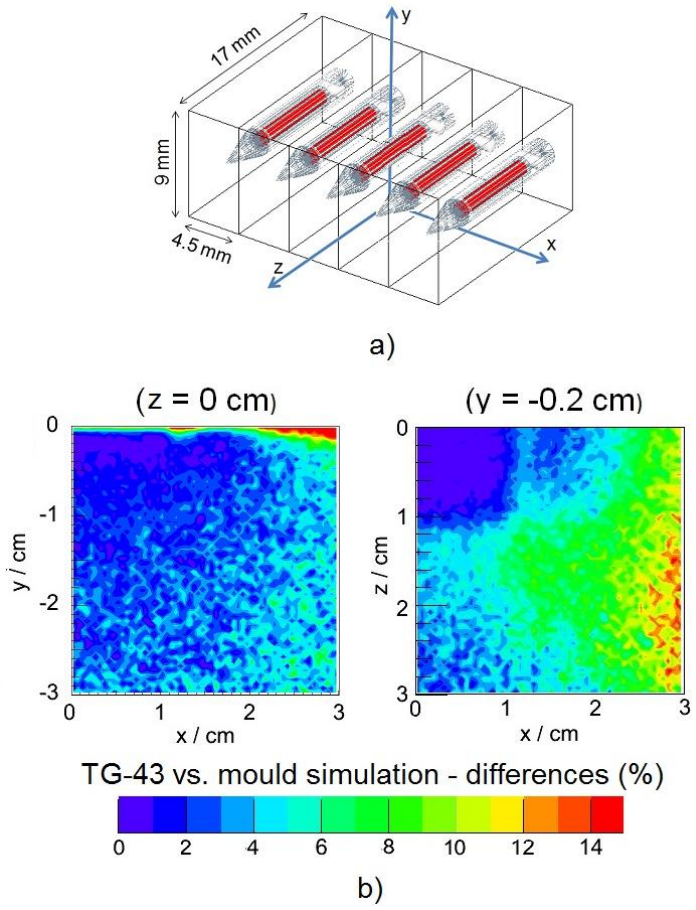

Figure 4-6*. a) Superficial mould mesh consisting of 5 needles inside a glass casing. In the MC simulations, this was placed over a 20 cm cubic water phantom. The origin of coordinates is placed at the interface between glass and water, just below the center of the central needle. b) Relative differences between absorbed doses to water calculated with TG-43 formalism and with a realistic MC simulation, in a coronal plane (plane perpendicular to the mould, at z = 0 cm) (left) and in a tangential plane (plane parallel to the mould, at y = -0.2 cm depth) (right).*

4.3.6 Absorbed dose at large distances

The absorbed dose rate at large distances can be determined using expressions (4-3) and (4-4). The coefficients obtained from the fitting of the MC results are: $a = 0.968$, $b = 1.205$ and $\mu = 0.0641$ cm^{-1}. When these values are used together with expression (4-3), the dose rate thus calculated differs from the MC calculation by less than 1.5% in the range 10 cm to 60 cm. Between 60 cm and 90 cm differences increase continuously up to 10%. The dose rates obtained from MC simulations and from expression (4-3) are shown in **Figure 4-7**, together with the relative difference between both data sets. Beyond roughly 95 cm the relative difference becomes quickly negative due to the lack of backscattering in the MC simulation beyond 100 cm.

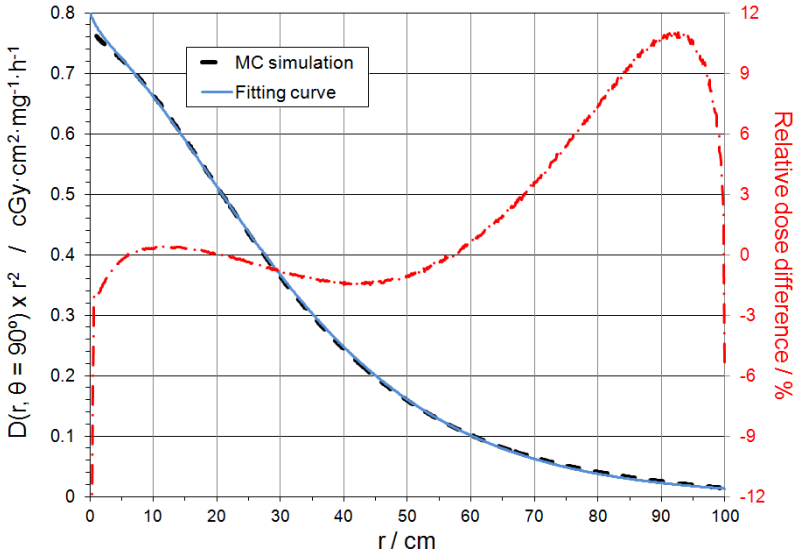

***Figure 4-7**. Absorbed dose rate as a function of the radial distance from a 10 mg ^{226}Ra point-like source. In red it is shown the relative difference between the dose rate calculated with GEANT4 and with expression (4-3) with the fitting parameters obtained in this study.*

4.3.7 Uncertainty analysis

As recommended by AAPM TG-138 (DeWerd *et al.*, 2011) and HEBD (Perez-Calatayud *et al.*, 2012) reports, an uncertainty analysis should be performed for the dosimetric data provided in this study. This was computed based on the method used by Rivard *et al.* (2004) and Granero *et al.* (2011). The type A statistical uncertainty of the absorbed dose rate calculated with GEANT4 was around 0.3%, increasing up to almost 1% near the longitudinal axis of the sources. On the other hand, the type B uncertainty components are roughly similar to the ones calculated by Granero *et al.* (2011). The overall uncertainty thus estimated (with coverage factor $k=1$) is roughly 1.2% for the absorbed dose rates at 1 and 5 cm, as well as for S_K. The Λ uncertainty is about 1.1% $(k=1)$. These are the uncertainties that may be attributed to the MC calculations, since they include the influence of the uncertainties due to: ^{226}Ra spectrum, MC physics, phantom composition, phantom cross-sections, tally volume averaging and tally statistics. However, these uncertainties are negligible in comparison with the uncertainty that should be assigned to the dose estimates made retrospectively. The reason is that any dose estimate requires the activity of the radium sources. Nevertheless, one of the drawbacks of old dosimetry is the lack of a measurable source strength; in fact, the uncertainty in source strength specified in terms of quantities like mg·Ra can be considered one of the largest sources of dosimetric uncertainty before measureable quantities were established (see, *e.g.*, Ref. (Visser, 1989; ICWG, 1990; Williamson, 2006)). Because the old sources are no longer available, the quantity mg·Ra needs to be used also with the data provided in this study, and so this drawback is present for both, the old and the new dosimetry. As reported in the literature reviewed, the size of the radium mass enclosed in the sources had an uncertainty of 10% to 15% (Dutreix *et al.*, 1982). Therefore, this can be the uncertainty assigned to each dose estimation at a given point, for the radium tube and the radium needle studied here.

4.4 Discussion

4.4.1 Comparison with older dosimetry data

The dosimetric formalisms used to calculate absorbed doses around radium sources changed considerably throughout the last century. The very first ones only considered primary radiation and the inverse square law for air (Mould, 2007). Later on, the dosimetric calculations based on the Sievert Integral became widely used. This model partitioned the line source into point sources, considering also the inverse square law and filtration corrections. In 1970, Goodwin *et al.* (1970) published tables of dose rate in tissue as a function of the platinum filtration thickness, source active length and the distances along-and-away. Tabulated data existed as a function of area or volume to be treated. Computerized treatment planning based on Sievert integration became available after that, and the Siemens Sidos system used at Radiumhemmet in Sweden was one of these (Feroldi *et al.*, 1992). A comparison of such systems showed differences among them in particular along the source long axis (Visser, 1989).

In order to test the accuracy of existing dose tables based on the Sievert Integral, the along-and-away table calculated by Young and Batho (1962) with an electronic computer for a needle similar to the one considered in this study is compared with data evaluated with the TG-43 formalism. **Table 4-2** shows the relative difference between both data sets. It is shown that at large distances (y >1 cm) and in the regions not bounded by the ends of the active source (z >0.77 cm), the difference increases, *i.e.* the dose calculated with TG-43 data is smaller. This is due to the fact that the other data set did not consider absorption and scattering in tissue. This result is consistent with the findings by Williamson *et al.*, who showed that the calculations based on the Sievert Integral overestimated the exposure rate per unit activity (Williamson *et al.*, 1983).

***Table 4-2**. Relative differences between dose rates around a ^{226}Ra needle calculated with the Sievert integral (as provided by Young and Batho (1962)) for a needle with 0.56 mm overall filtration (the platinum filter was 0.5 mm) and the TG-43 formalism.*

y / mm	*z* / mm							
	0	*3.08*	*4.62*	*7.70*	*15.4*	*23.1*	*30.8*	*38.5*
4.62	4.5	4.2	3.3	0.8	-4.4	-3.3	-0.8	2.9
6.16	3.1	3.5	2.6	0.7	-3.7	-5.1	-4.7	-1.9
7.70	2.4	2.0	1.6	0.3	-3.3	-5.0	-5.6	-4.3
11.6	0.9	0.6	0.2	-0.4	-2.2	-4.3	-5.6	-6.9
15.4	0.1	-0.3	-0.3	-0.8	-2.2	-4.1	-4.7	-6.4
19.3	-0.6	-0.7	-0.7	-1.2	-2.1	-3.7	-4.6	-5.9
23.1	-1.1	-1.2	-1.4	-1.5	-2.3	-3.5	-5.0	-6.3
30.8	-2.0	-2.4	-2.1	-2.7	-3.0	-3.9	-5.1	-6.2
38.5	-3.2	-3.7	-3.6	-3.4	-4.2	-5.0	-5.8	-6.5
46.2	-4.8	-4.4	-4.8	-4.8	-4.8	-5.9	-6.2	-7.1
61.6	-7.0	-6.7	-6.9	-7.2	-7.2	-7.8	-8.3	-9.5
77.0	-9.7	-9.7	-10.0	-9.6	-10.1	-11.5	-11.4	-12.3

In a previous study by Lundell (1994), absorbed dose rates were measured with TLDs in an anthropomorphic child phantom and calculated using the Sidos treatment planning system with simplified input regarding source filtration. In conjunction with that study, a radial dose profile was measured close to the 10 mg radium needle considered in this work with lithium fluoride TL dosimeters in full scatter conditions in PMMA (up to r=1 cm) and polystyrene (for $r \geq 1$ cm). **Figure 4-8** shows those data in comparison with MC results from the current study in water. For the TLD measurements, distances in PMMA were expressed in equivalent distances in liquid water (Lundell, 1994). For distances greater than r=1

cm, experimental and calculated results for the same ^{226}Ra needle agree within 13% and -10%. At distances shorter than r=1 cm, differences are between 4% and -13%. These differences are reasonable considering the experimental uncertainties in this steep dose-gradient area, but limit the accuracy of experimental dosimetric values near the sources, which have a high dose uncertainty even without considering the uncertainty in the mass of radium.

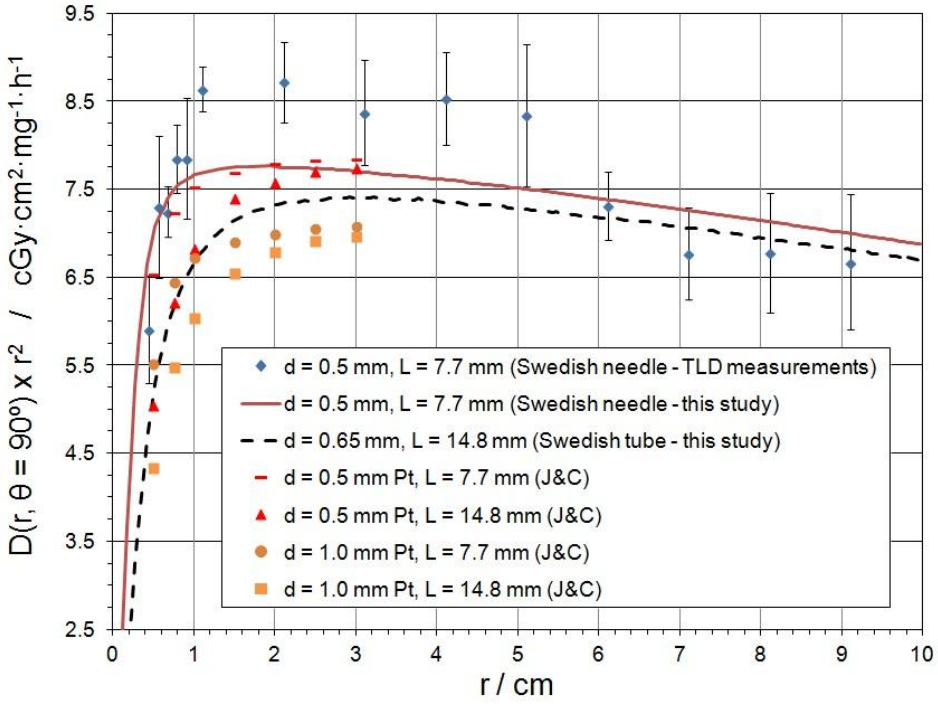

***Figure 4-8**. Absorbed dose rate on the transverse axis of the radium needle and radium tube calculated in this study, in comparison with experimental data from TLD measurements for the same radium needle. For comparison purposes, the dose rate shown by Johns and Cunnigham (1983) (J&C in the legend) for a given filtration thickness d and source active length L has been plotted.*

4.4.2 Applicability and limitations of this study

Retrospective risk assessments of ionizing radiation require dosimetric data as reliable as possible, as well as an estimate of its uncertainty. The dosimetric data provided in this study is important particularly in following up the large cohort of children treated for hemangioma through the Swedish cancer registry (Eidemüller *et al.*, 2009). Like survivors of the atomic bombs, those children data may be very helpful to determine the relationship between a specific late hazard effect and the absorbed dose (UNSCEAR, 2013), especially it will contribute to provide information on radiation sensitivity in early childhood, a topic of current interest (Candela-Juan *et al.*, 2014a). Earlier dosimetric data was restricted, *e.g.*, regards the number of source configurations and difficult to use when further individualization of absorbed doses was desired. Data provided here are the most accurate available for these sources and may be easily incorporated into current planning systems or home-made spreadsheets in order to perform retrospective studies of any source configuration.

In addition, for those epidemiologic studies in which absorbed doses to distant sensitive organs such as breasts, thyroid, brain or gonads are needed, the fitting parameters of a mathematical expression have been determined and provided. Candela-Juan *et al.* (2013) calculated organ equivalent doses in a voxelized phantom using ^{60}Co and ^{192}Ir sources applied to the prostate. Differences up to 20% were found between the simulations when the phantom was heterogeneous and when it is made just of water. Because the ^{226}Ra source has a mean photon energy spectrum between that of ^{60}Co and that of ^{192}Ir, those results are of reasonable applicability in this case. This 20% uncertainty, together in quadrature with the 10 to 15% uncertainty previously stated due to the generally unknown exact mass of radium, is assumed to give the best dose range estimation of absorbed doses. It is out of the scope of this study to evaluate if that uncertainty is acceptable for epidemiological studies since that may depend on each particular case and the amount of data available. It is surely important for the epidemiologic studies to be aware of this uncertainty before extracting their conclusions.

The sources considered in this study were a radium tube and a radium needle commonly used in Sweden and requested for ongoing epidemiologic studies. The TG-43 formalism has been shown to provide consistent results in comparison with MC simulations of a superficial mould implant within the regions bounded by the ends of the sources and a few cm extra margin, *i.e.*, these results are well suited to determine the absorbed dose in the treatment area. However, it is possible to estimate the influence of the source design on these results. **Figure 4-8** shows, besides the dose rate along the transversal axis of these Swedish sources, the dose rate along the transversal axis of two radium sources of the same active length than the needle and the tube, but with different platinum thicknesses. These data were obtained from the book by Johns and Cunningham (1983), and were evaluated through the Sievert Integral. Beyond 3 cm approximately, the dose rate becomes nearly independent of the active length of the source, an expected result. In addition, the difference due to the different platinum shielding used in each case is roughly 11%. The two platinum thicknesses considered (0.5 mm Pt and 1.0 mm Pt) represent the platinum range used by most of the radium sources. Thus, it is reasonable to consider that the TG-43 data and the dose rate at large distances that have been provided in this work may be applied to other sources similar in active length with an increased dose uncertainty of at most 11%.

4.5 Conclusions

Two independent Monte Carlo investigations have been performed to derive TG-43 parameters for a 8 mg ^{226}Ra tube and a 10 mg ^{226}Ra needle, previously used for brachytherapy at Radiumhemmet (Karolinska University Hospital, Stockholm, Sweden). The radial dose function, the 2D anisotropy function, the air-kerma strength per unit activity and dose rate constant are provided and can be used for these and similarly designed sources. Results from the TG-43 formalism have been shown to be accurate in cases with surface treatments and several sources inside glass casing. Thus, all these parameters can be put into a modern brachytherapy

treatment planning system in order to derive high quality dose estimations for retrospective dosimetry. In addition, the fitting parameters of a mathematical curve have been calculated in order to assess the absorbed dose to organs placed between 10 cm and 60 cm from the radium implant. This will allow improving the current knowledge that relates absorbed dose with long term radiation effects. Throughout a critical analysis of uncertainties it was estimates that absorbed doses assigned to organs in retrospective studies have an uncertainty of 20% to 25%.

Chapter 5. LEAD SHIELD FOR SURFACE HDR BRACHYTHERAPY

Most of the content of this chapter was published in the original research paper:

Candela-Juan C, Granero D, Vijande J, Ballester F, Perez-Calatayud J, Rivard MJ. *Dosimetric perturbations of a lead shield for surface and interstitial high-dose-rate brachytherapy*. Journal of Radiological Protection. 34: 297 – 311 (2014).

Kind permission was granted by the journal to reprint this article as a chapter of this dissertation.

5.1 Introduction

Skin brachytherapy with HDR sources is widely used. Based on tumor depth, superficial or interstitial modalities may be applied (Gerbaulet *et al.*, 2002*)*. In order to attenuate radiation that can reach radiosensitive organs in the patient, lead shields could be used to cover the implants on the body surface. For example, shields might be placed on the nose surface to attenuate radiation to the eye lens from a nasal implant, or around the breast to protect the thyroid from direct radiation coming from a breast treatment or even to protect the fetus in a hypothetical pregnant patient. This approach has two main dosimetric consequences.

1) Backscattering produces a dose enhancement in the patient in the vicinity of the shielding (Das *et al.*, 1989; Das *et al.*, 1995; Li *et al.*, 1999; Nath *et al.*, 1999; Das *et al.*, 2001; Das *et al.*, 2002; Lliso *et al.*, 2011). This overdose could be minimized by placing bolus with an appropriate thickness between lead and tissue. The backscatter dose enhancement has been reported for both kilovoltage and megavoltage photon beams, as well as for ^{60}Co equipment (Das *et al.*, 1989) and the Valencia applicators with HDR ^{192}Ir brachytherapy sources (Lliso *et al.*, 2011). Some reported data are based on experimental measurements with limitations related to the chamber size (*e.g.* volume averaging, effective measurement point, signal to noise ratio or chamber window for electrons), and so the need for additional Monte Carlo (MC) simulated radiation transport has been requested (Das *et al.*, 1995). This is even more important when discrepancies between experimental results and MC simulations have been reported (Das *et al.*, 2002). In addition, dose enhancement has not been evaluated in surface or interstitial BT with their corresponding boundary conditions.
2) Photon absorption reduces dose above the shield, downstream from the distal surface of the barrier. Radiation transmission data for radionuclides and materials relevant to BT facility shielding have been investigated for a point-like source placed in air, in broad-beam conditions typical of

radiation protection transmission studies (Papagiannis *et al.*, 2008). However, radiation transmission has not been evaluated in surface or interstitial BT for a typical clinical scenario.

Consequently, this work aims to study the dosimetric perturbations produced by the use of a lead shield in surface or interstitial BT using ^{60}Co, ^{192}Ir, or ^{169}Yb, and to provide the required bolus thicknesses that avoid overdose in the human tissue. This is examined for several shield thicknesses and for different source depths from the surface.

5.2 Methods and materials

Three different HDR radionuclides were considered: ^{60}Co ($T_{1/2}$=5.27 yr, $E_{\gamma,mean}$=1253 keV), ^{192}Ir ($T_{1/2}$=73.8 days, $E_{\gamma,mean}$=350 keV), and ^{169}Yb ($T_{1/2}$=32.0 days, $E_{\gamma,mean}$=93 keV). Both ^{60}Co and ^{192}Ir are commercially available for HDR BT, whereas ^{169}Yb has potential (MacPherson *et al.*, 1998) and might be available in the future. The corresponding source models were the Multisource HDR ^{60}Co model GK60M21 (Eckert & Ziegler BEBIG GmbH*)* and the HDR ^{192}Ir microSelectron mHDR-v2 (Nucletron BV, The Netherlands) source (Granero *et al.*, 2007; 2011). For HDR ^{169}Yb, since no commercial model is available and given that for the purpose of this work the exact geometry of the source has negligible effects, the source design has the same geometry as the microSelectron mHDR-v2. Results obtained herein for the studied source models should be generalizable to other commercially available models for the same radionuclides because energy spectra of photons that exit the different existent capsules are similar due to the energies involved.

Due to the intrinsic difficulties and limitations of absorbed dose measurements in very small depth intervals, MC simulated radiation transport has been used. The sources were radiologically characterized using the GEANT4 v.9.4 MC code (Agostinelli *et al.*, 2003), which has been used and validated extensively

in previous works in BT radiation transport simulations (Papagiannis *et al.*, 2008; Granero *et al.*, 2011; Vijande *et al.*, 2012). This code has been benchmarked in dosimetric evaluations of internal shielding in HDR BT with experimental measurements using radiochromic films (Lliso *et al.*, 2011). Instead of giving the energy spectra of emitted photons as an input to the MC code (Rivard *et al.*, 2010), in this work either ^{60}Co, ^{192}Ir, or ^{169}Yb radionuclides were placed inside the simulated sources, activating the GEANT4 radioactive decay module. This module generates all particles, including photons, electrons, recoil nucleus, and neutrinos (the latter are killed). Both photons and electrons were tracked, including secondary electrons generated by photons. The PENELOPE physics package included in the library of GEANT4 was used, although extra simulations were performed using the Livermore physics package of GEANT4, with no significant differences considering the statistical uncertainty of results shown in this work. Furthermore, results from GEANT4 were validated with the Monte Carlo code PENELOPE (Salvat *et al.*, 2008), which was used for a single case, providing consistent results with those shown in this work. The cutoff range for both types of particles simulated was set to 10 μm in all materials (Ballester *et al.*, 2009), considerably lower than the highest spatial resolution used in this work (100 μm). For photons, this range cutoff is roughly equivalent to an energy cutoff of 1 keV in air and water, and 6 keV in lead. For electrons, it is equivalent to 1 keV cutoff in air, 14 keV in water, and 58 keV in lead.

The geometry used in the simulations is shown in **Figure 5-1.** It mimics a typical clinical setup, although without catheters since the geometry reproduced here was considered to be the worst possible scenario from a radiation protection point of view. However, the catheter influence will be discussed later. The considered geometry is based on a 25×25×25 cm^3 cubic water phantom (Granero *et al.*, 2008) with a lead shield placed on its surface. While a large (25×25 cm^2) lead shield was considered, it can be smaller under clinical circumstances as long as it covers the full implant. The lead thickness t_{Pb} {0, 3, 6, and 10 mm} was changed between simulations. Depending on the source depth d_s, two cases were considered:

- Surface BT, with a single source placed on the surface $\left(d_s = 0\right)$, *i.e.*, between the water cube that represents the patient and the lead shield (**Figure 5-1a**).
- Interstitial BT, with the single source placed at a depth d_s {5, 10 mm} in the water cube (**Figure 5-1b**). A common width of the clinical target volume is 10 mm, and d_s = 5 mm is consequently a realistic value, which is the one used in these simulations. In order to further generalize these findings, simulations were repeated using d_s = 10 mm.

Therefore, three different geometry setups were considered in this work and, for each of them, four different lead thicknesses and three different BT radionuclides. This resulted in 36 independent simulations. The number of disintegrations simulated (*i.e.* number of radioactive atoms in the sources) was 9×10^8 for ^{60}Co, and 1.2×10^9 for ^{192}Ir and ^{169}Yb. Three independent simulations were performed for each geometry setup and the statistical (type A) uncertainty of the results was calculated as the standard deviation of the three data sets.

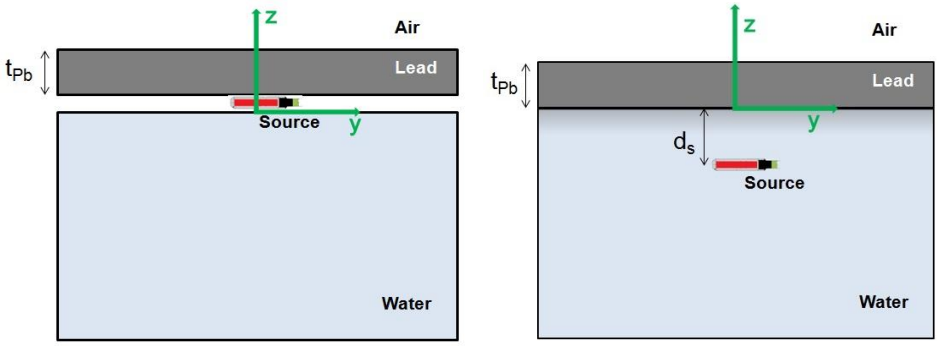

(a) (b)

Figure 5-1*. Scheme of the longitudinal section of the simulation setup, indicating some relevant parameters and the coordinate system used for a) surface brachytherapy, and b) interstitial brachytherapy. The figure is not to scale.*

For each considered simulation, total absorbed dose throughout the entire phantom volume was scored in 2D-histograms $D(z,\rho)$, being $\rho=\sqrt{x^2+y^2}$. Overdose at water phantom surface due to radiation backscatter in the lead shield was then evaluated comparing water absorbed dose with and without the shield, as a function of *z*. In order to quantitatively evaluate which radiation particles are responsible for the overdose at water phantom surface, absorbed dose due to photons and electrons coming from the lead shield were assessed. In order to separate the fraction of dose deposited by both types of radiation particles, the following process was followed. When a photon interacted with the lead shield and came back to the water phantom, all energy deposited by this photon and/or by all its secondary particles (including electrons) was scored in the histogram of dose deposited by photons. The same was done for electrons interacting with the lead shield and coming back to the water phantom. For all these histograms, bin thicknesses of 0.1 mm and 0.5 mm were used for *z* and ρ, respectively. The small scoring thickness in the z-axis was selected to avoid volume averaging due to the high dose gradient.

On the other hand, the dose reduction above the shield was evaluated by comparing air absorbed dose with and without shield. For absorbed dose in air, the histogram has a bin width of 1 mm in both, *z* and ρ. A forward overdose up to a few millimeters in air was expected due to contribution from particles created within the lead shield (Li *et al.*, 1999; Das *et al.*, 2001; Lliso *et al.*, 2011; Das, 1997). However, that overdose information is not relevant for the scope of this work due to their low range (Das, 1997) and given that no human tissue is expected to be located there. Hence, only attenuation in the above air volume is reported.

The geometry setup considered in the simulations represents a single source position. However, in a real clinical case the source has multiple dwell positions, remaining a specific time interval in each of them. In order to take this into account, the source configuration that allows irradiating uniformly a 50×50 mm^2 area located at a depth $z=-5$ mm and centered at $x=y=0$ was obtained. This was

achieved by considering 4 catheters with 8 dwell positions each. The distance between consecutive catheters was 10 mm, with the catheters axes parallel to the *y*-axis. Moving the source along the *y*-axis was done at 5 mm spatial intervals. For each particular dwell position, the required treatment time was calculated. Then, simulation results for a single source position were spatially displaced, weighted according to the dwell times, and superimposed, thus obtaining the dose distributions for a realistic clinical case with the phantom being water. This phantom material was chosen because planning systems in HDR brachytherapy make use of it and because our main aim was to obtain the required bolus thickness, being the bolus material equivalent to water. Despite these two reasons, the range of the dose perturbation was also evaluated in skin (density of 1.09 g/cm^3), comparing it with the range obtained in water (density of 1.00 g/cm^3).

In order to analyze and evaluate results, energy spectra of the simulated sources, of the back-scattered photons and electrons, and of the photons and electrons that cross the lead shield were assessed. Spectra correspond to those of photons and electrons emitted in all directions of the space, and not just in the transversal axis at a particular distance. All energy spectra were saved with a 1 keV bin width.

5.3 Results

5.3.1 Energy spectra

The GEANT4 radioactive decay module has been benchmarked comparing energy spectra of photons emitted by the simulated radionuclides with recommended data (Rivard *et al.*, 2010; Perez-Calatayud *et al.*, 2012) provided at http://www.nndc.bnl.gov/nudat2/indx_dec.jsp by the National Nuclear Data Center (NNDC). For ^{60}Co, differences between both spectra are 1% for mean energy and overall intensity when considering photons > 15 keV. If lower energy photon

emissions are considered, there are higher differences (up to 16%). For ^{192}Ir, differences are lower than 0.1% for both intensity and mean energy, whereas for ^{169}Yb differences are 1.5% and 0.7%. Again, higher discrepancies are found for energies below 15 keV. Those low energy lines hardly exit the source capsule and so their influence in absorbed dose is neglected. As shown by Rivard *et al.* (2010), differences between various reported energy spectra result in a negligible effect when obtaining absorbed dose ratios, which is the case of this work. Furthermore, as previously reported, the physics models used in GEANT4 have already been validated in dosimetric evaluations of internal shielding in HDR BT with experimental measurements (Lliso *et al.*, 2011). Therefore, the GEANT4 code used in this work can be considered to be validated for the scope of this study.

Figure 5-2 shows energy spectra of photons and electrons that go back from the lead shield to the water phantom, including backscattered photons and electrons, characteristic x-rays, and Auger electrons. The predominant energy lines in the backscattered photon spectra (**Figure 5-2a**) are those corresponding to characteristic x-rays coming from the deexcitation of lead atoms, with energies between 74 and 90 keV, in agreement with data reported by the Laboratoire National Henri Becquerel (LNHB) (http://www.nucleide.org/DDEP_WG/ /DDEPdata.htm). **Figure 5-2** also shows energy spectra of photons and electrons that traverse the lead shield or are emitted by it, for the specific case t_{Pb} = 3 mm and d_s = 5 mm. Characteristic x-rays from lead atoms are also observed in this case, although the predominant lines are still the ones associated with nuclear disintegration.

Table 5-1 shows, for all three HDR sources considered, mean energy of photons and electrons backscattered and that traverse the lead shield, as a function of source depth and lead thickness. The statistical uncertainty of the mean energy of both photons and electrons is generally lower than 2 keV. It is noted that:

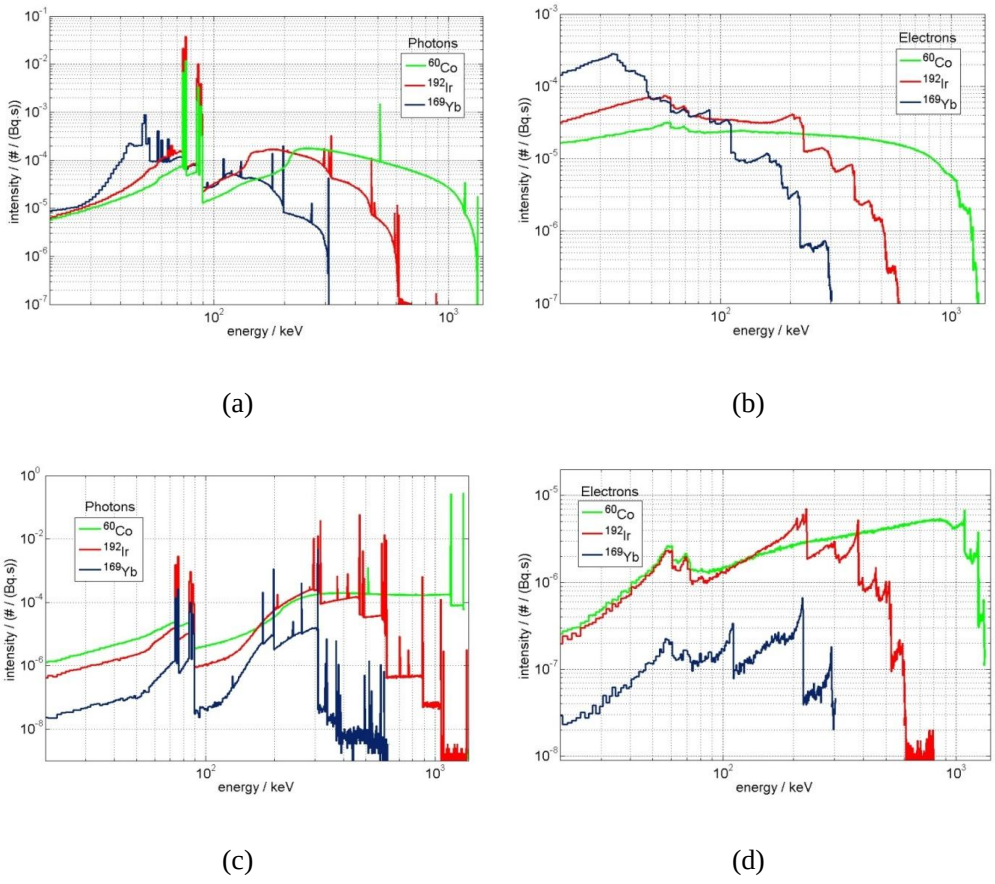

***Figure 5-2**. Energy spectra of a) photons and b) electrons that are backscattered from the lead shield to the water phantom, and energy spectra of c) photons and d) electrons that traverse the lead shield. Spectra correspond to the simulations with d_{Pb} = 5 mm and t_s = 3 mm, for all three HDR sources considered.*

***Table 5-1**. Mean energy of source photons and electrons that go back from the lead shield to the water phantom, and that traverse the lead shield, as a function of source depth d_s and lead thickness t_{Pb}.*

Nuclide	d_s (mm)	t_{Pb} (mm)	Mean photon energy (keV)		Mean electron energy (keV)	
			Backscatter	Traverse shield	Backscatter	Traverse shield
^{60}Co	0	3	418	1120	477	680
		6	425	1107	476	673
		10	427	1091	476	666
	5	3	374	1113	437	677
		6	386	1103	436	672
		10	388	1088	436	664
	10	3	343	1109	422	675
		6	357	1100	421	670
		10	360	1087	421	664
^{192}Ir	0	3	127	408	164	256
		6	128	446	164	279
		10	128	478	164	299
	5	3	117	406	144	254
		6	118	445	144	279
		10	118	478	144	299
	10	3	112	405	136	253
		6	112	445	136	278
		10	112	477	136	298
^{169}Yb	0	3	74	263	53	158
		6	74	287	53	168
		10	74	285	53	149
	5	3	74	263	51	159
		6	74	286	51	171
		10	74	285	51	153
	10	3	74	262	49	158
		6	74	286	49	170
		10	74	285	49	149

1) Mean energy of photons and electrons emitted in the backward direction (defined as the direction from shield to source) was lower than from the forward direction.
2) For a given lead thickness with ^{60}Co and ^{192}Ir, the mean energy of photons and electrons backscattered decreased when the source depth increases. For ^{169}Yb, the same was valid for the mean energy of backscattered electrons, whereas for photons there was no variation within 1 keV.
3) For a given lead thickness with ^{60}Co and ^{192}Ir, the mean energy of photons and electrons that traverse the lead shield slightly decreased when the

source depth increased. For ^{169}Yb, there was no variation within the relative uncertainty of these data.

4) For a given source depth and all three radionuclides, the mean energy of photons and electrons backscattered was independent of shield thickness (within the thickness range here considered), except for photons from ^{60}Co, whose mean energy slightly increased with lead thickness.
5) For a given source depth, lower energy photons were attenuated more than higher energy photons as the lead thickness increased. Consequently, the mean energy of photons and electrons that traversed the lead shield increased with t_{Pb} for ^{192}Ir. However for ^{60}Co, given that the predominant lines are almost exclusively 1,173 keV and 1,332 keV, the beam hardening effect was not observed given the negligible influence of the more attenuated lower energy lines. For ^{169}Yb, the mean energy of photons traversing the shield was also almost constant with t_{Pb} within the relative uncertainty of these data.

5.3.2 Backscattered dose perturbation

Figure 5-3 shows the shielded to unshielded absorbed dose ratio in the water phantom (along the *z*-axis, for $\rho = 0$) for the ^{60}Co, ^{192}Ir, and ^{169}Yb single dwell sources. For each *z* value, the statistical uncertainty was < 1.5% for ^{60}Co and < 3% for ^{192}Ir and ^{169}Yb. The dose enhancement profile was the same if the phantom was made of skin or water. For each source, all three geometrical configurations (surface BT and interstitial BT with d_s = 5 and d_s = 10 mm) are shown for t_{Pb} = 6 mm. For surface BT, the relative importance of backscattered dose in the *z*-axis is nearly negligible for all three HDR sources considered. This is due to the proximity of the source to the surface and to its high dose gradient. This is not the case with interstitial BT, where the backward dose perturbation reaches up to roughly 3 mm depth for ^{60}Co and 1 mm depth for both ^{192}Ir and ^{169}Yb, with the perturbation being higher in magnitude as the mean energy of gammas emitted by the radionuclide

decreases. The depth of the perturbation and the perturbation ratio at $z = -0.1$ mm (with $\rho = 0$) is independent of the lead thicknesses here considered (differences of perturbation ratios below 2% for all three sources).

For other ρ values, the dose enhancements due to the presence of the shielding are different than those reported in **Figure 5-3**: the dose enhancement generally increases with ρ for a single source position, although the range of the high dose perturbation remains nearly the same. The variation of the dose enhancement with ρ for a single dwell position is not considered to be relevant given that it is different than in a clinical case with multiple dwell positions. **Figure 5-4** shows the percentage excess dose (shielded to unshielded absorbed dose ratio minus 1, *i.e.* $100\% \times \left(D_{t_{Pb}} / D_{t_{Pb}=0} - 1 \right)$) throughout the water phantom (in the *x*-*z* plane) for a real clinical configuration with ^{192}Ir. The excess dose plots for ^{60}Co and ^{169}Yb are equivalent to the ones shown in **Figure 5-4**, although with different excess dose values and ranges of the perturbations. The following is noted within t the 50×50 mm^2 target region:

- For ^{60}Co, the range of the high dose enhancement reaches $z = -3$ mm. For greater depths, there is an excess dose of $2-3\%$ and $0-1\%$ for surface and interstitial BT cases, respectively. This nearly constant excess dose reaches a depth of, at least, $z = -30$ mm.

- For ^{192}Ir, the range of the high dose enhancement reaches $z = -1$ mm. For greater depths, there is an excess dose of $2-3.5\%$ and $1-2\%$ for surface and interstitial BT cases, respectively. This nearly constant excess dose reaches a depth of, at least, $z = -30$ mm.

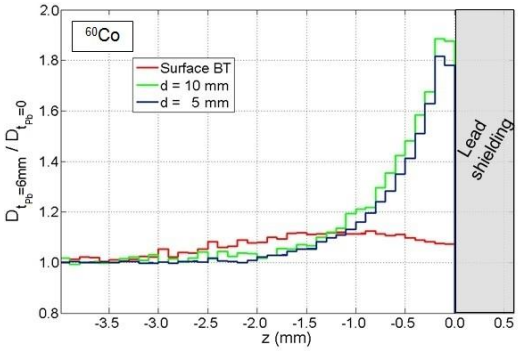

(a)

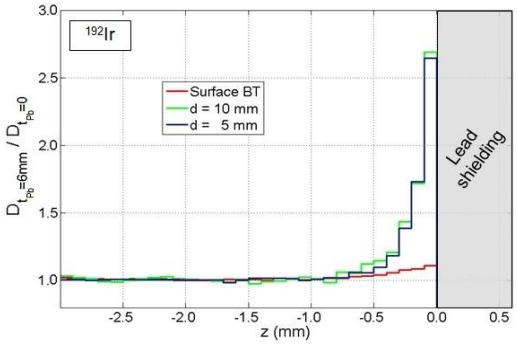

(b)

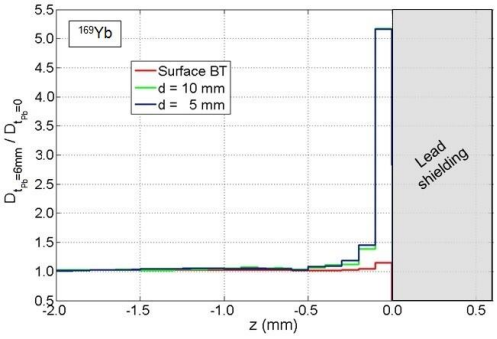

(c)

Figure 5-3*. Shielded to unshielded absorbed dose ratio in the z-axis (radial distance $\rho = 0$) for all sources and for the three configurations used according to source location: surface BT, and interstitial BT with d_s=5 mm and 10 mm.*

- For ^{169}Yb, the range of the high dose enhancement reaches almost $z = -1$ mm. For greater depths, there is an excess dose of $4-5.5\%$ for surface BT, although variations up to 9% are observed in planes without a dwell source position. For interstitial BT, the difference is $4-5\%$ up to $z = -2$ mm and $3-4\%$ for greater depths.

- For all three radionuclides, the excess dose in interstitial BT is negligible (<1%) at distances less than around 2 mm from the source (see grooves in **Figure 5-4b**).

Not only are the magnitude and depth of the backward dose perturbation important, but also is the type of ionizing radiation that produces it. **Figure 5-5** shows, for d_s = 5 mm and t_{Pb} = 6 mm, the shielded to unshielded absorbed dose ratio in the z-axis for each considered source, showing contribution of photons and electrons that backscatter from the lead shield to the water phantom, which have the spectra shown in **Figure 5-1**. Contamination from backscattered photons is nearly constant with *z*, for the depths close to the phantom surface. This is not the case for electrons, which are the main source of contamination near the surface, as previously suggested in works about backscatter dose perturbations by kilovoltage and megavoltage photon beams (Das *et al.*, 1989; Li *et al.*, 1999). However, their influence decreases quickly with depth: their dose curves can be fitted by an exponential function, as previously proposed (Klevenhagen *et al.*, 1982; Lambert *et al.*, 1982; Perez-Calatayud *et al.*, 2000). The current study confirms this behavior and quantifies it for the three HDR BT sources.

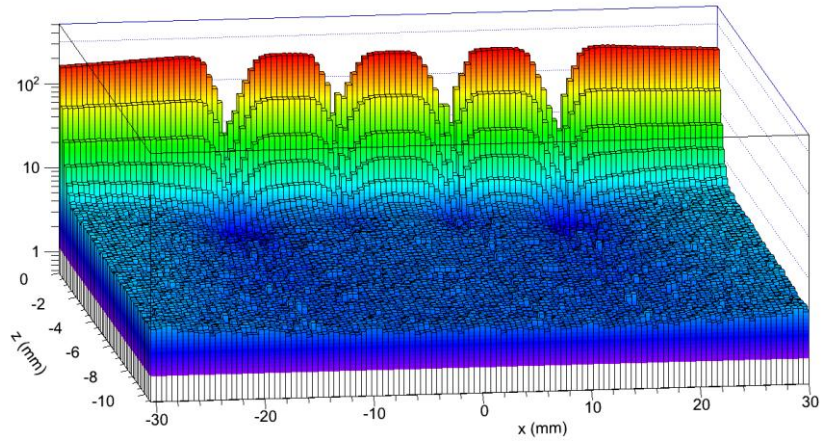

(a)

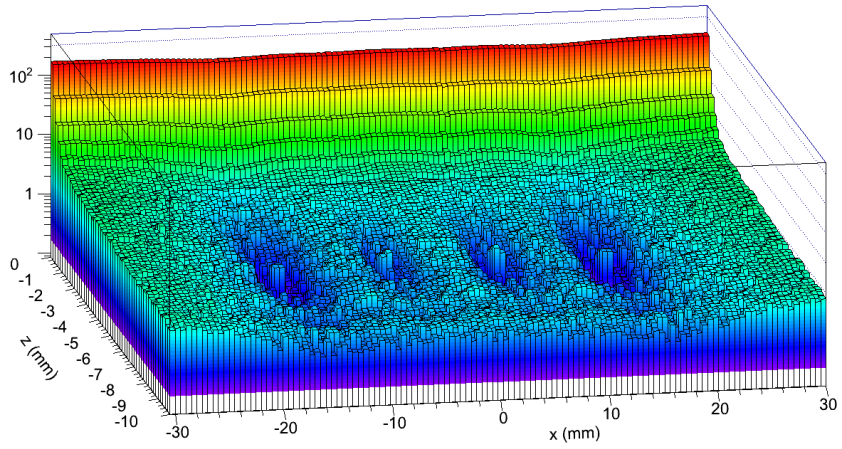

(b)

Figure 5-4*. Percentage excess dose (%) in the water phantom (y = 0) due to the lead shielding for a) surface (d_s = 0) and b) interstitial (d_s = 5 mm) HDR brachytherapy with 192Ir. This corresponds to a real configuration with the source having multiple dwell positions. Grooves appear at the different dwell positions. The bin widths are 0.2 mm and 0.5 mm for z and x, respectively.*

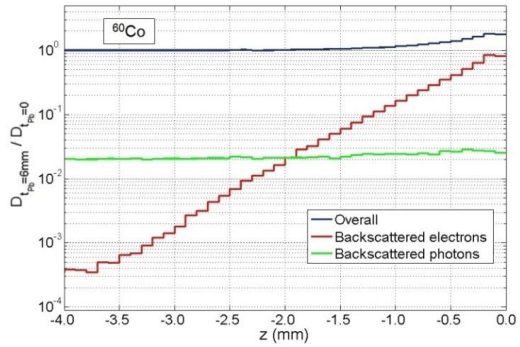

(a)

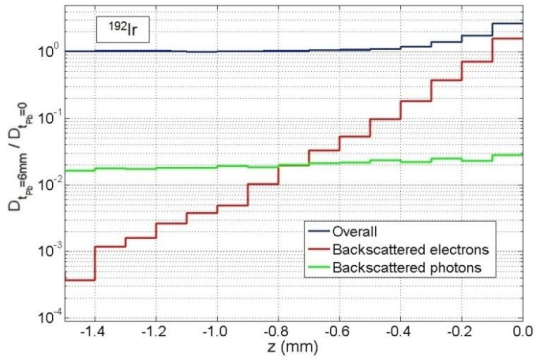

(b)

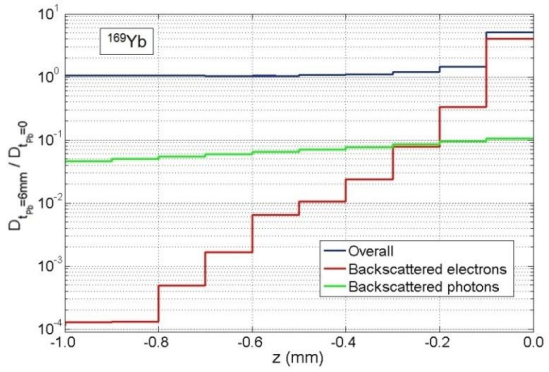

(c)

Figure 5-5*. Shielded to unshielded absorbed dose ratio in the z-axis for all three sources, using d_s=5 mm and t_{Pb}=6 mm, with contribution from backscattered photons and electrons.*

5.3.3 Transmission

Figure 5-6 shows the shielded to unshielded absorbed dose ratio above the lead shield for a ^{60}Co source placed at 5 mm depth and with lead shield of 6 mm thickness, considering a clinical case with multiple dwell positions. Similar figures were obtained for ^{192}Ir and ^{169}Yb, as well as for the other source depths and lead thicknesses considered. Given the multiple and limited source positions, the dose reduction is not constant throughout the whole space, and so giving a single transmission value in a real case with multiple dwell positions seems not appropriate. Instead, a transmission range for each considered case is provided (**Table 5-2**). The forward dose enhancement near the surface is not considered, as previously argued. In addition, the treatment area has 50 mm thickness and is centered at $x = 0$ mm. Thus, the transmission range is for the limits $20 < z < 100$ mm and $-25 < x < 25$ mm. Furthermore, an arbitrary reference point has been established at $(x = 0, y = 0, z = 50)$ mm, for which the transmission is also provided in **Table 5-2**.

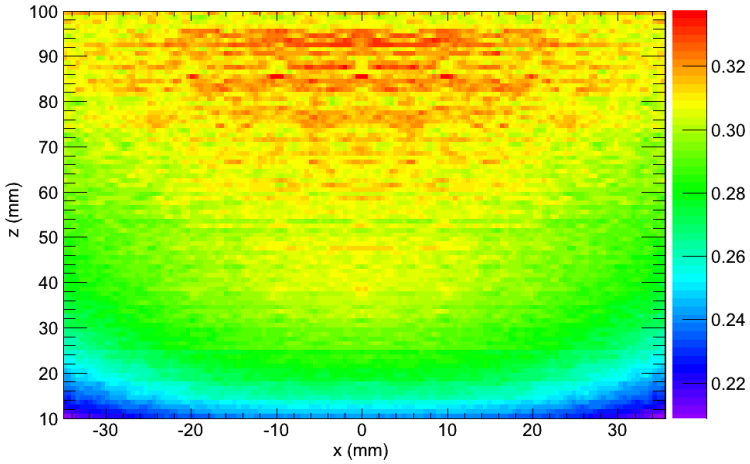

***Figure 5-6**. Shielded to unshielded absorbed dose ratio in the X-Z plane of the air volume due to the t_{Pb}=6 mm lead shielding for interstitial (d_s=5 mm) HDR brachytherapy with multiple dwell positions of a ^{60}Co source.*

***Table 5-2**. Transmission through the lead shield for ^{60}Co, ^{192}Ir, and ^{169}Yb, as a function of lead thickness t_{Pb} and source depth d_s. Transmission is evaluated in the x-z plane, in the range $20 < z < 100$ mm and $-25 < x < 25$ mm. The reference point is $P(x = 0, y = 0, z = 50)$ mm.*

Nuclide	t_{Pb} (mm)	d_s (mm)	Transmission (%)	
			Range	In reference point
^{60}Co	3	0	34 – 52	47
		5	37 – 46	42
		10	42 – 50	46
	6	0	23 – 38	33
		5	26 – 34	31
		10	31 – 38	35
	10	0	15 – 27	23
		5	18 – 26	22
		10	21 – 28	25
^{192}Ir	3	0	28 – 46	41
		5	47 – 60	57
		10	55 – 65	62
	6	0	09 – 18	15
		5	15 – 23	21
		10	18 – 25	23
	10	0	3.0 – 6.5	5.5
		5	5.0 – 9.0	7.5
		10	5.5 – 9.5	8.5
^{169}Yb	3	0	3.0 – 10	7.0
		5	8.0 – 12	10
		10	7.0 - 13	11
	6	0	0.4 – 2.0	1.0
		5	1.0 – 2.6	1.7
		10	1.0 – 4.0	2.0
	10	0	0.0 – 0.4	0.2
		5	0.0 – 0.6	0.3
		10	0.0 – 0.9	0.3

The statistical uncertainties of the transmission values reported are generally ~10% for ^{60}Co and ^{192}Ir, and ~50% for ^{192}Yb. Although these relative uncertainties may seem large, they are smaller or similar than the broad transmission range

shown in **Table 5-2** for each configuration. As expected, the transmission decreases as the lead thickness increases. For ^{60}Co, transmission data seem not sensitive to source depth, whereas for ^{192}Ir and ^{169}Yb, transmission is lower in surface BT than in interstitial BT, although with a large dose range.

5.4 Discussion

5.4.1 Backscattered dose perturbation

The range of the backscatter dose perturbation obtained in this work (along the *z*-axis) for ^{60}Co (3 mm) is similar to experimental data by Das *et al.* (1989) and MC simulations by Li *et al.* (1999) (3 to 4 mm), both for an external collimated beam and a lead shield immersed in water equivalent tissue.

Results of this work for the single dwell position are also consistent with those published for the particular case of the Valencia applicator with ^{192}Ir sources (Lliso *et al.*, 2011), in which the backward perturbation was reported to be around 0.5 mm (0.7 mm in this work, near 1 mm). The dose enhancement at the surface (within 0.1 mm depth) for the Valencia applicator configuration was a factor of 2. As shown in this work, this dose enhancement in the transversal axis depends on the distance between the source and the shielding, ranging between 2.7 for d_s=10 mm and 1.1 for d_s=0 (see **Figure 5-3b**). In addition, in the Valencia applicator configuration, the lead shield was immersed in water whereas it was only in contact with the upper surface in the current study. Due to backscattering in the water phantom, immersion in water increased absorbed dose when no shielding was placed. Scattered radiation is of lower energy and is more attenuated when the lead shield is used. This contributes to the fact that the ratio between the dose with and without the shield decreases in comparison to a shield placed between water and air.

The backscatter dose enhancements in water obtained in this work, observed to be equivalent to those for tissue, may be used to choose an appropriate bolus

thickness to be placed between the surface and the lead shield. As shown previously for a realistic clinical case, the high dose perturbation reaches 3 mm depth for ^{60}Co and 1 mm for ^{192}Ir and ^{169}Yb, and equivalent or larger bolus thicknesses are needed for each radionuclide source.

Nowadays, plastic is used to flatten the surface and keep rigid the catheter geometry (Nag *et al.*, 2001; Yang *et al.*, 2009) and so it seems adequate to investigate whether its thickness is enough to negate backscatter overdose. With this aim, the backscatter dose perturbation was also obtained in polyethylene ($\rho = 0.94$ g/cm^3) and the range of the perturbation was found to be equal to the range in water (within 0.1 mm) for ^{192}Ir and ^{169}Yb, whereas for ^{60}Co the range in plastic was 0.4 ± 0.1 mm larger, also negligibly different than water. Hence, polyethylene is equally valid to avoid surface overdose if it has the appropriate thickness previously obtained for water.

Bolus thicknesses determined in this work are required to avoid high overdoses produced by electrons, but there still remains a nearly constant contamination from photons which reaches at least a few centimeters depth. That contamination might be small taking into account that treatment planning systems currently used in HDR brachytherapy consider the source to be placed within an infinite water medium, thus not considering that there is air above the patient surface. Due to the negligible contribution of backscattering in air in comparison to backscattering in water, the calculated surface dose might be currently overestimated. The presence of the bolus and the lead shield could partly compensate this.

5.4.2 Transmission

For all three radionuclides considered, **Figure 5-7** plots the transmission at the reference point for the surface BT case, with error bars showing the range of transmissions given in **Table 5-2**. For comparison purposes, the transmission curve

fitted by Papagiannis *et al.* (2008) for brachytherapy facility shielding is also plotted. Discrepancies between both datasets appear as the energy of gammas emitted by the radionuclide increases. This is mainly due to the fact that in the work by Papagiannis *et al.* (2008) the source was placed in air and at a distance of 1 m of the lead shield, which covered the whole wall, and only photons emitted in the shield direction were considered. However, in this case the source was placed in contact with or near the lead shield and the water phantom, and there were several dwell positions. The water phantom in this work increased absorbed dose when no shield was used in comparison to an air phantom due to backscattering by air being negligible in comparison to water. Therefore, the shielded to unshielded absorbed dose ratio in the surface BT configuration is necessarily lower than that given by Papagiannis and colleagues. Since incoherent scattering is increasingly important as photon energies increase, the discrepancy is highest for ^{60}Co and almost negligible for ^{160}Yb. In addition, the transmission evaluated by Papagiannis *et al.* is the maximum one as it was obtained in the transversal axis of the wall and the source. When the source is displaced, its contribution along that axis is lower since their photons traverse a higher lead thickness.

Thus, the geometrical configuration can greatly influence the transmission values. It should be carefully evaluated for each particular case if a precise estimation of dose reduction is desired. For instance, data provided in this work can be used to estimate organ equivalent dose saving in a treatment with HDR surface or interstitial BT with lead shields. In addition, the dose reductions shown in this work justify the use of lead shields (with an appropriate bolus thickness) in some particular radiation treatments since they clearly compensate the small backscatter overdose.

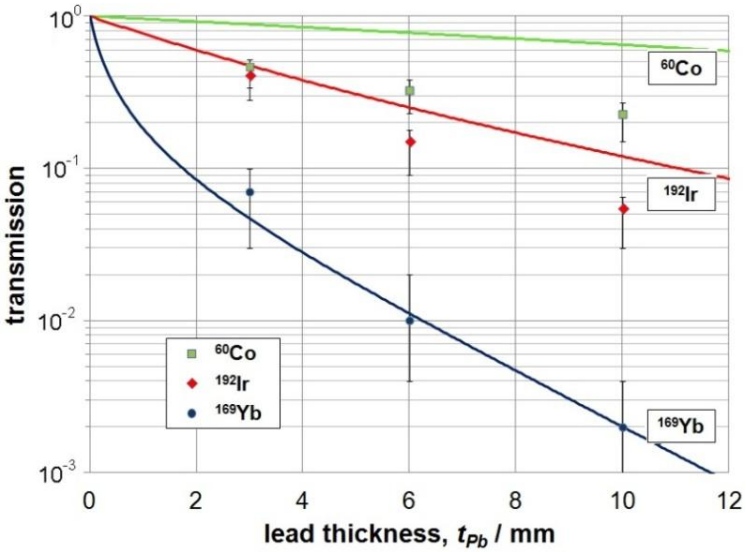

Figure 5-7*. Transmission dose through the lead shield calculated in this work at the reference point, for ^{60}Co, ^{192}Ir, and ^{169}Yb sources in the surface brachytherapy case. Error bars show the range of transmissions given in* ***Table 5-2****. Data are compared with the fitting curve by Papagiannis et al. (2008) (solid lines).*

5.5 Conclusions

In surface and interstitial BT, the high backscatter dose enhancement in the body surface due to use of a lead shield can be avoided by using a bolus thickness ≥ 3 mm for ^{60}Co, and ≥ 1 mm for ^{192}Ir and ^{169}Yb. It is due mainly to backscattered electrons and characteristic x-rays to a lesser extent.

Transmission data as a function of lead thickness have been provided for the three radioactive sources. These have been shown to differ with radiation transmission data for facility shielding with high energy sources due to the environment geometry (presence of water and multiple dwell positions). These data can be used to estimate organ equivalent dose saving in a real treatment with HDR surface or interstitial BT with lead shields.

Chapter 6. FETAL DOSE REDUCTION IN PREGNANT PATIENT WITH BREAST CANCER

Most of the content of this chapter is included in the original research paper:

Candela-Juan C, Gimeno-Olmos J, Pujades MC, Rivard MJ, Carmona V, Lliso F, Celada F, Ramírez-Coves JL, Ballester F, Tormo A, Pérez-Calatayud J. *Fetal dose measurements and shielding efficiency assessment in a custom setup of ^{192}Ir brachytherapy for a pregnant woman with breast cancer*. Physica Medica. (2015) doi: 10.1016/j.ejmp.2015.01.010.

Kind permission was granted by the journal to reprint this article as a chapter of this dissertation.

6.1 Introduction

Even though the incidence rate of cancer during pregnancy is low (roughly 0.1% of pregnant women have cancer (ASCO, 2014; Filipov *et al.*, 2013)), the magnitude of patients needing treatment is appreciable. In particular, many pregnant women are treated with radiation therapy. Given that ionizing radiation can also cause damage to the fetal cells, the possible risks to the developing baby should be carefully evaluated.

The effect of ionizing radiation to the fetus depends on the gestational age, equivalent dose and fractionation (Stovall *et al.*, 1995; ICRP, 2000; Nuyttens *et al.*, 2002; NCRP, 2013). A summary of these radiation effects, classified by gestational age, can be found in reports by the AAPM (Stovall *et al.*, 1995), the ICRP (2000) and, more recently, the NCRP (2013). Based on epidemiological data from atomic bomb survivors, from patients exposed to diagnostic X-rays, and from experiments with animals, it may be concluded that doses below 10 cGy do not produce observable deterministic effects in the fetus, although this dose threshold is reduced to 5 cGy in other studies (Kal *et al.*, 2005). In addition, the possibility that such low doses may produce a radiation-induced tumor is under debate (Candela-Juan *et al.*, 2014a). A large uncertainty exists for this dose threshold, and so the main aim of any radiation treatment should be tumor control with absorbed doses to the fetus made as low as possible, trying not to exceed the stated dose constraint. It may be helpful to clarify at this point that even though the original data used to determine the existent dose constraints was expressed in mSv, the units of absorbed dose (*i.e.*, cGy) are adopted in the current study for consistency with the reports by the AAPM (Stovall *et al.*, 1995), ICRP (2000) and NCRP (2013).

Radiation therapy in pregnant patients has been widely reported for Hodgkin's disease (Woo *et al.*, 1992; Cygler *et al.*, 1997; Antypas *et al.*, 1998; Nuyttens *et al.*, 2002; Mazonaquis *et al.*, 2003), as well as for head and neck tumors or brain carcinomas (Wong *et al.*, 1986; Sneed *et al.*, 1995; Podgorsak *et al.*, 1999; Haba *et al.*, 2004; Lliso *et al.*, 2004; Josipovic *et al.*, 2009). There are also

publications on radiotherapy for pregnant patients with breast cancer (Ngu *et al.*, 1992; Van Der Giessen *et al.*, 1997; Antypas *et al.*, 1998; Fenig *et al.*, 2001; Martín Rincón *et al.*, 2002; Filipov *et al.*, 2013; Kourinou *et al.*, 2015). However, to the best of our knowledge, all previously reported radiation treatments applied to a pregnant patient were based on EBRT. No prior study has examined fetal doses for women receiving breast BT, although Venselaar *et al.* (1996) evaluated the absorbed dose at large distances from BT sources and proposed the application of his evaluations to estimate fetal doses.

In EBRT, the peripheral dose depends mainly on the distance from the field edge (it approximately falls exponentially with the distance (Stovall *et al.*, 1995; Mutic *et al.*, 1999; Podgorsak *et al.*, 1999; ICRP, 2000; Josipovic *et al.*, 2009)), but also on the field size and, in a minor contribution, on the depth in tissue (Antypas *et al.*, 1998). The main sources of radiation outside the treatment area are head leakage radiation, radiation scattered in the collimators and the rest of the head of the accelerator, transmission through the collimators, and radiation scattered inside the patient (Antypas *et al.*, 1998; Mutic *et al.*, 1999). The use of physical wedges is ill-advised because of the higher amount of monitor units (MU) needed and the higher scatter component (Josipovic *et al.*, 2009; Filipov *et al.*, 2013). The use of high-energy photon beams (> 10 MV) should also be avoided as it leads to a higher proportion of the transmission and collimator scatter, as well as to generation of photoneutrons (Antypas *et al.*, 1998). In order to reduce peripheral dose, a tertiary multileaf collimator (MLC) may be used, which reduces collimator scatter and transmission through the primary and secondary collimators (Mutic *et al.*, 1999). Furthermore, shielding devices around the patient's abdomen or the gantry are highly recommended to minimize exposure to the fetus from leakage and collimator radiation scatter (Ngu *et al.*, 1992; Woo *et al.*, 1992; Stovall *et al.*, 1995; Nuyttens *et al.*, 2002; Lliso *et al.*, 2004; Josipovic *et al.*, 2009; Filipov *et al.*, 2013). The proposed lead thickness for EBRT is about 5 cm to 7 cm (Josipovic *et al.*, 2009), which results in a massive custom device.

Opposed to the traditional whole breast irradiation (WBI), accelerated partial breast irradiation (APBI) techniques have emerged in recent decades, either by interstitial or intracavitary BT, EBRT, or intraoperative radiation therapy (IORT). The American Society for Radiation Oncology (ASTRO) (Smith *et al.*, 2009), the Groupe Européen de Curiethérapie-European Society for Therapeutic Radiology and Oncology (GEC-ESTRO) (Polgar *et al.*, 2010), and the American Brachytherapy Society (ABS) (Shah *et al.*, 2013) have presented consensus statements for APBI. The rationale for APBI is that most of local relapses occur in proximity to the tumor bed (Polgar *et al.*, 2005; Vicini *et al.*, 2005). Thus, APBI may be another option to treat breast cancer in pregnant patients.

On the basis of the rapid dose fall off with distance (as a result of the inverse distance square law) from a BT implant, it is expected that this radiation technique reduces the dosage to organs at risk and the integral dose when compared to EBRT. This has been quantified for organs as the heart or lung (Patel *et al.*, 2007; Weed *et al.*, 2005). Also, in **Chapter 2**, based on MC simulations and patients with prostate cancer, a radiation protection advantage of BT over EBRT at large distances from the treatment volume was shown (Candela-Juan *et al.*, 2013). This advantage could be applied to fetal dose reduction. Although there are no data to determine the optimal technique for APBI, interstitial BT has the highest follow up and is the technique of choice at our center for breast BT. This technique uses a HDR ^{192}Ir source and an array of catheters inserted within the breast around the excision cavity.

The aim of the current study is to assess the radiation dose to the fetus when using interstitial breast HDR ^{192}Ir BT. In addition, a new patient setup and lead shielding technique placed around the breast was designed to reduce the fetal dose. Absorbed doses were evaluated without and with this shielding. The variation of dose with distance to the implant as well as dose homogeneity within a representative slice of the fetal position were measured experimentally. A case report is also presented.

6.2 Materials and methods

6.2.1 Case report

A 29-year-old woman in the 12th week of gestation (see **Figure 6-1**) was submitted for postoperative irradiation of the right breast. An interstitial HDR ^{192}Ir BT breast treatment was planned as described in section 6.2.2 because the fetal dose was estimated to be lower than the delivered by external radiotherapy (a comparison between both techniques can be found in the Discussion section of this chapter). Interstitial HDR ^{192}Ir breast BT was also recommended because the patient satisfied the recommendations of ASTRO (Smith *et al.*, 2009), GEC-ESTRO (Polgar *et al.*, 2010), and ABS (Shah *et al.*, 2013), except for the age restriction, which is discussed later. From ultrasound measurements, it was estimated that the distance from the lower edge of the breast to the uterine fundus (the most proximal position of the uterus) 1 week before treatment was 20 cm, whereas the pubis was located an additional 10 cm caudally. The methodology described below was used to evaluate dose to the fetus.

According to the NCRP Report 174 (2013), the minimum acute lethal dose is estimated to be > 100 cGy for the fetus between the 8th and the 15th week of gestation. However, this is the most vulnerable period for irreversible whole-body growth retardation, with no-adverse effects observed between 25 cGy and 50 cGy. Nevertheless, given that a dose threshold of 5 cGy has been suggested in other studies (Kal *et al.*, 2005), this conservative constraint was used in the current study to compare the treatment options.

6.2.2 Treatment planning

The patient was seated in a chair with her right breast positioned over a table in such a way that the fetus was located beneath the table (see **Figure 6-1**). The

radiation dose to the fetus can then be reduced when the breast is shielded (see section 6.2.3).

An interstitial breast HDR ^{192}Ir BT treatment was planned using Oncentra Brachy TPS v.4.3 (Elekta AB, Stockholm, Sweden). A total of 36 Gy in 8 fractions was prescribed at the 90% of the basal points, with two treatment fractions per day given in four consecutive days. Seven catheters were used, each of them having the HDR ^{192}Ir source dwell positions for 9 cm of active length. The catheters were positioned in two coronal, parallel planes (three catheters in one plane and four catheters in the deeper-seated plane, both parallel to the thoracic wall, and defining equilateral triangles of side 1.6 cm) using a template (see **Figure 6-2a**). The minimum distance between the closest catheter and the thoracic wall was about 2 cm.

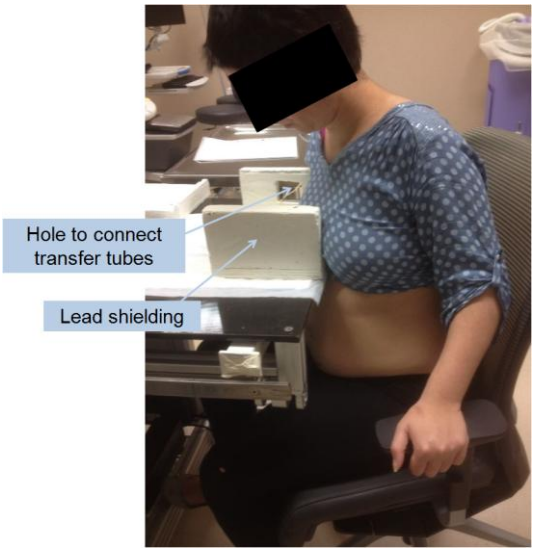

Figure 6-1*. Simulation of the proposed patient set-up in the HDR brachytherapy treatment room. The patient is seated in a chair, placing the breast to be treated over the lead shielding, which has a hole in the lateral wall to allow connecting the transfer tubes to the catheters. With this position, the fetus is maximally located beneath the shielded table.*

6.2.3 Shielding design

Absorbed dose to the fetus is due to primary radiation from the ^{192}Ir source and scattered radiation within the patient. The latter cannot be removed; however, the breast may be shielded to minimize dose contribution to the fetus from the primary component.

The shielding design consisted of a 3.5 cm thick layer of lead placed between the breast and the table. Thus, during the treatment, the breast rests over this lead shield. In addition, two lateral pieces of lead (3 cm thick each) were added (see **Figure 6-2**). The rationale for the use of this thickness was to attenuate most (over a factor of one-thousand, considering a tenth-value layer of 11 mm (Candela-Juan *et al.*, 2014b)) of the primary radiation component of the absorbed dose to the fetus such that it just receives the scattered radiation from inside the mother. The lateral blocks allowed placing an extra piece of lead (2.5 cm thick) above the breast, parallel to the first layer (see **Figure 6-2b**). The aim of this last layer was to shield primary radiation to the thyroids and eye lenses given the seated position of the patient. Its thickness was chosen as a compromise between providing radiation attenuation and patient setup feasibility given its weight.

One of the lateral layers had a hole through which the transfer tubes were connected to the catheters (see **Figure 6-1** and **Figure 6-2b**). In order to minimize the transit dose when the ^{192}Ir source exits and returns to the remote afterloader, a hollow lead tube (0.4 cm thick) was made, which covered the transfer tubes (see **Figure 6-2b**).

It is important to note that lead shielding placed in contact with patient skin can considerably increase the surface dose due to backscattering and electron contamination. This problem was in **Chapter 5** for surface and interstitial HDR ^{192}Ir BT. From that study, it was concluded that the surface overdose may be removed in the current study by placing a 0.1 cm thick layer of water-equivalent material between the lead shielding and the patient skin.

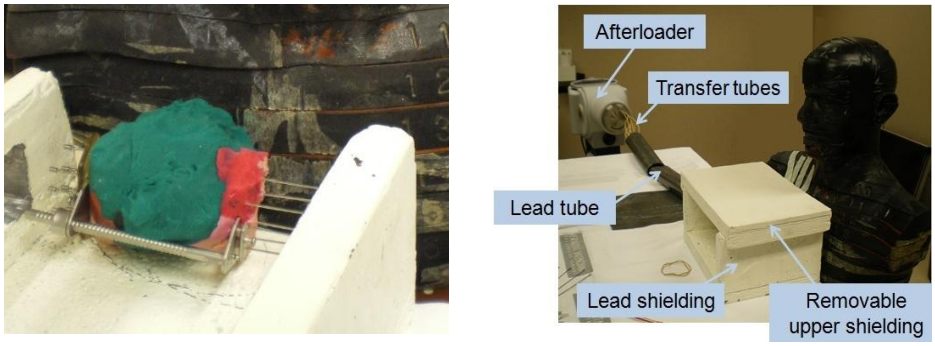

a) b)

***Figure 6-2**. Representation of the HDR ^{192}Ir brachytherapy treatment set-up, showing a) the implant within the breast phantom, and b) the assembled lead shielding arrangement.*

6.2.4 Fetal dose evaluation

6.2.4.1 Phantom measurements

Measurements of absorbed dose were made in a Rando phantom (Alderson Research Laboratories, Inc., Stanford, CT), which is sectioned into slices and is made of materials to radiologically mimic body tissues (see **Figure 6-2**). As a female-designed phantom was not available, the missing breast tissue was made of Roma Plastilina™ (JOVI S.A., Rubí, Spain). While this material is denser than a female human breast, the differences in attenuation at the photon energies examined in the current study (originating from ^{192}Ir) are expected to be negligible.

Because the patient was seated, her spine was oriented approximately vertically during treatment. Thus, it was decided to center the dosimeters at a position approximately representative of the center of the fetus, measuring the distance from the back of the patient. In this study, using data from Osei and

Faulkner (1999), it was estimated that the shortest distance between the fetus and the patient's back was about 10 cm for a median pregnant woman, whereas the largest distance might be about 20 cm. Then, the position representing the fetus center was estimated to be at about 15 cm from the phantom's back. Absorbed dose was measured at this central region, in several planes of the phantom, covering a distance d_z between 5 cm and 35 cm from the lower edge of the treated breast (or the upper surface of the lead shield) (see **Figure 6-3a**). This way, dose was estimated as a function of distance from the breast, hence allowing the application of the results to a wide range of gestational ages. Furthermore, four extra measurements were made at distances of 10 cm and 20 cm from the lower edge of the breast in order to evaluate the uniformity of the dose distribution. The location of the dosimeters in these three planes is depicted in **Figure 6-3b**.

Additionally, measurements were made at the eye lenses and thyroid of the phantom. All dose measurements were made without and with the previously described shielding design.

6.2.4.2 Radiochromic film dosimetry

The energy spectrum of radiation impinging the fetus is unknown, which may introduce a significant uncertainty in dosimeters with energy-dependent response. For this reason, in the current study, Gafchromic^{TM} EBT3 films (ISP, Wayne, NJ, USA) were used, whose energy response to monochromatic beams of 35 keV has been shown to differ by at most 3% when compared to calibration with 4 MV beams (Brown *et al.*, 2012). This energy dependence was considered as an additional term of the uncertainty for derivation of dose.

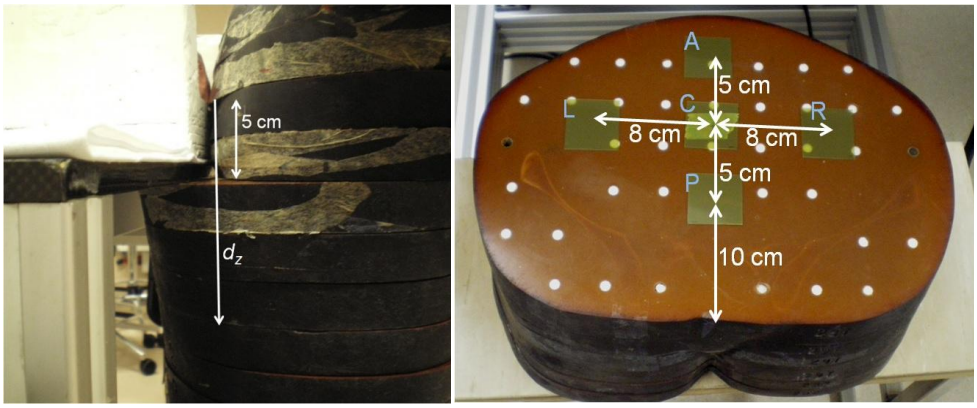

a) b)

Figure 6-3*. a) Lateral view of the Rando phantom showing vertical distances d_z from the caudal edge of the breast. b) Axial plane of the Rando phantom showing the location of the dosimeters and the distance between them. The location of each film is identified according to the notation: central C, anterior A, posterior P, right R and left L.*

In order to obtain readings above a few cGy even for the farthest dosimeters, five complete treatments (with 8 fractions each) were irradiated consecutively when shielding was used. When shielding was not used, the films were subjected to irradiation from a single treatment (8 fractions).

The films were cut into 3.2 cm × 3.2 cm pieces. Additionally, a set of films belonging to the same lot were irradiated at known doses of 0, 10, 20, 50 and 200 cGy, using a TrueBeam™ linear accelerator (Varian Medical Systems, Palo Alto, CA, USA) with 6 MV beams. Together with the calibration films, the irradiated films were scanned 4 days after irradiation using a model 11000XL scanner (Epson Canada, Ltd., Markham, Ontario, Canada), employing a resolution of 100 dpi and 16-bits per color. Scanned images were then analyzed using the Film QA Pro™

software (Ashland Inc., Wayne, NJ, USA) with the multichannel film calibration method and protocol recommended in the literature by the film and software manufacturers (Micke *et al.*, 2011; Lewis *et al.*, 2012). The dose-response data was fitted by a rational function, as shown in **Figure 6-4**. The quality of the fitting curve indicates the adequacy of these films even in the low dose range. Regions of interest subtending 1.3 cm × 1.3 cm were defined at the center of the irradiated films and the average dose and its standard deviation were determined.

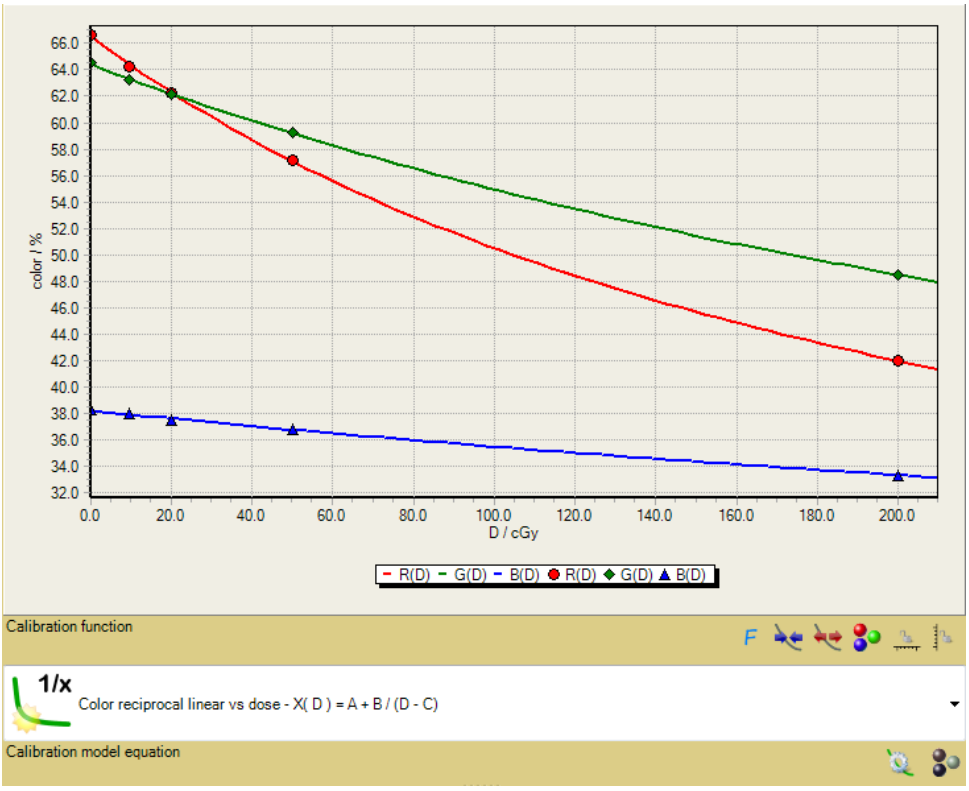

***Figure 6-4**. Calibration data and calibration function for all three channels (R, G, B) of the Gafchromic EBT3 films used in this study to convert pixel values to absorbed dose.*

6.3 Results

6.3.1 Dose distribution in the central region

Table 6-1 shows absorbed doses measured with radiochromic film at central region *C* (see **Figure 6-3b**). The uncertainty of the measurements was obtained considering the standard deviation of the selected ROI, which increases with distance d_z. Roughly, this uncertainty component is 3% at 5 cm and 45% at 25 cm. In addition, the uncertainty of the calibration curve at these low absorbed doses (roughly 3% according to the analysis software) was also considered as well as the uncertainties due to the variation of film sensitivity as a function of photon energy (3% according to Ref. (Brown *et al.*, 2012)). Results are reported without and with shielding. **Table 6-1** also shows the dose ratio for unshielded to shielded HDR-BT. The proposed shielding reduced the radiation exposure by a factor of two near the breast and more than an order of magnitude beyond 20 cm. The effect of shielding increased with increasing distance from the inferior edge of the breast. This was reasonable considering that at the closest axial planes there were still contributions from primary radiation that did not traverse the shielding to reach those regions within the patient. At farther distances, primary radiation was mostly attenuated and dose was mainly comprised of scattered radiation. For the experimental conditions, nearly constant attenuation factors of 15%/cm and 26%/cm (per unit d_z) were observed without and with shielding, respectively.

Absorbed dose was also evaluated without and with shielding at positions in the phantom to estimate dose to the thyroid and the right eye lens. The upper lead shield had no effect on thyroid dose (40 cGy in both cases) as in this case it was not close enough to the thoracic wall to shield primary radiation. However, it shielded the ocular lenses and reduced absorbed dose by a factor of 20 (from 72.8 to 3.6 cGy).

***Table 6-1**. Absorbed dose after a complete (36 Gy) brachytherapy treatment, measured with EBT3 radiochromic films placed between slices of the phantom, at 15 cm from the phantom's back. Distance d_z was measured from the axial slice at the lower edge of the breast. Estimated uncertainties (with coverage factor $k = 1$) are given in parentheses.*

d_z / cm	Mean absorbed dose / cGy		Unshielded to shielded dose ratio
	Without shielding	With shielding	
5.0	96.4 (7.0)	49.6 (2.5)	1.9 (0.2)
7.5	70.8 (5.1)	24.3 (1.4)	2.9 (0.2)
10.0	53.5 (3.5)	13.2 (0.8)	4.1 (0.4)
12.5	40.8 (2.6)	7.0 (0.6)	5.8 (0.6)
15.0	31.4 (2.1)	3.9 (0.4)	8.1 (1.0)
17.5	20.4 (1.6)	2.6 (0.3)	8.0 (1.1)
20.0	15.0 (1.4)	1.4 (0.2)	10.7 (2.1)
22.5	11.8 (1.3)	1.1 (0.3)	11.1 (3.0)
25.0	6.9 (1.3)	0.5 (0.2)	13.8 (6.7)
27.5	4.7 (1.2)	0.4 (0.3)	11.2 (9.1)
30.0	2.7 (1.1)	< 0.1 (0.1)	

***Table 6-2**. Relative difference between absorbed dose at a given point on the axial plane (see **Figure 6-3b**) and absorbed dose D_C at the center C of the same axial plane (from **Table 6-1**), after a complete (36 Gy) brachytherapy treatment.*

Position	Without shielding		With shielding	
	$d_z = 10.0$ cm	$d_z = 20.0$ cm	$d_z = 10.0$ cm	$d_z = 20.0$ cm
Anterior	+44%	+7%	–56%	–39%
Posterior	–46%	–25%	+10%	+39%
Right	+33%	+3%	–7%	+1%
Left	–45%	–47%	–27%	–13%

6.3.2 Dose homogeneity on an axial plane

Table 6-2 shows the measured relative difference between the dose at a given position (*A* (anterior), *P* (posterior), *R* (right) or *L* (left), as seen in **Figure 6-3b**) of an axial plane and the dose in the center *C* of that same plane, for axial planes given by $d_z = 10.0$ cm and $d_z = 20.0$ cm.

The dose heterogeneity observed for HDR ^{192}Ir interstitial breast BT (**Table 6-2**) can be explained considering the inverse-distance square law and the contribution from primary and scattered radiation. The implant was in the right breast and in the anterior part of the phantom. When shielding is used, primary radiation to the anterior part of the abdomen is attenuated and there are contributions only from scattered radiation, which traveled a larger distance to reach the anterior part than the central part. Thus, shielding reduced dose to the anterior part of the phantom. The same argument applied to the left region of the patient abdomen. However, the distance that the scattered radiation has to traverse to reach the posterior part of the phantom is shorter than to the central region. When also accounting for contributions from primary radiation, dose to the posterior part commensurately increases. On the right side of the phantom, the dose variation is nearly negligible when compared to the dose at the center. Without shielding, the inverse-distance square law dominates and regions that are nearer the implant receive a higher dose.

6.3.3 Case report

According to ultrasound measurements, the most proximal part of the fetus was 20 cm below the caudal edge of the breast one week before the planned treatment, with the pubis located at 30 cm. Considering a cranially growth of the fetus of 1 cm per week (Podgorsak *et al.*, 1999) and that the fetus was still mainly in the central region, the highest absorbed dose to be received by the example fetus in this case report was estimated to be 2 cGy, whereas the estimated pubis dose was

less than 0.1 cGy. These values are notably below the 5 cGy constraint that was established for the current study.

6.4 Discussion

6.4.1 Clinical considerations

ASTRO, GEC-ESTRO and ABS have published recommendations for patient selection criteria for APBI (Smith *et al.*, 2009; Polgar *et al.*, 2010; Shah *et al.*, 2013), and identify a high-risk group that should not be treated with APBI outside of clinical trials. This group, among other factors, includes patients younger than 40 to 50 years. These recommendations are based on the fact that young age has been documented to be a dominant adverse prognostic factor for local failure, and that the majority of studies with successful results for APBI included an age restriction for patient selection. However, the association of youth and local failure is based on data after WBI. There are retrospective analyses that do not find differences between the different ASTRO risk groups using APBI (Wilkinson *et al.*, 2013). Sensitive decisions, such as radiation therapy in a pregnant woman, should be made on an individual basis, and always assessing techniques that adequately reduce the fetal dose.

6.4.2 Analysis of the dose as a function of depth

Based on the measured rate of dose falloff as a function of d_z, for HDR ^{192}Ir BT without and with shielding, for the experimental conditions of this study an uncertainty of 1 cm in measuring d_z would result in a dose measurement uncertainty of 15% and 26%, respectively. For the measured values shown in **Table 6-1**, the magnitude of the measurement uncertainties without and with shielding exceeded the rate of dose falloff as a function of d_z at approximately 24 cm. In retrospect,

perhaps the uncertainties at larger distances could have been diminished if extended detector irradiation times were utilized.

However, differences up to 50% compared with the central region are present for a given axial plane with HDR ^{192}Ir BT, as examined in the current study. The exact location of the uterine fundus within a given axial plane is thus the largest contributor to the uncertainty of the evaluated fetal dose. Given the patient setup geometry and practical desire to minimize imaging of the fetus, a robust means of measuring the distance from the fetus to the implant, and the position of the uterine fundus is elusive to satisfy the dose constraint. Radiochromic films seem appropriate to provide quantitative, patient-specific dose measurements as long as adequate signal is generated (through delivery of multiple treatment fractions).

Based on this analysis, it seems reasonable to state that the estimated maximum fetal dose may be evaluated in HDR ^{192}Ir BT with roughly a maximum conservative uncertainty of 50%. This magnitude is considered acceptable for radiation protection applications. If the measured doses with shielding were increased by this factor of 1.5, the maximum fetal dose would still be lower than the 5 cGy constraint considered in this study for distances d_z larger than about 17 cm.

6.4.3 HDR ^{192}Ir BT vs. EBRT

Other published studies on radiotherapy during pregnancy used EBRT techniques. In the current study, interstitial HDR ^{192}Ir BT is proposed as a therapeutic option to treat breast cancer in pregnant patients, as previously argued. From an exposure perspective, differences exist between both radiotherapy techniques when applied to this malignancy. BT offers over EBRT the advantages of a smaller prescribed dose, a smaller number of treatment fractions, and a smaller overall treatment time, which facilitates maintaining the distance between the breast and the fetus as large as possible. However, BT delivers higher doses per fraction, which can increase the fetal toxicity, even though this has not been proven at low

radiation doses (< 10 cGy). On the other hand, peripheral dose in a given axial plane is nearly homogeneous in EBRT, whereas large dose heterogeneities have been observed in this study for the HDR-BT case.

It may be also interesting to compare accumulated fetal doses reported in other studies using EBRT with results obtained in the current study. **Figure 6-5** shows data from the current study (without and with shielding) in the central region (see **Table 6-1**) compared with peripheral doses measured by Martín Rincón *et al.* (2002) when using EBRT without wedges. The latter used tangential 6 MV photon beams, prescribing 50 Gy to the right breast. **Figure 6-5** shows that peripheral dose decreases nearly exponentially in all cases (with an exponential fit provided for the different datasets). The slope of the depth-dose curve is steeper for the case of BT with shielding. When comparing this case with 'EBRT – 6 MV' (from Martín Rincón *et al.* (2002)), it is observed that shielded BT is advantageous from a radiation protection point of view beyond 10 cm from the caudal edge of the breast. It was the only examined treatment modality able to deliver less than 5 cGy as identified as the threshold for fetal toxicity. Differences with reported data by Martín Rincón *et al.* increase up to almost a factor of ten at 25 cm.

The treatment planning system only allows dose calculations near the source (up to roughly 10 cm) and so it cannot be used to validate results obtained in this study. MC simulations could have been performed to evaluate the photon energy spectrum at large distance, thus allowing the use of other detectors such as TLDs. Nevertheless, Venselaar *et al.* (1996) evaluated the peripheral dose rate at large distances from a ^{192}Ir radioactive source, and adjusted the data to a fitting curve. For comparison purposes, this curve has been also represented in **Figure 6-5** after converting the radial distances to d_z distances, as used in the current study. The agreement between the dose values measured in the current study without shielding and those data by Venselaar *et al.* is good considering the uncertainties and the different geometrical conditions in both cases, which validates the results obtained in this study with radiochromic films.

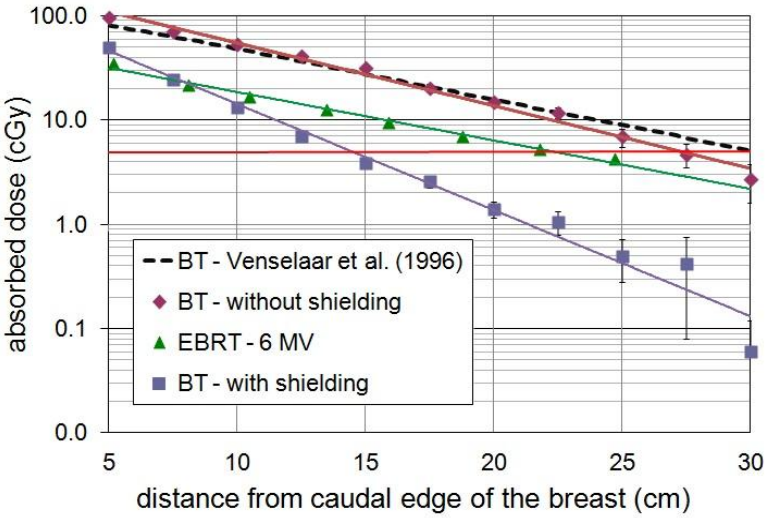

Figure 6-5*. Comparison of accumulated absorbed doses in the central region of a phantom after 50 Gy whole breast treatment using external-beam radiotherapy (EBRT) 6 MV X-rays without any wedges or shielding (from Martín Rincón et al. (2002)), and 36 Gy interstitial brachytherapy (BT) without and with shielding (from the current study). Dose values have been fitted by exponential curves. The curve by Venselaar et al. (1996) has also been plotted. The 5 cGy constraint presumed in this study is depicted with a red horizontal line.*

Other authors have also reported the estimated fetal doses in pregnant patients with breast cancer using EBRT. Ngu *et al.* (1992) treated a woman in the late fetal stage using 6 MV photons and tangential wedged fields, covering the patient's abdomen with 0.9 cm of lead shielding and using an additional lead block below the breast. A prescription dose of 50 Gy was prescribed and the maximum estimated fetal dose was estimated to be 14 cGy to 18 cGy. Van der Giessen (1997) evaluated the peripheral dose as a function of distance in breast radiotherapy for both, open and wedged beams, from photon energies covering ^{60}Co gamma radiation and 6 to 25 MV X-rays. Fetal dose as a function of pregnancy stage was

reported from those measurements for a target dose of 50 Gy. The estimated maximum fetal doses were a factor 5 to 7 and 2 to 4 times higher than in the study by Martín Rincón *et al.* (2002) for the ^{60}Co and 6 MV photon beams, respectively. Antypas *et al.* (1998) treated a 45-year-old woman at the second gestation week, using 6 MV X-ray beams and two opposing tangential fields, prescribing an overall absorbed dose of 46 Gy in 20 fractions. The distance between uterine fundus and the lower limit of the radiation fields was 29 cm, where the estimated absorbed dose was almost 4 cGy, a dose ten times higher than with the method proposed herein for the same distance. On the other hand, Filipov *et al.* (2013) evaluated fetal doses using a "pregnant" humanoid phantom irradiated with 6 MV photon beams and wedges. Measurements were done without and with a combination of 1.5 cm and 4 cm-thick lead blocks, placed around the abdominal region. The minimum fetal doses were achieved when using the dynamic wedge and the lead shielding. In that case, the estimated dose to the uterine fundus was 13.8 cGy, whereas the pubis received 1.8 cGy, which is higher than obtained in the shielded BT approach proposed herein. Also, Kourinou *et al.* (2015) have recently evaluated the fetal dose for a breast treatment with 6 MV tangential beams, without wedges or shielding, performing measurements with an anthropomorphic phantom. The measured fetal doses ranged from 3.9 cGy at 60 cm from the isocenter to 24.8 cGy at 17.5 cm distance, also higher than in the shielded BT case.

While the use of abdominal shielding in EBRT has decreased the peripheral dose, delivery of absorbed dose is dependent on each particular case where dose reductions up to 60% have been achieved (Islam *et al.*, 2001; Filipov *et al.*, 2013). If this dose reduction is applied to the data in **Figure 6-5**, shielded BT would still be advantageous for d_z > 12 cm. Therefore, interstitial breast HDR ^{192}Ir BT with shielding has been demonstrated to be more advantageous for pregnant patients than EBRT, as long as the distance to the uterine fundus is more than 12 cm.

The prescription doses and radiobiological equivalence of the EBRT doses could be adjusted to match the HDR-BT circumstances. However, these alterations would not produce a more fair comparison since the documented prescription doses

represent those that are practically prescribed, and the magnitude of any radiobiological corrections at these low doses are governed by the uncertainties in their methodological assumptions.

Dose thresholds given in the literature do not specify if they should be related to a certain fetal volume, or if they should be considered as a maximum dose or a mean value. From a radiation protection perspective, the maximum dose value is typically used. If the maximum value would not be as important, but rather the mean or a certain dose volume, given the higher gradient of the BT peripheral dose, this BT shielding technique would be even more advantageous (recall that the estimated fetal dose at a distance of 30 cm from the caudal edge of the breast was below 0.1 cGy).

Besides the stated dosimetric advantage of HDR-BT over EBRT, there is another factor to consider, the shielding. The shielding mass proposed herein (over 40 kg) is notably lower than needed for EBRT (over 200 kg (Stovall *et al.*, 1995; Josipovic *et al.*, 2009)) where the abdomen, larger than the breast needs to be shielded. This makes the BT shielding more manageable, with a lower likelihood of accident or couch damage.

The shielding described in the current study also allows protection of the ocular lenses and the healthy contralateral breast, as opposed to those generally used in EBRT, which only cover the abdomen region. The threshold dose above which the cataract formation could occur has been recently reduced to 50 cGy (Bouffler *et al.*, 2012), although a linear relationship with no-threshold dose between probability of cataract formation and lens absorbed dose has not been discarded.

6.4.4 Comparison of ^{192}Ir with other HDR-BT sources

The technique described herein is based on an ^{192}Ir source, the most popular radionuclide for HDR-BT. However, breast BT may be also performed nowadays

with ^{60}Co sources or the 50 kV electronic brachytherapy (eBT) source (Xoft, Inc., Sunnyvale, CA, USA) (Rivard *et al.*, 2006; Mille *et al.*, 2010). Even though photons emitted by ^{60}Co are more energetic than those emitted by ^{192}Ir, up to a distance of about 25 cm from the source, the energy deposited by both radionuclides is nearly the same (^{60}Co deposits a few percent smaller dose than ^{192}Ir (Candela-Juan *et al.*, 2013) in this depth range). Hence, ^{60}Co sources may be also appropriate for this application, although a wider breast shielding might be required.

On the other hand, the eBT source emits photons of a considerably lower energy than ^{192}Ir, and has been shown to give a smaller dose beyond a few centimeters. Through MC simulations, Mille *et al.* (2010) evaluated the absorbed dose to the normal uterus for a reference female phantom being treated to 34 Gy with balloon breast BT. Accumulated dose to the uterus was (11.20±0.03) cGy when using ^{192}Ir and (0.153±0.002) cGy with the eBT sources, with a mean distance of 31.5 cm between the balloon center and uterus. Adjusting results of the current study to match the lower prescription dose and differing implant distances, HDR-BT for the breast without and with shielding at the 34 Gy prescription dose and distance d_z =25 cm provides 6.5 and 0.5 cGy, respectively. Consequently, eBT sources appear more favorable for breast BT than ^{192}Ir for pregnant patients, even without addition of external shielding.

6.4.5 Applicability of the current study to other setups

The treatment modality, patient setup geometry, and shielding proposed in the current study may be an important treatment method to consider, especially at the early gestational ages when the fetus is more sensitive to ionizing radiation and there is a higher probability to fetal death, malformations or mental retardations (NCRP, 2013). However, results presented herein are valid for the specific conditions reported in section 6.2.2 and for the shielding described in section 6.2.3, and so they should be carefully extrapolated to other conditions or systems.

Considering treatment delivery, the geometrical setup used in the current study is based on a patient seated in a chair with the breast over a table and lead shielding surrounding the breast. An alternative setup could be the patient lying in the prone position, placing the breast to be treated inside a leaded box. This could distance the implant from the thoracic wall, thus achieving a higher attenuation of primary radiation. A lateral decubitus setup could be also considered, which may be more comfortable than the prone position, with the treated breast positioned closest to the shielding. Both of these two setup options should be evaluated from a dosimetric perspective before clinical use.

Finally, the treatment method described herein could also be applied to skin lesions of the extremities in which similar shielding could protect the fetus from primary radiation, thus achieving similar or even better dose reductions than in the current study.

6.5 Conclusions

The optimized delivery of radiation therapy to pregnant patients with breast cancer is a demanding task in which the main aim should be tumor control while constraining dose delivered to the fetus beneath a fixed value. Previous studies evaluated the fetal dose delivered by EBRT. In the current study, HDR ^{192}Ir BT has been proposed as an alternative method to reduce the fetal exposure. A specific patient setup and shielding design has been suggested. The peripheral dose has been evaluated as a function of the distance to the lower edge of the breast. Comparison with previously reported fetal doses from EBRT techniques showed a dosimetric advantage of shielded HDR-BT over EBRT beyond 10 cm. This option is thus an alternative method to be considered as long as the pathologic factors included in societal recommendations are satisfied, especially at the early gestational ages when the fetus is most sensitive to ionizing radiation and deterministic effects.

Chapter 7. GENERAL DISCUSSION

From **Chapter 2** to **Chapter 6** we have presented five different studies related to the radiation protection of patients undergoing HDR brachytherapy. Each of these chapters has a specific discussion section and so the reader is referred to those sections for a deeper debate on each of the previous topics considered. In this section, a general discussion is presented relating the different studies of this dissertation.

Chapter 2 was the first study performed, and it was of relevance for the others. This chapter evaluated the peripheral dose for a patient undergoing HDR BT, either with ^{60}Co or ^{192}Ir sources. Because relative dosimetric differences around ^{60}Co and ^{192}Ir sources are less significant than prescription technique and the optimization parameters, no clinically significant differences exist between them. This means that, from a practical point of view where the goal is dose coverage of the lesion and dose minimization to healthy tissue, performing an HDR BT treatment with a ^{60}Co source is equivalent to performing a treatment with a ^{192}Ir source as long as their specific air-kerma strength or activity is considered. In other words, the same BT treatment plan (the same number of catheters and dwell positions) can be used for both sources with equivalent clinical results. Biological differences between them have been also stated to be negligible (Richter *et al.*, 2008; Strohmaier *et al.*, 2011). This makes the comparison between these two sources independent on the technician and optimization parameters, which allows us to make a fair comparison between them, as presented in **Chapter 2**. MC simulations performed in this study showed that, from a patient radiation protection point of view, there is an advantage of ^{60}Co over ^{192}Ir up to ~25 cm, whereas ^{192}Ir is increasingly advantageous beyond that distance. From the literature review performed in **Chapter 3** it was found that most of the induced tumors appear within the high dose region. Thus, it might be expected from a theoretical point of view a slight increase of tumor induction with ^{192}Ir than with ^{60}Co, although the relative dose difference between these two sources is below 10% within this high dose region to healthy tissues and so in a practical point of view, this difference might result in negligible differences in the rate of cancer induction. Between 30 cm and

80 cm from the implant, organ equivalent doses are well below 0.1 Sv for common prescription doses, for which the probability to induce a tumor has been shown to be near the background level and with high uncertainties. Thus, even though at these large distances differences between the two sources for organ equivalent doses can be up to a factor of five, this is expected to result in negligible differences when considering the probability of cancer induction.

The second important point of discussion from **Chapter 2** is the difference between different radiation techniques in terms of doses to healthy tissues. Equivalent doses here obtained were also compared with estimations made from EBRT with 3D-CRT, IMRT or proton therapy. As recently stated by a group of the GEC-ESTRO, second primary cancer risks must be also considered when deciding which patients should be irradiated and which techniques should be used (Murray *et al.*, 2014). A recent study by Georg *et al.* (2014) has evaluated the dose to the nearest organs (bladder wall, rectal wall, femoral heads, urethra and pelvic tissue) of a prostate treatment, considering different treatment options: volumetric modulated arc therapy, intensity-modulated proton therapy, intensity-modulated carbon-ion therapy, LDR brachytherapy (with ^{125}I sources) and HDR brachytherapy (with a ^{192}Ir source). It was concluded that BT techniques were clearly superior in terms of rectal wall, bladder wall, and normal tissue sparing, with even lower values for HDR-BT. This study considered ten patients and it might not be generalizable since large differences exist among the literature and between different patients. In our study, similar organ doses were found between these different techniques for the nearest organs. Thus, it can be concluded that differences might be institution and patient dependent for the nearest organs. In our study, we also compared these techniques for large distances, and it is clear that BT is superior as the distance increases.

The fact that the studies by GEC-ESTRO (Murray *et al.*, 2014) and Georg *et al.* (2014) are very recent denote the current importance and concern of the scientific and medical society about cancer risks and dose to healthy tissues resulting from different radiation techniques. In **Chapter 2** and **Chapter 3** we hope

to have been contributed to this aspect by comparing different sources and different radiation techniques in terms of second cancer risks, and to have been done an overview of the risks. Due to the large uncertainties in cancer risk estimates at low radiation doses, we do not advocate the use of MC simulations (highly time-consuming) for individual patients.

Despite **Chapter 2** was applied to a prostate carcinoma, results can be extended to other treatments such as the gynecological ones, which is the most extended application of HDR brachytherapy. The comparison between ^{192}Ir and ^{60}Co is also of application for any other treatment region.

Results from **Chapter 3** concerning the current limitations of knowledge on tumor induction at low radiation doses motivated our interest in the study presented in **Chapter 4**. Epidemiologists and medical physicists from Sweden contacted us to perform MC simulations to characterize radium sources widely used during the first part of last century. As stated by the UNSCEAR committee in 2013, the extensive group of children treated with ^{226}Ra sources may be very helpful to determine the relationship between a specific late hazard effect and the absorbed dose (UNSCEAR, 2013). Thus, while the topic might seem esoteric, the lack of accurate dosimetric data for the sources that were used in Sweden, and an evaluation of uncertainties, made it difficult to take the most profit of their extended data on patient follow-up. Therefore, it is expected that the dosimetric data presented in **Chapter 4** are important for retrospective epidemiological studies.

Reducing the high absorbed doses to organs near the treatment volume is of importance to improve the treatment outcome in terms of toxicity. This was the aim of **Chapter 5** when applied to the treatment of surface lesions. Typically moulds and flaps are used on superficial skin brachytherapy for treatment depths up to about 5 mm. The use of superficial skin shielding applicators is an efficient solution because these reduce significantly the absorbed dose to the surrounding healthy tissues. Currently there are radionuclide based HDR ^{192}Ir applicators as well as electronic sources. All these applicators restrict the useful beam to cross-sectional

circular beams of some specific diameters. On the other hand, the use of moulds and flaps allows producing irregular dose distributions, which might be of more interest in some cases. In **Chapter 5** we extended the advantage of shielding applicators to moulds and flaps by adding a lead shield above the implant. For example, shields might be placed on the nose surface to attenuate radiation to the eye lens from a nasal implant, or around the breast to protect the thyroid from direct radiation coming from a breast treatment. The study presented in **Chapter 5** has allowed making this efficiently by evaluating the bolus thickness required to be placed between the implant and the lead shielding in order to avoid a large surface overdose due to electron contamination and backscattering in the lead shield. This study also allowed evaluating the dose reduction near the shielding. Thus, this study and the methodology proposed is easy, economical and effective to implement in clinical practice to allow irregular dose distributions in the surface while shielding some of the nearest organs, as achieved with specifically designed surface applicators.

The study presented in **Chapter 6** concerning the reduction of the fetal dose in a pregnant patient with breast cancer was motivated by the experience and knowledge acquired from the other studies of this thesis. It was March 2013 when a pregnant patient with breast cancer was submitted to the radiotherapy oncology department of La Fe University and Polytechnic Hospital (Valencia, Spain). Besides the tumor control, the reduction of the fetal dose was a priority. To our knowledge, all previously reported cases of radiotherapy applied to pregnant patients were based on EBRT. However, **Chapter 2** had revealed that BT was advantageous over EBRT at large distances. In addition, we had recently evaluated the influence of lead shielding, and knew how to avoid surface overdose. **Chapter 5** also allowed obtaining the thickness of the lead shielding required to absorb most of the primary beam that could contribute to increase notably the absorbed dose to the fetus, and this information was used to build the shielding presented in **Chapter 6**. The results with this setup and shielding were very promising when compared with previously reported data from EBRT, allowing the reduction of the fetal dose in

comparison with EBRT for distances between the caudal edge of the breast and the uterine fundus larger than 10 cm. Differences reach more than one order of magnitude at 30 cm distance. In 1983 it was estimated that 1 out of 1000 pregnant women were diagnosed with cancer (Donegan, 1983). This number is expected to increase as the age of pregnancy increases. Many of those patients need radiotherapy, and so the proposed setup and shielding can be of great benefit for them.

SUMMARY

The use of HDR ^{192}Ir brachytherapy has increased substantially since the 1990s and it is expected to grow even more in the near future (Guedea, 2014), thus becoming a fundamental therapeutic tool. Compared to EBRT, BT has the advantages of a rapid fall off of dose around the sources and shorter overall treatment duration, herein reducing the risk of tumor repopulation. However, the dose distribution is not homogeneous and accuracy in source positioning is critical (Gerbaulet *et al.*, 2002).

During radiation therapy not only the tumor volume absorbs dose, but also all the remaining tissues of the body. This may result in some cases in acute, sub-acute and/or long-term side-effects, which depend on the location of the target volume, the amount of absorbed dose and dose rate, and the type of radiotherapy that is used. Reducing the absorbed dose to healthy tissues will surely improve the treatment success.

Due to improved long-term survival rates, long-term side-effects such as the induction of a second primary tumor related to the radiation treatment are becoming increasingly important. The scientific community tries to establish a relationship between organ equivalent doses and the probability that a specific tumor is induced. If the relationship were known, the secondary cancer induction from a typical brachytherapy treatment could be obtained and compared with the probability from other radiation techniques. The AAPM Task Group 158 and the NCRP Scientific Committee have excluded brachytherapy from their studies due to lack of data (Xu

et al., 2008), which confirms the necessity to make a complete study regarding peripheral doses from HDR brachytherapy.

The goal of this thesis was threefold. Firstly, to evaluate the peripheral dose in a typical clinical scenario and discern which HDR radionuclide is more advantageous from a patient radiation protection point of view (see **Chapter 2**). Secondly, the risk of secondary malignancies induced by the BT treatment was reviewed (see **Chapter 3**). Concerning to this second point, because epidemiological data with higher dose estimation accuracy are needed, we provided a more accurate dosimetry based on the currently used formalism for old radium brachytherapy sources, for which a large and long patient follow-up exists (see **Chapter 4**). Thirdly, we aimed to reduce the peripheral dose received by organs and tissues near the implant using specifically designed implant shielding (see **Chapter 5** and **Chapter 6**). Below is a summary of the information contained in each of the chapters of this dissertation.

In **Chapter 1** a general introduction extending the information that has been summarized in the previous paragraphs was presented, along with the objectives of the thesis and an outline of it.

In **Chapter 2** the peripheral dose to a patient undergoing HDR brachytherapy applied to a localized prostate carcinoma was obtained for both, ^{60}Co and ^{192}Ir sources. These are nowadays the only commercially-available radionuclides for HDR BT. MC simulations in GEANT4 were performed using a voxelized phantom described in ICRP Publication 110, which reproduces masses and shapes from an adult reference man defined in ICRP Publication 89. Point sources of ^{60}Co or ^{192}Ir with photon energy spectra corresponding to those exiting their capsules were placed in the center of the prostate, and equivalent doses per clinical absorbed dose in this target organ were obtained in several radiosensitive organs. Values were corrected to account for clinical circumstance with the source located at various positions with differing dwell times throughout the prostate. This methodology was repeated for a homogeneous water phantom. A database of organ

equivalent doses when applying HDR brachytherapy to the prostate with either ^{60}Co or ^{192}Ir was provided.

The results were that, for the nearest organs considered (bladder, rectum, testes, small intestine, and colon), equivalent doses given by a ^{60}Co source were roughly 10% smaller than from ^{192}Ir. However, as the distance increases, the more penetrating gamma rays produced by ^{60}Co deliver higher equivalent doses. Thus, according to physical considerations, ^{192}Ir is dosimetrically advantageous over ^{60}Co sources at large distances, but not in the closest organs. The overall result is that effective dose per clinical absorbed dose from a ^{60}Co source (11.1 mSv/Gy) is roughly 10% lower than from a ^{192}Ir source.

Regarding the differences between calculations in a heterogeneous and a homogeneous water phantom, it was concluded that equivalent doses were the same for those soft tissues closer to the prostate than about 30 cm. As the distance increased, the differences of photoelectric effect in water and soft tissue, and appearance of other materials such as air, bone or lungs, produced variations between both phantoms which were at most 35% in the considered organ equivalent doses.

Finally, peripheral doses from HDR brachytherapy sources were compared with reported values from proton therapy and IMRT. Damage to distant healthy organs per clinical absorbed dose is lower with brachytherapy than with IMRT or protons, although the overall effective dose per Gy given to the prostate was very similar. Given that there are several possible fractionation schemes, which result in different total amounts of therapeutic absorbed dose, advantage of a radiation treatment (according to equivalent dose to healthy organs) is treatment and facility dependent, although BT is advantageous over EBRT for the furthest organs.

In **Chapter 3**, the current knowledge on cancer induction from ionizing radiation was reviewed. It was aimed to determine if a well established relationship between organ equivalent dose and probability of cancer induction was already

known, which could facilitate and improve the comparison between different radiation modalities performed in the previous chapter.

Graphically, three main areas can be identified in this dose–effect curve (Hall *et al.*, 2004). In the central zone (between 0.1 Sv and 2.5 Sv) there appears to be a linear relationship in which, as the organ equivalent dose increases so does the probability of tumor induction.

At higher organ equivalent doses (> 2.5 Sv), radiation induced cell sterilization, cell repopulation, and proliferation may cause a deviation from a linear dose response (Nguyen *et al.*, 2015). Phenomenological risk models based on fitting parameters have been applied to estimate the risk of inducing a tumor in organs inside the primary radiation field, *i.e.*, at doses in excess of 2.5 Gy. In particular, recent studies have applied a model developed by Schneider (2009), which is based on the linear-quadratic formula, to estimate the outcome of different treatment modalities (Nguyen *et al.*, 2015). Linear, linear-exponential, and plateau models have been also used (Abo-Madyan *et al.*, 2014). A review study by Xu *et al.* (2008) showed that the cumulative risk for the development of second cancers has been estimated as ranging from 5% to 12% over a 25 year follow-up interval, although there exists a high dispersion of data. The model parameters have been determined with limited data and, therefore, uncertainties will limit the model predictions. Nguyen *et al.* (2015) have recently estimated that the uncertainties associated with model predictions are higher than 100%. This implies that, currently, it might not be feasible to reliably predict cancer risks based on treatment plan information and phenomenological risk models.

At low radiation doses (less than 0.1 Sv) also different models have been proposed based on observations. Because of its simplicity, reasonability, and conservative approach, international committees such as the ICRP and the NCRP recommended extrapolating the linear relationship to the lowest dose range. However, the available evidence for this has not been statistically significantly better for predicting cancer than other methods based on a threshold dose (Fletcher

et al., 2013) owing to high background incidence cases. Uncertainties in past epidemiological data of irradiation exposures within the diagnostic dose range did not rule out a possible threshold dose below which no excess cases of cancer appeared. This threshold dose might be within the range of 10 to 60 mSv (Xu *et al.*, 2008; Pauwels *et al.*, 2011). Thus, the risks, if existent, are of the same order of magnitude than background levels.

From a deep literature review of studies concerning radiation therapy and cancer risks for organs receiving low radiation doses, Xu *et al.* (2008) concluded that many of the past dosimetry studies were based on inconsistent and sometimes confusing dose quantities, which reduces the possibility that they can be used to perform more sophisticated epidemiological studies. We thus conclude that retrospective risk assessments of ionizing radiation require more reliable dosimetric data and epidemiological studies, as well as an estimate of their uncertainty before general conclusions can be established.

During the first part of the 20th century, ^{226}Ra was the most used radionuclide for brachytherapy. Thus, like survivors of the atomic bombs, data of children treated with ^{226}Ra sources may be very helpful to determine the relationship between a specific late hazard effect and the absorbed dose. As recently noted by the UNSCEAR committee, the latter is of current interest in the search for improved knowledge on dose-response relationships for cancer induction and other late effects due to exposure to ionizing radiation in early childhood (UNSCEAR, 2013). Related to this, Sweden has long held a complete registry on cancer incidence coupled to unique citizen ID numbers. Together with detailed knowledge about the children that underwent ^{226}Ra treatment, these data are of interest to use in research on late radiation effects. However, earlier dosimetric data for the sources that were used in Sweden were restricted. The aim of **Chapter 4** was to dosimetrically characterize two ^{226}Ra sources, commonly used in Sweden during the first half of the 20th century, for retrospective dose-effect studies, as requested by Swedish epidemiologists.

An 8 mg ^{226}Ra tube and a 10 mg ^{226}Ra needle, used at Radiumhemmet (Karolinska University Hospital, Stockholm, Sweden) from 1925 to the 1960s, were modeled in two independent MC radiation transport codes: GEANT4 and MCNP5. Absorbed dose and collision kerma around the two sources were obtained, from which the TG-43 parameters that can be implemented in current planning systems were derived for the secular equilibrium state. Furthermore, results from this dosimetric formalism were compared with results from a realistic MC simulation with a superficial mould constituted by 5 needles inside a glass casing, placed over a water phantom, trying to mimic a typical clinical set-up. The aim of this comparison was to validate the use of dosimetric data in the format of TG-43 parameters for surface treatments, where lack of backscattering at the water surface could give place to errors in the dose calculation. Furthermore, calculated absorbed doses using the TG-43 formalism were also compared with previously reported measurements and calculations based on the Sievert Integral. Finally, the dose rate at large distances from a ^{226}Ra point-like-source placed in the center of 1 m radius water sphere was calculated with GEANT4, and data were fitted by an analytical function to allow estimation of absorbed dose at large distances from the sources.

From this study, TG-43 parameters (including $g_L(r)$, $F(r,\theta)$, Λ and s_K) have been provided for epidemiological studies, and the fitting parameters of a mathematical curve that provides the dose rate between 10 cm and 60 cm from the source have been calculated. Results from TG-43 formalism are consistent within the treatment volume with those of a MC simulation of a typical surface clinical scenario. Comparisons with reported measurements made with TLDs show differences up to 13% along the transverse axis of the radium needle. It was estimated that the uncertainty associated to the absorbed dose within the treatment volume is 10% to 15%, whereas uncertainty of absorbed dose to distant organs is roughly 20% to 25%.

The results provided in **Chapter 4** facilitate retrospective dosimetry studies of ^{226}Ra using modern treatment planning systems, which may be used to improve knowledge on long term radiation effects. It is surely important for the

epidemiologic studies to be aware of the estimated uncertainty provided here before extracting their conclusions.

The following two chapters of this dissertation were aimed to reduce the peripheral dose received by organs and tissues near the implant using specifically designed implant shielding. In particular, in surface HDR brachytherapy with either ^{60}Co, ^{192}Ir, or ^{169}Yb sources (the latter has potential as HDR source and might be available in the future), some radiosensitive organs near the surface may be exposed to high absorbed doses. This may be reduced by covering the implants with a lead shield on the body surface, which has two main dosimetric consequences. Firstly, backscattering produces a dose enhancement in the patient in the vicinity of the shielding. Secondly, photon absorption reduces dose above the shield, downstream from the distal surface of the barrier. Radiation transmission data had not been evaluated in surface or interstitial BT for a typical clinical scenario. **Chapter 5** was aimed to evaluate the dosimetric perturbation produced by lead shields that are used in some surface HDR BT treatments.

Monte Carlo simulations in GEANT4 were performed for the three radionuclides placed at a single dwell position. Four different shield thicknesses (0, 3, 6, and 10 mm) and three different source depths (0, 5, and 10 mm) in water were considered, with the lead shield placed at the phantom surface. From these simulations, backscatter dose enhancement and transmission data were obtained. Finally, results were corrected to account for a realistic clinical case with multiple dwell positions.

From this study it was concluded that the range of the high backscatter dose enhancement in water is 3 mm for ^{60}Co and 1 mm for both ^{192}Ir and ^{169}Yb. Thus, as stated in **Chapter 5**, the backscatter overdose produced by the lead shield can be avoided just using a few millimeters of bolus, herein justifying the use of lead shields. On the other hand, transmission data for ^{60}Co and ^{192}Ir are smaller than those reported by Papagiannis *et al.* (2008) for brachytherapy facility shielding. For ^{169}Yb, the difference is negligible.

The previous study is of application in several clinical scenarios. For example, shields might be placed on the nose surface to attenuate radiation to the eye lenses from a nasal implant, or around the breast to protect the thyroid from direct radiation coming from a breast treatment. Another application of the previous approach is to minimize the fetal dose in a pregnant patient with breast cancer needing radiotherapy.

Chapter 6 aimed to assess the radiation dose to the fetus of a pregnant patient undergoing HDR ^{192}Ir interstitial breast brachytherapy, and to design a new patient setup and lead shielding technique that minimizes the fetal dose. To do that, the pregnant woman was planned to be seated in a chair with the breast over a table and inside a leaded box specifically designed to protect the fetus. A total of 36 Gy in 8 fractions were prescribed. The shielding design consisted of a 3.5 cm thick layer of lead placed between the breast and the table. Thus, during the treatment, the breast rested over this lead shield. In addition, two lateral pieces of lead (3 cm thick each) were added. One of the lateral layers had a port through which the transfer tubes were connected to the catheters. The lateral blocks allowed placing an extra piece of lead (2.5 cm thick) above the breast, parallel to the first layer, aiming to reduce primary radiation to the thyroids and eye lenses. In addition, in order to minimize the transit dose when the ^{192}Ir source exits and returns to the remote afterloader, a hollow lead tube was made, which covered the transfer tubes. Finally, a layer of water-equivalent material (1 mm thick) was placed between the lead shielding and the patient skin to minimize the backscattering and electron contamination coming from the shield, as had been determined in the previous chapter.

Dose measurements were done with radiochromic films that were placed between the slices of an anthropomorphic phantom modeling the patient. Dose variation as a function of distance from the implant volume as well as dose homogeneity within a representative slice of the fetal position was evaluated without and with shielding. Results with the previous setup were very promising. With shielding, the peripheral dose ranged from 50 cGy at 5 cm from the caudal

edge of the breast to < 0.1 cGy at 30 cm. The shielding reduces absorbed dose by a factor of two near the breast and more than an order of magnitude beyond 20 cm. The dose is heterogeneous within a given axial plane, with variations from the central region within 50%. From a literature analysis, it was also observed that interstitial HDR ^{192}Ir brachytherapy with breast shielding can be more advantageous than EBRT from a radiation protection point of view, as long as the distance between the caudal edge of the breast and the uterine fundus is higher than about 10 cm. At 30 cm distance, absorbed dose is more than a factor of ten smaller with shielded HDR brachytherapy than with EBRT. Furthermore, the weight of the shielding here proposed is notably lower than that needed in EBRT. Therefore, the shielded breast brachytherapy setup presented in **Chapter 6** may benefit pregnant patients needing localized radiotherapy, especially during the early gestational ages when the fetus is more sensitive to ionizing radiation.

Finally, **Chapter 7** presented a general discussion previous to this summary.

SUMMARY IN SPANISH / *RESUMEN EN ESPAÑOL*

La braquiterapia (BT) es una modalidad de tratamiento de radioterapia en la que se coloca una fuente radiactiva encapsulada cerca, en contacto o en el interior del volumen a tratar. La desintegración de esta fuente produce la emisión de energía, lo que puede dar lugar a la muerte celular. Una dosis absorbida muy elevada (la dosis absorbida se define como la energía absorbida por unidad de masa) se deposita en un corto período de tiempo y en un pequeño número de fracciones. Para poder realizar un tratamiento de BT se requiere que el volumen de tratamiento sea accesible y bien delimitado en tamaño y forma. La BT se utiliza comúnmente como una modalidad de tratamiento eficaz para el cáncer de cuello uterino, de próstata, de mama y de piel. También ha demostrado ser eficaz para tratar tumores de la región del cerebro, cabeza y cuello (por ejemplo, labios o lengua), ojo, la tráquea y los bronquios, el aparato digestivo y el tracto urinario (por ejemplo, la vejiga, el recto, el ano, la uretra o el pene), el tracto reproductor femenino (útero, vagina y vulva), y otros tejidos blandos (Gerbaulet *et al.*, 2002).

En función de la tasa de dosis D alrededor de la fuente radiactiva empleada, la BT se clasifica en: BT de alta tasa de dosis (HDR) (D>12 Gy/h), BT de media tasa de dosis (MDR) (D=2-12 Gy/h)), BT de tasa de dosis pulsada (PDR) (pulsos cortos de radiación, generalmente una vez una hora) y BT de baja tasa de dosis (LDR) (D<2 Gy/h). En detrimento de la LDR, la HDR se está convirtiendo hoy en día en la modalidad más extendida en todo el mundo (Guedea, 2014). Las ventajas de la HDR sobre la terapia LDR incluyen la reducción de exposición del personal a

radiación ionizante, la reducción del tiempo de tratamiento global, la aplicación del tratamiento de forma remota, así como un ahorro económico (Bastin *et al.*, 1993). Además, para el caso particular de la braquiterapia de próstata, se minimizan algunos de los problemas comunes relacionados con los implantes de semillas permanentes, tales como la incapacidad para corregir la posición de las semillas, incapacidad para optimizar la dosis absorbida una vez que las semillas están en su lugar, y la discrepancia entre la distribución de dosis planeada y la definitiva (Demanes *et al.*, 2014). Por contra, se ha estimado que con la BT HDR existe un mayor riesgo de efectos secundarios (Dale, 1985). Por todas estas razones, la terapia de HDR es la técnica de BT considerada en este estudio que trata la protección radiológica del paciente.

El uso de la BT HDR se ha incrementado sustancialmente desde la década de 1990 y se espera que crezca aún más en un futuro próximo (Guedea, 2014), convirtiéndose así en una herramienta terapéutica fundamental. En comparación con la radioterapia externa (EBRT), la BT tiene la ventaja de una rápida caída de la dosis con la distancia a la fuente y una duración del tratamiento total menor, siendo así un tratamiento más localizado y que reduce el riesgo de repoblación tumoral. Sin embargo, la distribución de dosis no es homogénea y la precisión en el posicionamiento de la fuente radiactiva es crítica (Gerbaulet *et al.*, 2002).

Durante un tratamiento de radioterapia no sólo el volumen del tumor absorbe dosis, sino también todos los tejidos restantes del cuerpo, en mayor o menor medida. Órganos cercanos o en contacto con el tejido a irradiar pueden recibir también altas dosis de radiación, mientras que el tejido más alejado se expone a dosis de radiación bajas. Esto puede resultar en algunos casos en efectos secundarios agudos, sub-agudos y/o efectos de largo plazo. La aparición de estos efectos depende de la ubicación del volumen a tratar, de la cantidad de dosis prescriba, de la tasa de dosis, y del tipo de radioterapia que se utiliza. Es seguro que la reducción de la dosis absorbida por los tejidos sanos mejora el éxito del tratamiento en relación a las secuelas.

Debido al incremento de la tasa de supervivencia a largo plazo, los efectos secundarios tales como la inducción de un tumor secundario están convirtiéndose cada vez más importantes. La comunidad científica intenta establecer una relación entre dosis equivalentes a órganos y la probabilidad de que se induzca un tumor. Si se conociera dicha relación, se podría obtener cuál es la probabilidad de inducir un tumor tras un tratamiento típico de braquiterapia, comparándola con la probabilidad derivada de otras técnicas de tratamiento con radiaciones. El Grupo de Trabajo 158 de la Sociedad Americana de Físicos Médicso (AAPM) y el Comité Científico del Consejo Nacional Americano de Protección y Medición de Radiación (NCRP) han excluido la braquiterapia de sus estudios de tumores radio inducidos debido a la falta de datos (Xu *et al.*, 2008), lo que confirma la necesidad de realizar un estudio completo con respecto a las dosis periféricas en braquiterapia HDR.

Tres son los objetivos principales de esta tesis. En primer lugar, evaluar la dosis periférica en un escenario clínico típico de BT HDR y discernir qué fuente radiactiva de HDR es más ventajosa desde el punto de la protección radiológica del paciente (véase el **Capítulo 2**). En segundo lugar, se pretende realizar una revisión bibliográfica sobre el riesgo de inducir un tumor secundario tras un tratamiento de BT (véase el **Capítulo 3**). Con respecto a este segundo punto, ya que se necesitan más datos epidemiológicos con mayor precisión en la estimación de la dosis, llevamos a cabo una caracterización dosimétrica precisa de antiguas fuentes de ^{226}Ra para las cuales existe un extenso y completo seguimiento, basada en el formalismo utilizado actualmente para fuentes de BT (véase el **Capítulo 4**). En tercer lugar se tiene como objetivo reducir la dosis periférica recibida por los órganos y los tejidos cercanos al implante de BT HDR, utilizando para ello blindajes que hemos diseñado especialmente para este objetivo (véase el **Capítulo 5** y el **Capítulo 6**).

A continuación se muestra un resumen de la información contenida en cada uno de los capítulos de esta tesis.

En el **Capítulo 1** se presentó una introducción general que extiende la información que se ha resumido en los párrafos anteriores. Además, se introdujeron los objetivos de la tesis y un esbozo de lo contenido en cada uno de ellos.

En el **Capítulo 2** se obtuvo la dosis periférica en un paciente sometido a BT HDR aplicada a un carcinoma de próstata localizado tanta con fuentes de ^{60}Co como de ^{192}Ir. Estos dos radionúclidos son hoy en día los únicos comercialmente disponibles para HDR BT. Para llevar a cabo el objetivo de este estudio se realizaron simulaciones MC con GEANT4, utilizando un maniquí voxelized proporcionado por la Publicación 110 de la Comisión Internacional de Protección Radiológica (ICRP). Este maniquí reproduce las masas y formas de todos los órganos del hombre adulto considerado de referencia. Las fuentes puntuales de ^{60}Co o ^{192}Ir se colocaron en el centro de la próstata y se simuló la emisión de fotones con un espectro de energía igual al que sale de las fuentes reales. A partir de estas simulaciones se obtuvo la dosis equivalente en todos los órganos del cuerpo, normalizado por la dosis absorbida por la próstata. Los valores fueron corregidos para tener en cuenta la circunstancia clínica según la cual la fuente no se lleva a una única posición en el centro de la próstata, sino que se sitúa en varias posiciones a lo largo de toda la próstata, con diferentes tiempos de permanencia en cada una de estas posiciones. Esta metodología se repitió para un maniquí igual que el anterior, pero en el que la composición de todos los vóxeles se sustituyó por agua. Esto último tenía por objetivo comparar los resultados dosimétricos en un maniquí realista respecto a cuándo se considera todo el cuerpo hecho de agua, que es la situación actual en la planificación de tratamientos de braquiterapia.

Este estudio proporcionó una base de datos de dosis equivalentes a órganos tras aplicar braquiterapia HDR a la próstata, ya sea con fuentes de ^{60}Co o de ^{192}Ir. Lo que se observó fue que en los órganos cercanos considerados (vejiga, recto, testículos, intestino delgado y colon), las dosis equivalentes dadas por la fuente de ^{60}Co son aproximadamente un 10% inferiores a las derivadas de un tratamiento con ^{192}Ir. Sin embargo, a largas distancias (más de 30 cm aproximadamente), el ^{60}Co proporciona dosis equivalentes superiores debido a una mayor energía media de los

fotones que emite. Así, de acuerdo a las consideraciones físicas, el ^{192}Ir es dosimétricamente ventajoso sobre el ^{60}Co a grandes distancias, pero no en los órganos cercanos. El resultado global es que la dosis efectiva por dosis clínica absorbida en la próstata es 11.1 mSv/Gy cuando se hace uso de una fuente de ^{60}Co, y un 10% aproximadamente inferior cuando se hace uso de una fuente de ^{192}Ir.

En cuanto a las diferencias entre los cálculos en un maniquí heterogéneo y un maniquí homogéneo de agua, se concluyó que las dosis equivalentes eran iguales para los tejidos blandos que estaban a un máximo de unos 30 cm de la próstata, es decir, cerca del implante. A medida que aumentaba la distancia, las diferencias de efecto fotoeléctrico en el agua y los tejidos blandos, y la aparición de otros materiales tales como aire, hueso o pulmones, producen variaciones entre ambos maniquíes, alcanzado las diferencias entre la dosis equivalente a órganos un 35% en el peor de los casos.

Finalmente, las dosis periféricas derivadas de tratamientos con fuentes de BT HDR se compararon con los valores reportados en la literatura para tratamientos con protones y radioterapia externa de intensidad modulada (IMRT). Se vio que el daño a los órganos sanos distantes es menor con braquiterapia que con IMRT o protones, aunque la dosis efectiva total por Gy a la próstata es muy similar en los tres casos. Dado que hay varios posibles esquemas de fraccionamiento, que resultan en diferentes cantidades totales de dosis absorbida terapéutica, la ventaja de un tipo de tratamiento de radioterapia frente a otro (según dosis equivalente a órganos sanos) es dependiente del propio tratamiento y del fraccionamiento utilizado en la instalación, aunque en cualquier caso la BT es ventajosa sobre la EBRT y los protones para los órganos más alejados.

En el **Capítulo 3** se revisa el conocimiento actual sobre la inducción de cáncer debido a las radiaciones ionizantes. El objetivo fue determinar si existía una relación bien establecida entre la dosis equivalente a órganos y la probabilidad de inducción de cáncer, lo que podría facilitar y mejorar la comparación entre diferentes modalidades de tratamiento de radiación realizada en el capítulo anterior.

Se pueden identificar tres regiones diferentes en el gráfico que relaciona la dosis equivalente a órgano con la probabilidad de inducir un tumor (Hall *et al.*, 2004). En la zona central (entre 0.1 y 2.5 Sv) hay una relación lineal según la cual, un aumento de la dosis absorbida incrementa proporcionalmente la probabilidad de inducir un tumor.

A mayores dosis equivalentes a órganos (> 2.5 Sv), los efectos de esterilización celular debida a la radiación, la repoblación de células y la proliferación pueden causar una desviación en la respuesta lineal (Nguyen *et al.*, 2015). Para realizar estimaciones en los órganos que se encuentran dentro del campo de radiación y que, por lo tanto, reciben más de 2.5 Sv, los investigadores han aplicado modelos de riesgo fenomenológicos basados en diversos parámetros de ajuste. En particular, estudios recientes han aplicado un modelo desarrollado por Schneider (2009) que se basa en la fórmula lineal-cuadrática para estimar el resultado de diferentes modalidades de tratamiento (Nguyen *et al.*, 2015). Otros modelos como el de meseta-lineal y lineal-exponencial también han sido utilizados para hacer estimaciones (Abo-Madian *et al.*, 2014). Un estudio de revisión realizado por Xu *et al.* (2008) mostró que el riesgo acumulado para el desarrollo de tumores secundarios se ha estimado que va desde el 5% al 12% tras un intervalo de seguimiento de 25 años, aunque existe una alta dispersión en los datos. Los parámetros del modelo se han determinado con datos limitados y, por tanto, las incertidumbres limitarán las predicciones realizadas. Nguyen *et al.* (2015) han estimado recientemente que las incertidumbres asociadas con las predicciones de estos modelos son superiores al 100%. Esto implica que, en la actualidad, podría no ser factible predecir de forma fiable los riesgos de cáncer basándonos en la información del plan de tratamiento y modelos de riesgo fenomenológicas.

En dosis bajas de radiación (menos de 0.1 Sv) también existen diferentes modelos, algunos basados en la teoría y otros en observaciones. Debido a su simplicidad, razonabilidad, y el enfoque conservador, los comités internacionales como la ICRP y la NCRP recomiendan extrapolar la relación lineal a este rango de dosis bajas. Sin embargo, la evidencia disponible no es estadísticamente más

significativa para predecir el cáncer inducido que la de otros modelos basados en una dosis umbral (Fletcher *et al.*, 2013), lo cual es debido a los altos valores de fondo. Las incertidumbres en los datos epidemiológicos no descartan una posible dosis umbral por debajo de la cual no hay un exceso de casos de cáncer. Por lo tanto, los riesgos derivados de bajas dosis de radiación, en el caso de que existan, son del mismo orden de magnitud que los niveles de fondo.

A partir de una revisión bibliográfica llevada a cabo por Xu *et al.* (2008), la cual se centraba en las pequeñas dosis de radiación derivadas de tratamientos de radioterapia, se llegó a la conclusión que muchos de los estudios dosimetría realizados hasta la fecha se basaron en cantidades de dosis inconsistentes y, a veces, confusas, lo que reduce la posibilidad de que puedan ser utilizados para llevar a cabo estudios epidemiológicos más sofisticados. Por lo tanto, concluimos que las evaluaciones de riesgo retrospectivas de las radiaciones ionizantes requieren datos dosimétricos más fiables, así como una estimación de su incertidumbre antes que se puedan extraer conclusiones más generales.

Durante la primera parte del siglo 20, el ^{226}Ra fue el radionúclido más usado en braquiterapia. Por lo tanto, al igual que los sobrevivientes de las bombas atómicas, los datos de los niños tratados con fuentes de ^{226}Ra pueden ser muy útiles para determinar la relación entre un determinado efecto radioinducido y la dosis absorbida. Como señaló recientemente el Comité Científico de las Naciones Unidas en el Efecto de las Radiaciones Atómicas (UNSCEAR, 2013), este último grupo es de interés actual en la búsqueda de un mejor conocimiento sobre las relaciones dosis-efecto. En relación con esto, Suecia ha mantenido durante mucho tiempo un registro completo de la incidencia de cáncer en todos los pacientes tratados. Junto con un conocimiento detallado acerca de los niños que se sometieron al tratamiento de ^{226}Ra, estos datos son de interés para su uso en la investigación sobre los efectos tardíos de la radiación. Sin embargo, los datos dosimétricos hasta la fecha utilizados para las fuentes que se utilizaron en Suecia son escasos y de presentan dudas.

A petición de epidemiólogos suecos, el objetivo del **Capítulo 4** fue caracterizar dosimétricamente dos fuentes de ^{226}Ra comúnmente utilizadas en Suecia durante la primera mitad del siglo 20 con el fin de llevar a cabo estudios retrospectivos. Para ello, un tubo de 8 mg de ^{226}Ra y una aguja de 10 mg de ^{226}Ra, utilizados en Radiumhemmet (Hospital Universitario Karolinska, Estocolmo, Suecia) desde 1925 hasta la década de 1960, fueron reproducidos en dos códigos MC que simulan el transporte de radiaciones y su interacción con la materia. Los códigos independientes utilizados fueron GEANT4 y MCNP5. Con ellos se obtuvieron las distribuciones de dosis absorbida y kerma de colisión alrededor de las dos fuentes, a partir de las cuales se derivaron los parámetros del TG-43 que se pueden implementar en los sistemas actuales de planificación. Además, los resultados de este formalismo dosimétrico se compararon con los resultados de una simulación realista también hecha con MC con un molde superficial constituido por 5 agujas dentro de una funda de vidrio. Ésta se colocó sobre un maniquí de agua que simulaba el paciente, tratando de imitar un típico caso clínico de tratamiento de piel. El objetivo de esta comparación fue validar el uso de los datos dosimétricos proporcionados en el formalismo del TG-43 para tratamientos superficiales, teniendo en cuenta que el TG-43 considera un medio infinito de agua mientras que en un tratamiento de piel hay una falta de retrodispersión en la superficie del agua, que podría dar lugar a errores en el cálculo de la dosis. Además, las dosis absorbidas calculadas utilizando el formalismo del TG-43 también se compararon con las mediciones y cálculos previamente reportados en la literatura que se basaban en el antiguo formalismo de la Integral de Sievert. Por último, la tasa de dosis a grandes distancias de un una fuente de ^{226}Ra colocada en el centro de una esfera de agua de 1 m de radio se calculó con GEANT4, y la tasa de dosis en función de la distancia se ajustó con una función analítica para permitir la estimación de la dosis absorbida a largas distancias de la fuentes (entre 10 y 60 cm de la fuente).

Los resultados del formalismo del TG-43 son coherentes dentro del volumen de tratamiento con los de una simulación MC de un escenario clínico. Por otro lado,

las comparaciones con medidas realizadas en 1994 con dosímetros termolunimiscentes muestran diferencias de hasta un 13% a lo largo del eje transversal de la aguja. La incertidumbre estimada para la dosis absorbida en el volumen de tratamiento está entre el 10% y el 15%, mientras que la incertidumbre de la dosis absorbida a órganos distantes es aproximadamente un 20% a un 25%.

Se espera que los resultados presentados en el **Capítulo 4** permitan facilitar estudios de dosimetría retrospectiva con fuentes ^{226}Ra, usando sistemas de planificación de tratamientos modernos, que pueden ser utilizados para mejorar el conocimiento sobre los efectos de la radiación a largo plazo. Sin duda, es importante que los estudios epidemiológicos sean conscientes de la incertidumbre estimada aquí antes de extraer sus conclusiones.

Los siguientes dos capítulos de esta tesis se orientaron a reducir la dosis periférica recibida por los órganos y los tejidos cercanos al implante, utilizando para ello blindajes diseñados específicamente para este propósito. En particular, en tratamientos superficiales con fuentes HDR de BT, ya sea con ^{60}Co, ^{192}Ir, o ^{169}Yb (éste último tiene potencial como fuente HDR y puede estar disponible en el futuro), algunos órganos radiosensibles cerca de la superficie pueden estar expuestos a altas dosis absorbidas. Esto puede reducirse cubriendo los implantes con un blindaje de plomo situado en la superficie del cuerpo. Este blindaje tiene principalmente dos repercusiones dosimétricas. En primer lugar, la retrodispersión producida en el plomo puede generar una sobredosificación importante en la superficie del paciente, la cual no es deseada. En segundo lugar, el blindaje reduce la dosis al otro lado del mismo. Antes de realizar este estudio no existían datos de transmisión de radiación a través de barreras de plomo de distintos espesores utilizados en braquiterapia superficial e intersticial. El **Capítulo 5** está dirigido a evaluar la perturbación dosimétrica producida por estos blindajes de plomo que se utilizan en algunos tratamientos superficiales de BT HDR.

Para llevar a cabo este estudio se realizaron simulaciones MC con GEANT4, simulando los tres radionúclidos previamente citados. Se consideraron cuatro

espesores diferentes de plomo (0, 3, 6 y 10 mm) y tres profundidades de localización de las fuentes diferentes (0, 5 y 10 mm) en agua, estando el blindaje colocado en la superficie del maniquí. A partir de estas simulaciones, se obtuvieron las componentes de retrodispersión y transmisión. Los resultados fueron corregidos para tener en cuenta un caso clínico realista con múltiples posiciones de permanencia de las fuentes.

De este estudio se concluyó que el rango de la sobredosificación en piel debida a la retrodispersión es de 3 mm para ^{60}Co y 1 mm tanto para fuentes de ^{192}Ir como de ^{169}Yb. Por lo tanto, como se dijo en el **Capítulo 5**, se concluye que la retrodispersión producida por el blindaje de plomo se puede evitar simplemente usando unos pocos milímetros de bolus colocado entre el blindaje y la superficie del paciente. Este simple montaje justifica el uso de blindajes de plomo. Por otro lado, se observó que los datos de transmisión para ^{60}Co e ^{192}Ir son más pequeños que los reportados por Papagiannis *et al.* (2008) para los blindajes de una instalación de braquiterapia. En cambio, para el ^{169}Yb la diferencia era insignificante.

El estudio anterior es de aplicación a varias situaciones clínicas. Por ejemplo, los blindajes pueden ser colocados sobre la superficie de la nariz para atenuar la alta dosis de radiación a la que se ven expuestos los cristalinos en un implante nasal, o alrededor de la mama para proteger la tiroides de la radiación directa procedente de un tratamiento de mama. Otra aplicación podría ser la reducción de la dosis fetal en una paciente embarazada con cáncer de mama que necesite radioterapia.

El **Capítulo 6** tuvo como objetivo evaluar la dosis de radiación al feto de una paciente embarazada que se somete a un tratamiento de BT intersticial con una fuente HDR de ^{192}Ir, así como diseñar una nueva posición de tratamiento y un blindaje específico que minimice al máximo esa dosis fetal. Para ello, se planeó sentar a la paciente, colocando el pecho a tratar sobre una mesa, en el interior de una caja de plomo específicamente diseñado para proteger al feto. La dosis prescrita al volumen a irradiar fue de 36 Gy en 8 fracciones. El diseño del blindaje consistió en una gruesa capa de 3.5 cm de plomo colocada entre el pecho y la mesa. Por lo

tanto, durante el tratamiento, la mama descansaba sobre este blindaje de plomo, atenuando así la radiación directa al feto. Además, se añadieron dos piezas laterales de plomo (3 cm de espesor cada una). Una de las capas laterales tenía un agujero a través del cual los tubos de transferencia por los cuales se transporta la fuente de forma remota se conectaron a los catéteres que se introducen dentro de la mama. Los bloques laterales permiten la colocación de una pieza extra de plomo (2.5 cm de espesor) por encima de la mama, paralelo a la primera capa, con el objetivo de reducir la radiación primaria al tiroides y los cristalinos. Además, con el fin de minimizar la dosis de tránsito debido a los movimientos de salida y entrada de la fuente de ^{192}Ir, se hizo un tubo de plomo hueco, que cubría los tubos de transferencia. Por último, una capa de material equivalente agua (con 1 mm de espesor) se colocó entre el blindaje de plomo y la piel del paciente para minimizar la retrodispersión de electrones, tal y como se había determinado en el capítulo anterior.

Las medidas de la dosis fetal se hicieron con películas radiocrómicas colocadas entre las rodajas de un maniquí antropomórfico que simulaba al paciente. Así se obtuvo la variación de la dosis en función de la distancia desde el volumen del implante, así como la homogeneidad dentro de un corte representativo de la posición fetal. Las medidas dosimétricas se realizaron tanto con blindaje como sin blindaje, para evaluar su eficiencia. Los resultados con la configuración anterior fueron muy prometedores. Con el blindaje, la dosis periférica varió de 50 cGy a 5 cm del borde caudal de la mama a menos de 0.1 cGy a los 30 cm de distancia. El blindaje redujo la dosis absorbida en un factor dos cerca de la mama y en más de un orden de magnitud más allá de los 20 cm. La dosis es heterogénea dentro de un corte axial dado, con variaciones respecto a la zona central del paciente de hasta un 50%. De un análisis de la literatura, también se observó que la braquiterapia intersticial de HDR con fuentes de ^{192}Ir y con el blindaje aquí desarrollado es más ventajoso que la EBRT desde un punto de vista de la reducción de la dosis al feto, siempre y cuando la distancia entre el extremo caudal de la mama y el fondo uterino sea mayor a 10 cm. A 30 cm de distancia, la dosis fetal es más de un factor 10

inferior con braquiterapia de HDR y el blindaje aquí diseñado que con EBRT. Además, el peso del blindaje aquí propuesto es notablemente inferior al recomendado en EBRT. Por lo tanto, la braquiterapia intersticial de mama con el blindaje presentado en el **Capítulo 6** puede beneficiar a pacientes embarazadas que necesiten radioterapia localizada, especialmente durante las primeras edades de gestación, cuando el feto es más sensible a la radiación ionizante.

Por último, el **Capítulo 7** ha presenta una discusión general que ha precedido a este resumen.

REFERENCES

Abo-Madyan Y, Aziz MH, Aly MM, Schneider F, Sperk E, Clausen S, *et al.* (2014) Second cancer risk after 3D-CRT, IMRT and VMAT for breast cancer. Radiother Oncol. 110: 471-476.

Agostinelli S, Allison J, Amako K, Apostolakis J, Araujo H, Arce P, *et al.* (2003) GEANT4 – a simulation toolkit. Nucl Instrum Meth A. 506: 250-303.

Allison J, Amako K, Apostolakis J, Araujo H, Dubois PA, Asai M, *et al.* (2006) GEANT4 developments and applications. IEEE Trans Nucl Sci. 53: 270-278.

American Association of Physicists in Medicine (2011) AAPM Position Statement on Radiation Risks from Medical Imaging Procedures. Available via http://www.aapm.org/org/policies/details.asp?id=318&type=PP. Last accessed 26 June 2013.

American Association of Physicists in Medicine (2012) CT scans are an important diagnostic tool when used appropriately. Available via http://www.aapm.org/publicgeneral/CTScansImportantDiagnosticTool.asp. Last accessed: 26 June 2013.

ASCO - American Society of Clinical Oncology (2014) Available online: http://www.cancer.net/coping-and-emotions/sexual-and-reproductive-health/cancer-during-pregnancy. Last accessed: October 18, 2014.

Andrássy M, Niatsetsky Y, Pérez-Calatayud J (2012) Controversies: Co-60 versus Ir-192 in HDR brachytherapy: scientific and technological comparison. Rev Fis Med. 13: 125-130.

Antypas C, Sandilos P, Kouvaris J, Balafouta E, Karinou E, Kollaros N, *et al.* (1998) Fetal dose evaluation during breast cancer radiotherapy. Int J Radiation Oncology Biol Phys. 40: 995-999.

Aronowitz JN (2002) Buried emanation; the development of seeds for permanent implantation. Brachytherapy. 1: 167-178.

Aroua A, Samara ET, Bochud FO, Meuli R, Verdum FR (2013) Exposure of the Swiss population to computed tomography. BMC Med Imaging. 13:22.

Attix FH, Ritz VH (1957) A determination of the gamma-ray emission of radium. J Res Natl Bur Stand. 56: 123.

Ballester F, Granero D, Perez-Calatayud J, Melhus CS, Rivard MJ (2009) Evaluation of high-energy brachytherapy source electronic disequilibrium and dose from emitted electrons. Med Phys. 36: 4250–4256.

Bastin K, Podgorsak M, Thomadsen B (1993) The transit dose component of high dose rate brachytherapy: direct measurements and clinical implications. Int J Radiation Oncology Biol Phys. 26: 695-702.

Bateman H (1910) Solution of a System of Differential Equations Occurring in the Theory of Radio-active Transformations. Proc Cambridge Phil Soc IS. 423.

Beaulieu L, Carlsson Tedgren Å, Carrier J-F, Davis SD, Mourtada F, Rivard MJ, *et al.* (2012) Report of the Task Group 186 on model-based dose calculation methods in brachytherapy beyond the TG-43 formalism: current status and recommendations for clinical implementation. Med Phys. 39: 6208-6236.

Bednarz B, Hancox C, Xu XG (2009) Calculated organ doses from selected prostate treatment plans using Monte Carlo simulations and an anatomically realistic computational phantom. Phys Med Biol. 54: 5271-5286.

Bednarz B, Athar B, Xu XG (2010) A comparative study on the risk of second primary cancers in out-of-field organs associated with radiotherapy of localized prostate carcinoma using Monte Carlo-based accelerator and patient models. Med Phys. 37: 1987-1994.

BEIR VII (2006) Health risks from exposure to low levels of ionizing radiation. BEIR VII Phase 2, The National Academic Press, Washington.

Berrington de Gonzalez A, Apostoaei AI, Veiga LH, Rajaraman P, Thomas BA, Hoffman FO, *et al.* (2012) RadRAT: a radiation risk assessment tool for lifetime cancer risk projection. J Radiol Prot. 32: 205-222.

Berris T, Mazonakis M, Kachris S, Damilakis J (2014) Peripheral organ doses from radiotherapy for heterotopic ossification of non-hip joints: is there a risk for radiation-induced malignancies? Phys Med. 30: 309-313.

Billings MP, Yucker WR (1973) Summary final report: the Computerized Anatomical Man (CAM) Report, McDonnell Douglas Corporation MDC G4655.

Boice JD Jr, Day NE, Andersen A, Brinton LA, Brown R, Choi NW, *et al.* (1985) Second cancers following radiation treatment for cervical cancer: an international collaboration among cancer registries. J Natl Cancer Inst. 74: 955–975.

Boice JD, Engholm G, Kleinerman RA, Blettner M, Stovall M, Lisco H, *et al.* (1988) Radiation dose and second cancer risk in patients treated for cancer of the cervix. Radiat Res. 116: 3-55.

Bouffler S, Ainsbury E, Gilvin P, Harrison J (2012) Radiation-induced cataracts: the Health Protection Agency's response to the ICRP statement on tissue reactions and recommendations on the dose limit for the eye lens. J Radiol Prot. 32: 479-88.

Brenner DJ, Elliston CD, Hall EJ, Berdon WE (2001) Estimated risks of radiation-induced fatal cancer from pediatric CT. AJR Am J Roentgenol. 176: 289-296.

Brenner DJ (2002) Estimating cancer risks from pediatric CT: going from the qualitative to the quantitative. Pediatr Radiol. 32: 228-231.

Brenner DJ, Sachs RK (2006) Estimating radiation-induced cancer risks at very low doses: rationale for using a linear no-threshold approach. Radiat Environ Biophys. 44: 253-256.

Brenner DJ (2008) Effective dose: a flawed concept that could and should be replaced. Br J Radiol. 81: 521-523.

Brenner DJ (2012a) Medical imaging in the 21st century – getting the best bang for the rad. N Engl J Med. 11: 943-945.

Brenner DJ, Hall EJ (2012b) Cancer risks from CT scans: Now we have data, what next? Radiology. 265: 330-331.

Briesmeister JF (2004) MCNP5 general Monte Carlo N-particle transport, Los Alamos National Laboratory, Report No. LA-12625.

Brix G, Nissen-Meyer S, Lechel U, Nissen-Meyer J, Griebel J, Nekolla EA, *et al.* (2009) Radiation exposures of cancer patients from medical X-rays: how relevant are they for individual patients and population exposure? Eur J Radiol. 72: 342-347.

Brown TA, Hogstrom KR, Alvarez D, Matthews KL, Ham K, Dugas JP (2012) Dose-response curve of EBT, EBT2, and EBT3 radiochromic films to synchrotron-produced monochromatic x-ray beams. Med Phys. 39: 7412-7417.

Brucer M (1952) Therapeutic potentialities of radioisotopes. The Merck report 61: 9-15.

Calandrino R, Ardu V, Corletto D, del Vecchio A, Origgi D, Signorotto P, *et al.* (2012) Evaluation of second cancer induction risk by CT follow-up in oncological long-surviving patients. Health Phys. 104:1-8.

Candela-Juan C, Perez-Calatayud J, Ballester F, Rivard MJ (2013) Calculated organ doses using Monte Carlo simulations in a reference male phantom undergoing HDR brachytherapy applied to localized prostate carcinoma. Med Phys. 033901.

Candela-Juan C, Montoro A, Ruiz-Martínez E, Villaescusa JI, Martí-Bonmatí L (2014a) Current knowledge on tumour induction by Computed Tomography should be used carefully. Eur Radiol. 24: 649-656.

Candela-Juan C, Granero D, Vijande J, Ballester F, Perez-Calatayud J, Rivard MJ (2014b) Dosimetric perturbation of a lead shield used for surface and interstitial high-dose-rate brachytherapy. J Radiol Prot. 34: 297-311.

Candela-Juan C, Gimeno-Olmos J, Pujades MC, Rivard MJ, Carmona V, Lliso F, Celada F, Ramírez-Coves JL, Ballester F, Tormo A, Pérez-Calatayud J (2015) Fetal dose measurements and shielding efficiency assessment in a custom setup of ^{192}Ir brachytherapy for a pregnant woman with breast cancer. Phys Med. doi: 10.1016/j.ejmp.2015.01.010

Caon M (2004) Voxel-based computational models of real human anatomy: a review. Radiat Env Biophys. 42: 229-235.

Carlsson GL (1985) Theoretical basis for dosimetry, in the dosimetry of ionizing radiation, edited by K. R. Kase, B. E. Bjärngard and F. H. Attix. (Academic, New York, 1985), Vol I.

Cullen DE, Hubbell JH, Kissel L (1997) EPDL97: the evaluated photo data library `97 version, Lawrence Livermore National Laboratory.

Cuttler JM, Pollycove M (2009) Nuclear energy and health: and the benefits of low-dose radiation hormesis. Dose Response. 7: 52–89.

Cygler J, Ding GX, Kendal W, Cross P (1997) Fetal dose for a patient undergoing mantle field irradiation for Hodgkin's disease. Med Dosim. 22: 135-137.

Dale RG (1985) The application of the linear quadratic dose-effect equation to fractionated and protracted radiotherapy. Br J Radiol. 58: 515-528.

Das IJ, Kahn FM (1989) Backscatter dose perturbation at high atomic number interfaces in megavoltage photon beams. Med Phys. 16: 367–375.

Das IJ, Chopra KL (1995) Backscatter dose perturbation in kilovoltage photon beams at high atomic number interfaces. Med. Phys. 22: 767–773.

Das IJ (1997) Forward dose perturbation at high atomic number interfaces in kilovoltage x-ray beams. Med Phys. 24: 1781–1787.

Das IJ, Kassaee A, Verhaegen F, Moskvin VP (2001) Interface dosimetry: Measurements and Monte Carlo simulations of low-energy photon beams. Radiat Phys Chem. 61: 593–595.

Das IJ, Moskvin VP, Kassaee A, Tabata T, Verhaegen F (2002) Dose perturbations at high-Z interfaces in kilovoltage photon beams: comparison with Monte Carlo simulations and measurements. Radiat Phys Chem. 64: 173–179.

Demanes DJ, Ghilezan MI (2014) High-dose-rate brachytherapy as monotherapy for prostate cancer. Brachytherapy. 13: 529-541.

DeWerd LA, Ibbott GS, Meigooni AS, Mitch MG, Rivard MJ, Stump KE, *et al.* (2011) A dosimetric uncertainty analysis for photon-emitting brachytherapy sources: report of AAPM Task Group No. 138 and GEC-ESTRO. Med Phys. 38, 782-801.

Dondon M-G, de Vathaire F, Shamsaldin A, Doyon FC, Diallo I, Ligot L, *et al.* (2004) Cancer mortality after radiotherapy for a skin hemangioma during childhood. Radiother Oncol. 72: 87-93.

Donegan WL (1983) Cancer and pregnancy. CA Cancer J Clin. 33: 194-214.

Dorr W, Herrmann T (2002) Second primary tumors after radiotherapy for malignancies, treatment-related parameters. Strahlenther Onkol. 178: 357–362.

Durand DJ, Mahesh M (2012) Understanding CT dose display. J Am Coll Radiol. 9: 669-671.

Dutreix A, Marinello G, Wambersie A (1982) Dosimétrie en curiethérapie. Masson (Paris).

Dutreix J, Tubiana M, Pierquin B (1998) The hazy dawn of brachytherapy. Radiother Onc. 49: 223-232.

ECRP (2008) European Commission Radiation Protection No. 154. European guidance on estimating population dose from medical x-ray procedures. Available via: http://ddmed.eu/_media/background_of_ddm1:rp154.pdf. Last accessed 26 June 2013.

Eidemüller M, Holmberg E, Jacobs P, Lundell M, Karlsson P (2009) Breast cancer risk among Swedish hemangioma patients and possible consequences of radiation-induced genomic instability. Mutat Res. 669: 48–55.

Eisenberg JD, Harvey HB, Moore DA, Gazelle GS, Pandharipande PV (2012) Falling prey to the sunk cost bias: a potential harm of patient radiation dose histories. Radiology. 263: 626-628.

Eschner W, Schmidt M, Dietlein M, Schicha H (2010) PROLARA: prognosis-based lifetime attributable risk approximation for cancer from diagnostic radiation exposure. Eur J Nucl Med Mol Imaging. 37: 131-135.

Fenig E, Mishaeli M, Kalish Y, Lishner M (2001) Pregnancy and radiation. Cancer Treat Rev. 27: 1-7.

Feroldi P, Galelli M, Belletti S (1992) A comparison of accuracy of computer treatment planning systems in brachytherapy. Radiother Oncol. 24: 147-154.

Ferrari A, Sala PR, Fassò A, Ranft J (2005) FLUKA: a multi-particle transport code (Program version 2005), CERN-2005-10, INFN/TC-05/11, SLAC-R-773 (CERN, Geneva).

Filipov D, Schelin HR, Soboll DS, Denyak V (2013) Evaluation of fetal dose in breast radiotherapy with shielding and wedges. IEEE Trans Nuc Sci. 60: 792-796.

Fitzwilliams DCL (1930) The technique of radium therapy to-day. Brit Med J. 2: 309-311.

Fletcher JG, Kofler JM, Coburn JA, Bruining DH, McCollough CH (2013) Perspective on radiation risk in CT imaging. Abdom Imaging. 38: 22-31.

Fontenot J, Taddei P, Zheng Y, Mirkovic D, Jordan T, Newhauser W (2008) Equivalent dose and effective dose from stray radiation during passively scattered proton radiotherapy for prostate cancer. Phys Med Biol. 53: 1677-1688.

Fontenot JD, Lee AK, Newhauser WD (2009) Risk of secondary malignant neoplasms from proton therapy and intensity-modulated x-ray therapy for early-stage prostate cancer. Int J Radiat Oncol Biol Phys. 74: 616-622.

Georg D, Hopfqartner J, Gòra J, Kuess P, Kragl G, Berger D, *et al.* (2014) Dosimetric considerations to determine the optimal technique for localized prostate cancer among external photon, proton, or carbon-ion therapy and high-dose-rate or low-dose-rate brachytherapy. Int J Radiat Oncol Biol Phys. 88: 715-722.

Gerbaulet A, Mazeron JJ (1998) The centenary of discovery of radium. Radiother Oncol. 49: 205-216.

Gerbaulet A, Pötter R, Mazeron JJ, Meertens H, Limbergen EV (2002) The GEC ESTRO handbook of brachytherapy (Leuven, Belgium: European Society for Therapeutic Radiology and Oncology).

Goodwin PN, Quimby EH, Morgan RH (1970) Physical Foundations of Radiology (Harper and Row, New York).

Goorley T, James M, Booth T, Brown F, Bull J, Cox LJ *et al*. (2012) Initial MCNP6 release overview. Radiat Trans Protect. 180: 298–315.

Granero D, Perez-Calatayud J, Ballester F (2007) Technical note: Dosimetric study of a new Co-60 source used in brachytherapy. Med Phys. 34: 3485–3488.

Granero D, Perez-Calatayud J, Pujades-Claumarchirant MC, Ballester F, Melhus CS, Rivard MJ (2008) Equivalent phantom sizes and shapes for brachytherapy dosimetric studies of ^{192}Ir and ^{137}Cs. Med Phys. 35: 4872–4877

Granero D, Vijande J, Ballester F, Rivard MJ (2011) Dosimetry revisited for the HDR ^{192}Ir brachytherapy source model mHDR-v2. Med. Phys. 38: 487-494.

Granero D, Perez-Calatayud J, Vijande J, Ballester F, Rivard MJ (2014) Limitations of the TG-43 formalism for skin high-dose-rate brachytherapy dose calculations. Med Phys. 41: 021703.

Guedea F (2014) Perspectives of brachytherapy: patterns of care, new technologies, and new biology. Cancer Radiother. 18: 434-436.

Haba Y, Twyman N, Thomas SJ, Overton C, Dendy P, Burnet NG (2004) Radiotherapy for glioma during pregnancy: Fetal dose estimates, risk assessment and clinical management. Clin Oncol. 16: 210-214.

Haie-meder C, Chargari C, Rey A, Dumas I, Morice P, Magné N (2009) DVH parameters and outcome for patients with early-stage cervical cancer treated with preoperative MRI-based low dose rate brachytherapy followed by surgery. Radiother Oncol. 93: 316–321.

Hall EJ (2004) Henry S. Kaplan Distinguished Scientist Award 2003. The crooked shall be made straight; dose-response relationships for carcinogenesis. Int J Radiat Biol. 80: 327-337.

HPS - Health Physics Society (2004) Radiation risk in perspective. Position Statement of the Health Physics Society: PS010-1.

HPA - Health Protection Agency (2011) Radiation risks from medical x-ray examinations as a function of the age and sex of the patient. HPA-CRCE-028.

Hendee WR, O'Connor MK (2012) Radiation risks of medical imaging: Separating fact from fantasy. Radiology. 264: 312-321.

Hendee WR (2013) Risk of medical imaging. Med Phys 40: 040401.

Hilaris BS (1975) Handbook of interstitial brachytherapy, 123.

Howell RM, Hertel NE, Wang Z, Hutchinson J, Fullerton GD (2006) Calculation of effective dose from measurements of secondary neutron spectra and scattered photon dose from dynamic MLC IMRT for 6 MV, 15 MV, and 18 MV beam energies. Med. Phys. 33: 360-368.

IARC (2001) Worldwide Cancer Incidence Statistics—Prostate, JNCI Cancer Spectrum. Oxford University Press.

ICRP (2000) Pregnancy and medical radiation. Annals ICRP, Publication 84. Ottawa, Canada.

ICRP (2002) Basic anatomical and physiological data for use in radiological protection: reference values. A report of age- and gender-related differences in the anatomical and physiological characteristics of reference individuals. ICRP Publication 89, Ann ICRP 32.

ICRP (2007) The 2007 Recommendations of the International Commission on Radiological Protection. ICRP publication 103, Ann ICRP 37.

ICRP (2008) Nuclear decay data for dosimetric calculations. ICRP Publication 107, Ann ICRP 38.

ICRP (2009) Realistic reference phantoms: an ICRP/ICRU joint effort. A report of adult reference computational phantoms. ICRP Publication 110, Ann ICRP 39.

ICWG (1990) Interstitial Collaborative Working Group. Interstitial Brachytherapy: Physical, Biological and Clinical Considerations, edited by L. L. Anderson, R. Nath, and K. A. Weaver (Raven, New York).

Islam MK, Saeedi F, Al-Rajhi N (2001) A simplified shielding approach for limiting fetal dose during radiation therapy of pregnant patients. Int J Radiat Oncol Biol Phys. 49: 1469-1473.

Ivanov VK, Tsyb AF, Mettler FA, Menyaylo AN, Kashcheev VV (2012) Methodology for estimating cancer risks of diagnostic medical exposure: with an example of risks associated with computed tomography. Health Phys. 103: 732-739.

Ivanov VK, Kashcheev VV, Chekin SY, Menyaylo AN, Pryakhin EA, Tsyb AF, *et al*. (2013) Estimation of risk from medical radiation exposure based on effective and organ dose: how much difference is there? Radiat Prot Dosimetry. 155: 317-328.

Jemal A, Bray F, Center MM, Ferlay J, Ward E, Forman D (2011) Global cancer statistics. CA Cancer J Clin. 61: 69-90.

Johns HE, Cunningham JR (1983) The physics of radiology, 4th ed. (Charles C. Thomas, Springfield IL).

Josipovic M, Nyström H, Kjaer-Kristoffersen F (2009) IMRT in a pregnant patient: how to reduce the fetal dose? Med Dosim. 34: 301-310.

Kal HB, Struikmans H (2005) Radiotherapy during pregnancy: Fact and fiction. Lancet Oncol. 6: 328-333.

Kim KP, Berrington de González A, Pearce MS, Salotti JA, Parker L, McHugh K, *et al*. (2012) Development of a database of organ doses for paediatric and young adult CT scans in the United Kingdom. Radiat Prot Dosimetry. 150: 415-426.

Klevenhagen SC, Lambert GD, Arbabi A (1982) Backscattering in electron beam therapy for energies between 3 and 35 MeV. Phys Med Biol. 27: 363–373.

Kornelsen RO, Young MEJ (1981) Brachytherapy build-up factors. Br J Radiol. 54:136.

Kourinou KM, Mazonakis M, Lyraraki E, Stratakis J, Damilakis J (2013) Scattered dose to radiosensitive organs and associated risk for cancer development from head and neck radiotherapy in pediatric patients. Phys Med. 29: 650-655.

Kourinou KM, Mazonakis M, Lyraraki E, Damilakis J (2015) Photon-beam radiotherapy in pregnant patients: Can the fetal dose be limited to 10 cGy or less? Phys Med. 31: 85-91.

Kry SF, Salehpour M, Followill DS, Stovall M, Kuban DA, White RA, *et al.* (2005) Out-of-field photon and neutron dose equivalents from step-and-shoot intensity-modulated radiation therapy. Int J Radiat Oncol Biol Phys. 62: 1204-1216.

Lambert GD, Klevenhagen SC (1982) Penetration of backscattered electrons in polystyrene for energies between 1 and 25 MeV. Phys Med Biol. 27: 721–725.

Lewis D, Micke A, Yu X (2012) An efficient protocol for radiochromic film dosimetry combining calibration and measurement in a single scan. Med Phys. 39: 6339-50.

Li XA, Chu JC, Chen W, Zusag T (1999) Dose enhancement by a thin foil of high-Z material: a Monte Carlo study. Med Phys. 26: 1245–1251.

Lindberg S, Karlsson P, Arvidsson B, Holmberg E, Lundberg LM, Wallgren A (1995) Cancer incidence after radiotherapy for skin haemangioma during infancy. Acta Oncol. 34: 735-740.

Lliso F, Pérez-Calatayud J, Casal E, Carmona V, Soriano A, Manzano F, *et al.* (2004) Dosimetría y garantía de calidad en el tratamiento radioterápico de pacientes embarazadas. Rev Física Médica. 5: 39-41.

Lliso F, Granero D, Perez-Calatayud J, Carmona V, Pujades M C, Ballester F (2011) Dosimetric evaluation of internal shielding in a high dose rate skin applicator. J Contem Brachyther. 3: 32–35.

Lundell M, Fürst CJ, Hedlund B, Holm LE (1990) Radium treatment for hemangioma in early childhood. Reconstruction and dosimetry of treatments, 1920-1959. Acta Oncol. 29: 551-556.

Lundell M (1994) Estimates of absorbed dose in different organs in children treated with radium for skin hemangiomas. Radiat Res. 140: 327-333.

Lundell M, Holm L-E (1995) Risk of solid tumors after irradiation in infancy. Acta Oncol. 24: 727-734.

Lundell M, Mattsson A, Karlsson P, Holmberg E, Gustafsson A, Holm L-E (1999) Breast cancer risk after radiotherapy in infancy: A pooled analysis of two Swedish cohorts of 17,202 infants. Radiat Res. 151: 626-632.

MacPherson MS, Battista JJ (1998) Radioactivity measurements of ytterbium-169 brachytherapy sources. Australas Phys Eng Sci Med. 21: 18–23.

Martin CJ (2007) Effective dose: how should it be applied to medical exposures? Br J Radiol. 80:639-647.

Martín Rincón C, Jerez Sainz I, Modolell Farré I, España López ML, López Franco P, Muñiz JL, *et al.* (2002) Evaluation of the peripheral dose to uterus in breast carcinoma radiotherapy. Radiat Prot Dosim. 101: 469-471.

Mathews JD, Forsythe AV, Brady Z, Butler MW, Goergen SK, Byrnes GB, *et al.* (2013) Cancer risk in 680 000 people exposed to computed tomography scans in childhood or adolescence: data linkage study of 11 million Australians. BMJ 346:f2360.

Mazonakis M, Varveris H, Fasoulaki M, Damilakis J (2003) Radiotherapy of Hodgkin's disease in early pregnancy: Embryo dose measurements. Radiother Oncol. 66: 333-339.

Mazonakis M, Berris T, Varveris C, Lyraraki E, Damilakis J (2014) Out-of-field organ doses and associated radiogenic risks from para-aortic radiotherapy for testicular seminoma. Med Phys. 41: 051702.

Micke A, Lewis DF, Yu X (2011) Multichannel film dosimetry with nonuniformity correction. Med Phys. 38: 2523-2534.

Miglioretti DL, Johnson E, Williams A, Greenlee RT, Weinmann S, Solberg LI, *et al.* (2013) The use of computed tomography in pediatrics and the associated radiation exposure and estimated cancer risk. JAMA Pediatr. E1-E8.

Mille MM, Xu XG, Rivard MJ (2010) Comparison of organ doses for patients undergoing balloon brachytherapy of the breast with HDR ^{192}Ir or electronic sources using Monte Carlo simulations in a heterogeneous human phantom. Med Phys. 37: 662-671.

Moteabbed M, Yock TI, Paganetti H (2014) The risk of radiation-induced second cancers in the high to medium dose region: A comparison between passive and scanned proton therapy, IMRT and VMAT for pediatric patients with brain tumors. Phys Med Biol. 59: 2883–2899.

Mould RF (2007) Radium history mosaic (Institute of Oncology, Warsaw).

Murray L, Henry A, Hoskin P, Siebert F-A, Venselaar J (2014) Second primary cancers after radiation for prostate cancer: a systematic review of the clinical data and impact of treatment technique. Radiother Oncol. 110: 213-228.

Mutic S, Klein EE (1999) A reduction in the AAPM TG-36 reported peripheral dose distributions with tertiary multileaf collimation. Int J Radiat Oncol Biol Phys. 44: 947-953.

Myers WG (1948) Applications of artificially radio-actives isotopes in therapy. Am J Roentgenol. 60: 816-823.

Nag S, Kuske RR, Vicini FA, Arthur DW, Zwicker RD (2001) Brachytherapy in the treatment of breast cancer Oncology (Williston Park) 15: 195-202, 205; discussion 205–197.

Nath R, Anderson LL, Luxton G, Weaver KA, Williamson JF, Meigooni AS (1995) Dosimetry of interstitial brachytherapy sources: recommendations of the AAPM Radiation Therapy Committee Task Group No. 43. American Association of Physicists in Medicine. Med Phys. 22: 209-234.

Nath R, Yue N, Weinberger J (1999) Dose perturbations by high atomic number materials in intravascular brachytherapy. Cardiovasc Radiat Med. 1: 144–153

NCRP (2001) National Council on Radiation Protection and Measurements. Evaluation of the linear nonthreshold dose-response model for ionizing radiation. NCRP Report 136. Bethesda, MD: NCRP.

NCRP (2013) National Commission on Radiological Protection. Preconception and prenatal radiation exposure: Health effects and protective guidelines. NCRP Report No. 174. NCRP (Bethesda, MD).

Nelson WR, Hirayama H, Rogers DWO (1985) The EGS4 Code System. Report SLAC-265 (Stanford Linear Accelerator Center, Stanford, CA).

Ngu SL, Duval P, Collins C (1992) Foetal radiation dose in radiotherapy for breast cancer. Australas Radiol. 36: 321-322.

Nguyen J, Moteabbed M, Paganetti H (2015) Assessment of uncertainties in radiation-induced cancer risk predictions at clinically relevant doses. Med Phys. 42: 81-89.

Nikjoo H, Khvostunov IK (2003) Biophysical model of the radiation-induced bystander effect. Int J Radiat Biol. 79: 43-52.

Nuyttens JJ, Prado KL, Jenrette JM, Williams TE (2002) Fetal dose during radiotherapy: clinical implementation and review of the literature. Cancer/Radiother. 6: 352-357.

Oikarinen H, Meriläinen S, Pääkkö E, Karttunen A, Nieminen MT, Tervonen O (2009) Unjustified CT examinations in young patients. Eur Radiol. 19: 1161-1165.

Osei EK, Faulkner K (1999) Fetal position and size data for dose estimation. Br J Radiol. 72: 363-370.

Paganetti H, Athar BS, Moteabbed M, Adams JA, Schneider U, Yock TI (2012) Assessment of radiation-induced second cancer risks in proton therapy and IMRT for organs inside the primary radiation field. Phys Med Biol. 57: 6047–6061.

Palmer A, Hayman O, Muscat S (2012) Treatment planning study of the 3D dosimetric 400 differences between Co-60 and Ir-192 sources in high dose rate (HDR) brachytherapy for cervix cancer. J Contemp Brachyther. 4: 52–59.

Pandharipande PV, Eisenberg JD, Avery LL, Gunn ML, Kang SK, Megibow AJ, *et al.* (2013) How radiation exposure histories influence physician imaging decisions: a multicenter radiologist survey study. Am J Roentgenol 200: 1275-1283.

Papagiannis P, Baltas D, Granero D, Perez-Calatayud J, Gimeno J, Ballester F, *et al.* (2008) Radiation transmission data for radionuclides and materials relevant to brachytherapy facility shielding. Med Phys. 35: 4898–4906.

Patel RR, Becker SJ, Das RK, Mackie TR (2007) A dosimetric comparison of accelerated partial breast irradiation techniques: Multicatheter interstitial brachytherapy, three-dimensional conformal radiotherapy, and supine versus prone helical tomotherapy. Int J Radiat Oncol Biol Phys. 68: 935-942.

Pauwels EK, Bourguignon M (2011) Cancer induction caused by radiation due to computed tomography: a critical note. Acta Radiol. 52: 767-773.

Pearce MS, Salotti JA, Little MP, McHugh K, Lee C, Kim KP, *et al.* (2012) Radiation exposure from CT scans in childhood and subsequent risk of leukaemia and brain tumours: a retrospective cohort study. Lancet. 380: 499-505.

Perez-Calatayud J, Ballester F, Serrano MA, Lluch JL, Casal E, Carmona V (2000) Dosimetric characteristics of backscattered electrons in lead. Phys Med Biol. 45: 1841–1849.

Perez-Calatayud J, Ballester F, Das RK, Dewerd LA, Ibbott GS, Meigooni AS, *et al.* (2012) Dose calculation for photon-emitting brachytherapy sources with average energy higher than 50 keV: report of the AAPM and ESTRO. Med Phys. 39: 2904–2929.

Perisinakis K, Seimenis I, Tzedakis A, Papadakis AE, Damilakis J (2012) Triple-rule-out computed tomography angiography with 256-slice computed tomography scanners: patient-specific assessment of radiation burden and associated cancer risk. Invest Radiol. 47:109-115.

Pickles T, Keyes M, Morris WJ (2009) Brachytherapy or Conformal External Radiotherapy for Prostate Cancer: A Single-Institution Matched-Pair Analysis. Int J Radiat Oncol Biol Phys. 76: 43–49.

Pierce DA, Shimizu Y, Preston DL, Vaeth M, Mabuchi K (1996) Studies of the mortality of atomic bomb survivors. Report 12, part 1. Cancer: 1950-1990. Radiat Res. 146:1-27.

Pierce DA, Preston DL (2000) Radiation-related cancer risks at low doses among atomic bomb survivors. Radiat Res. 154:178-186.

Pieters BR, De Back DZ, Koning CCE, Zwinderman AH (2009) Comparison of three radiotherapy modalities on biochemical control and overall survival for the treatment of prostate cancer: A systematic review. Radiother Oncol. 93: 168–173.

Podgorsak MB, Meiler RJ, Kowal H, Kishel SP, Orner JB (1999) Technical management of a pregnant patient undergoing radiation therapy to the head and neck. Med Dosim. 24: 121-128.

Polgar C, Strnad V, Major T (2005) Brachytherapy for partial breast irradiation: the European experience. Semin Radiat Oncol. 15: 116-122.

Polgar C, Van Limbergen E, Potter R, Kovacs G, Polo A, Lyczek J, *et al.* (2010) Patient selection for accelerated partial-breast irradiation (APBI) after breast-

conserving surgery: Recommendations of the Groupe Europeen de Curietherapie-European Society for Therapeutic Radiology and Oncology (GEC-ESTRO) breast cancer working group based on clinical evidence. Radiother Oncol. 94: 264-273.

Preston DL, Kusumi S, Tomonaga M, Izumi S, Ron E, Kuramoto A, *et al.* (1994) Cancer incidence in atomic bomb survivors. III. Leukemia, lymphoma and multiple myeloma. Radiat Res. 137: 1950-1987.

Pujades MC, Camacho C, Perez-Calatayud J, Richart J, Gimeno J, Lliso F, *et al.* (2011) The use of nomograms in LDR-HDR prostate brachytherapy. J Contemp Brachyther. 3: 121-124.

Recchia V, Dodaro A, Braga L (2013) Event-based versus process-based informed consent to address scientific evidence and uncertainties in ionising medical imaging. Insights Imaging. DOI 10.1007/s13244-013-0272-6.

Rehani MM (2009) Smart protection. IAEA Bull. 50. Available via: http://www.iaea.org/Publications/Magazines/Bulletin/Bull502/50205813137.html. Last accessed 26 June 2013.

Rehani MM, Frush DP (2011) Patient exposure tracking: the IAEA Smart Card Project. Radiat Prot Dosimetry. 147: 314-316.

Reniers B, Liu D, Rusch T, Verhaegen F (2008) Calculation of relative biological effectiveness of a low-energy electronic brachytherapy source. Phys Med Biol. 53: 7125-7135.

Richter J, Baier K, Flentje M (2008) Comparison of ^{60}Co and ^{192}Ir sources in high dose rate afterload brachytherapy. Strahlenther Onkol. 184: 187-192.

Rivard MJ, Coursey BM, DeWerd LA, Hanson WF, Huq MS, Ibbott GS, *et al.* (2004) Update of AAPM Task Group No. 43 Report: A revised AAPM protocol for brachytherapy dose calculations. Med Phys. 31: 633-674.

Rivard MJ, Davis SD, DeWerd LA (2006) Calculated and measured brachytherapy dosimetry parameters in water for the Xoft Axxent x-ray source: An electronic brachytherapy source. Med Phys. 33: 4020-4032.

Rivard MJ, Granero D, Perez-Calatayud J, Ballester F (2010) Influence of photon energy spectra from brachytherapy sources on Monte Carlo simulations of kerma and dose rates in water and air. Med Phys. 37: 869–876.

Ron E, Modan B, Boice JD Jr, Alfandary E, Stovall M, Chetrit A, *et al.* (1988) Tumors of the brain and nervous system after radiotherapy in childhood. N Engl J Med. 319:1033-1039.

Rossi HH, Kellerer AM (1972) Radiation carcinogenesis at low doses. Science. 175: 200-202.

Rzeszowska-Wolny J, Przybyszewsky WM, Widel M (2009) Ionizing radiation-induced bystander effects, potential targets for modulation of radiotherapy. Eur J Pharmacol. 625: 156-164.

Salvat F, Fernández-Varea JM, Sempau J (2008) PENELOPE-2008: a code system for Monte Carlo simulation of electron and photon transport, 2008. Issy-les-Moulineaux, France.

Salvat F, Fernández-Varea JM, Sempau J (2011) PENELOPE 2011: A code system for Monte Carlo simulation of electron and photon transport, OECD Nuclear Energy Agency, Issy-les-Moulineaux, France. Available: NEA web page.

Samei E, Li X, Chen B, Reiman R (2013) The effect of dose heterogeneity on radiation risk in medical imaging. Radiat Prot Dosimetry. 155: 42-58.

Schneider U, Lomax A, Pemler P, Besserer J, Ross D, Lombriser N, Kaser-Hotz B (2006) The impact of IMRT and proton radiotherapy on secondary cancer incidence. Strahl Onkol. 182: 647-652.

Schneider U, Lomax A, Besserer J, Pemler P, Lombriser N, Kaser-Hotz B (2007) The impact of dose escalation on secondary cancer risk after radiotherapy of prostate cancer. Int J Radiat Oncol Biol Phys. 68: 892-897.

Schneider U (2009) Mechanistic model of radiation-induced cancer after fractionated radiotherapy using the linear-quadratic formula. Med Phys. 36: 1138–1143.

Shah C, Vicini F, Wazer DE, Arthur D, Patel RR (2013) The American Brachytherapy Society consensus statement for accelerated partial breast irradiation. Brachytherapy. 12: 267-277.

Shen X, Keith SW, Mishra MV, Dicker AP, Showalter TN (2012) The impact of brachytherapy on prostate cancer-specific mortality for definitive radiation therapy of high-grade prostate cancer: a population-based analysis. Int J Radiat Oncol Biol Phys. 83: 1154-1159.

Smith BD, Arthur DW, Buchholz TA, Haffty BG, Hahn CA, Hardenbergh PH, *et al.* (2009) Accelerated partial breast irradiation consensus statement from the American Society for Radiation Oncology (ASTRO). Int J Radiat Oncol Biol Phys. 74: 987-1001.

Smith-Bindman R, Lipson J, Marcus R, Kim KP, Mahesh M, Gould R, *et al*. (2009) Radiation dose associated with common computed tomography examinations

and the associated lifetime attributable risk of cancer. Arch Intern Med. 169: 2078-2086.

Smocovitis D (1966) Absorption and scattering of radium gamma radiation in water (The University of British Columbia).

Sneed PK, Albright NW, Wara WM, Prados MD, Wilson CB (1995) Fetal dose estimates for radiotherapy of brain tumors during pregnancy. Int J Radiat Oncol Biol Phys. 32: 823-830.

Sodickson A (2013) CT radiation risks coming into clearer focus. BMJ. 346:f3102.

Stathakis S, Li J, Ma CC (2007) Monte Carlo determination of radiation-induced cancer risks for prostate patients undergoing intensity- modulated radiation therapy. J Appl Clin Med Phys. 8: 2685.

Stiller CA (2007) Childhood cancer in Britain: Incidence, survival, mortality. Oxford: Oxford University Press.

Stovall M, Blackwell CR, Cundiff J, Novack DH, Palta JR, Wagner LK, *et al.* (1995) Fetal dose from radiotherapy with photon beams: Report of AAPM radiation therapy committee Task Group No. 36. Med Phys. 22: 63-82.

Strandqvist M (1939a) A new technique and dosage system for gamma ray therapy in surface application of radium. Acta Radiol. 20: 1-15.

Strandqvist M (1939b) Radium treatments of cutaneous cavernous haemangiomas, using surface application of radium tubes in glass capsules. Acta Radiol. 20: 185-211.

Strohmaier S, Grzegorz Z (2011) Comparison of 60Co and 192Ir sources in HDR brachytherapy. J Contemp Brachyther. 3: 199-208.

Teeuwisse W, Geleijns J, Veldkamp W (2007) An inter-hospital comparison of patient dose baed on clinical indications. Eur Radiol. 17: 1795-1805.

Tubiana M (2005) Dose-effect relationships and estimation of the carcinogenic effects of low doses of ionizing radiation: the joint report of the Académie des Sciences (Paris) and of the Académie Nationale de Médecine. Int J Radiat Oncol Biol Phys. 63: 317-319.

Tubiana M, Aurengo A, Averbeck D, Masse R (2006) Recent reports on the effect of low doses of ionizing radiation and its dose-effect relationship. Radiat Environ Biophys. 44: 245-251.

UNSCEAR (1994) United Nations Scientific Committee on the Effects of Atomic Radiation. Report to the General Assembly. Annex B. Adaptive responses to radiation in cells and organisms. New York: United Nations.

UNSCEAR (2010) United Nations Scientific Committee on the Effects of Atomic Radiation. Report to the General Assembly. New York: United Nations.

UNSCEAR (2012) United Nations Scientific Committee on the Effects of Atomic Radiation. Report of the UNSCEAR. 59th session. May 21-25. General Assembly Official Records. 67th session, Supplement No. 46.

UNSCEAR (2013) United Nations Scientific Committes on the Effects of Atomic Radiation. Sources, effects and risks of ionizing radiation. Report. Vol. II. Scientific Annex B: Effects of radiation exposure of children.

Van der Giessen PH (1997) Measurement of the peripheral dose for the tangential breast treatment technique with Co-60 gamma radiation and high energy x-rays. Radiother Oncol. 42: 257-264.

Van der Giessen P-H (2001) Peridose, a software program to calculate the dose outside the primary beam in radiation therapy. Radiother Oncol. 58: 209-213.

Venselaar JL, Van der Giessen PH, Dries WJ (1996) Measurement and calculation of the dose at large distances from brachytherapy sources: Cs-137, Ir-192, and Co-60. Med Phys. 23: 537-543.

Venselaar J, Perez-Calatayud J (2008) European guidelines for quality assurance in radiotherapy, ESTRO booklet no. 8, a practical guide to quality control of brachytherapy equipment. ISBN 90-804532-8 ESTRO (Belgium).

Vicini FA, Arthur DW (2005) Breast brachytherapy: North American experience. Semin Radiat Oncol. 15: 108-115.

Vijande J, Granero D, Perez-Calatayud J, Ballester F (2012) Monte Carlo dosimetric study of the Flexisource Co-60 high dose rate source. J. Contemp. Brachytherapy. 4: 34–44.

Villforth JC (1964) Problems in Radium Control, Public Health Reports (1896-1970) 79: 337-342.

Visser AG (1989) An intercomparison of the accuracy of computer planning systems for brachytherapy. Radiother Oncol. 15: 245-258.

Viswanathan AN, Petereit DG (2007) Brachytherapy. Applications and Techniques. Devlin PM (Ed) (Philadelphia, PA, LWW).

Wall BF, Kendall GM, Edwards AA, Bouffler S, Muirhead CR, Meara JR (2006) What are the risks from medical X-rays and other low dose radiation? Br J Radiol. 69: 285-294.

Weed DW, Edmundson GK, Vicini FA, Chen PY, Martinez AA (2005) Accelerated partial breast irradiation: A dosimetric comparison of three different techniques. Brachytherapy. 4: 121-129.

White EC, Kamrava MR, Demarco J, Park S-J, Wang P-C, Kayode O, *et al.* (2013) High-dose-rate prostate brachytherapy consistently results in high quality dosimetry. Int J Radiation Oncol Biol Phys. 85: 543-548.

Wilkinson JB, Beitsch PD, Shah C, Arthur D, Haffty BG, Wazer DE, *et al.* (2013) Evaluation of current consensus statement recommendations for accelerated partial breast irradiation: A pooled analysis of William Beaumont Hospital an American Society of Breast Surgeon Mammosite Registry Trial Data. Int J Radiat Oncol Biol Phys. 85: 1179-1185.

Williamson JF, Morin RL, Khan FM (1983) Monte Carlo evaluation of the Sievert integral for brachytherapy dosimetry. Phys Med Biol. 28: 1021-1032.

Williamson JF (1987) Monte Carlo evaluation of kerma at a point for photon transport problems. Med Phys. 14: 567-576.

Williamson JF (2006) Brachytherapy technology and physics practice since 1950: a half-century of progress. Phys Med Biol. 51: R303-325.

Wong F, Sai-Ki O, Cheung F, Shiu W (1986) Pregnancy outcome following radiotherapy to naso-pharyngal carcinoma. Eur J Obstet Gynecol Reprod Biol. 22: 157-160.

Woo SY, Fuller LM, Cundiff JH, Bondy ML, Hagemeister FB, McLaughlin P, *et al.* (1992) Radiotherapy during pregnancy for clinical stages IA-IIA Hodgkin's disease. Int J Radiat Oncol Biol Phys. 23: 407-412.

X-5 Monte Carlo Team (2003) MCNP-A general Monte Carlo N-particle transport code, version 5, Report LA-UR-03-1987 (Los Alamos National Laboratory, Los Alamos, NM).

Xu XG, Bednarz B, Paganetti H (2008) A review of dosimetry studies on external-beam radiation treatment with respect to second cancer induction. Phys Med Biol. 53: R193-R241.

Xu XG, Eckerman KF (2010) Handbook of anatomical models for radiation dosimetry. (CRC Press/Taylor & Francis Group, Boca Raton, FL).

Yamada Y, Rogers L, Demanes DJ, Morton D, Prestidge BR, Pouliot J, *et al.* (2012) American Brachytherapy Society consensus guidelines for high-dose-rate prostate brachytherapy. Brachytherapy. 11: 20-32.

Yang Y, Rivard MJ (2009) Monte Carlo simulations and radiation dosimetry measurements of peripherally applied HDR ^{192}Ir breast brachytherapy D-shaped applicators. Med Phys. 36: 809–815.

Young MEJ, Batho HF (1962) Dose tables for linear radium sources calculated by an electronic computer. Br J Radiol. 37: 38-44.

Zaidi H, Xu SG (2007) Computational anthropomorphic models of the human anatomy: the path to realistic Monte Carlo modeling in radiological sciences. Annu Rev Biomed Eng. 9: 471-500.

Zhang J, Na YH, Caracappa PF, Xu XG (2009) RPI-AM and RPI-AF, a pair of mesh-based, size-adjustable adult male and female computational phantoms using ICRP-89 parameters and their calculations for organ doses from monoenergetic photon beams. Phys Med Biol. 54: 5885-5908.

LIST OF PUBLICATIONS

PUBLISHED ARTICLES:

1. **Candela-Juan C**, Karlsson M, Lundell M, Ballester F, Carlsson Tedgren A. *Dosimetric characterization of two radium sources for retrospective dosimetry studies*. (Under review by Medical Physics)

2. **Candela-Juan C**, Gimeno-Olmos J, Pujades MC, Rivard MJ, Carmona V, Lliso F, Celada F, Ramírez-Coves JL, Ballester F, Tormo A, Pérez-Calatayud J. *Fetal dose measurements and shielding efficiency assessment in a custom setup of ^{192}Ir brachytherapy for a pregnant woman with breast cancer*. Phys Med 2015; doi: 10.1016/j.ejmp.2015.01.010.

3. Pons-Llanas O, Ballester-Sánchez R, Celada-Álvarez FJ, **Candela-Juan C**, García-Martínez T, Llavador-Ros M, Botella-Estrada R, Barker CA, Ballesta A, Tormo-Micó A, Rodríguez S, Perez-Calatayud J. *Clinical implementation of a new electronic brachytherapy system for skin brachytherapy*. J Contemp Brachytherapy 2014; 6: 417-423.

4. El Bitar Z, Pino F, **Candela-Juan C**, Domenec R, Pavía J, Rannou F, Ruibal A, Aguilar P. *Performance of hybrid analytical-Monte Carlo system response matrix in pinhole SPECT reconstruction*. Phys Med Biol 2014; 59: 7573-7585.

5. Gimeno J, Pujades MC, García T, Carmona V, Lliso F, Palomo R, **Candela-Juan C**, Richart J, Perez-Calatayud J. *Commissioning and initial experience with a commercial software for in vivo volumetric dosimetry*. Phys Med 2014; 30: 954-959.

6. **Candela-Juan C**, Granero D, Vijande J, Ballester F, Perez-Calatayud J, Rivard MJ. *Dosimetric perturbations of a lead shield for surface and interstitial high-dose-rate brachytherapy*. J Radiol Prot 2014; 34: 297 - 311.

7. **Candela-Juan C**, Montoro A, Ruiz-martínez E, Villaescusa JI, Martí-Bonmatí L. *Current knowledge on tumour induction by Computed Tomography should be used carefully*. Eur Radiol 2014; 24: 649-656.

8. Montoro A, Sebastià N, **Candela-Juan C**, Barquinero JF, Soriano JM, Almonacid M, Alonso O, Guasp M, Marques-Sule E, Cervera J, Such E, Arnal C, Villaescusa JI. *Frequency of dicentrics and contamination levels in Ukrainian children and adolescents from areas near Chernobyl 20 years after the nuclear plant accident*. Int J Radiat Biol 2013; 89: 944-949.

9. **Candela-Juan C**, Perez-Calatayud J, Ballester F, Rivard MJ. Calculated organ doses using Monte Carlo simulations in a reference male phantom undergoing HDR brachytherapy applied to localized prostate carcinoma. Med Phys 2013; 40: 033901.

10. Montoro A, Sebastià N, **Candela C,** Barquinero J F, Soriano J M, Almonacid M, Sahuquillo V, Alonso O, Cervera J, Such E, Silla M A, Arnal C, Villaescusa J I. *Frecuencia de dicéntricos en niños y adolescentes ucranianos de zonas cercanas a Chernobyl 20 años después del accidente de la central nuclear*. Radioprotección 2012; 73: 12-17.

11. **Candela Juan C**, Crispin-Ortuzar M, Aslaninejad M. *Depth-dose distribution of proton beams using inelastic-collision cross sections of liquid water*. Nucl Instr Meth Phys Res B 2011; 269: 189–196.

BOOK CHAPTERS:

12. Villaescusa JI, **Candela-Juan C**, García GA, Pernot E, Sebastià N, Soriano JM, Montoro A. *Últimos avances en radioprotectores de origen natural. Capítulo I: La radiación y sus efectos.* Editado por Consejo de Seguridad Nuclear (CSN), Referencia: DID-21.13 (2013).

STUDIES PRESENTED IN CONFERENCES:

13. Gimeno J, Palomo R, **Candela-Juan C**, García T, Carmona V, Lliso F, Richart J, Ballester F, Perez-Calatayud J. *Evaluation of a commercial EPID-based in vivo dosimetric system in the presence of lung tissue heterogeneity*. **Poster** presented at the **56th Annual Meeting & Exhibition (AAPM)** in Austin (USA), in July 2014.

14. Palomo R, Gimeno J, Pujades MC, Carmona V, Lliso F, **Candela-Juan C**, Ballester F, Perez-Calatayud J. *Evaluation of the lense dose on the cone beam IGRT procedures*. **Poster** presented at the **56th Annual Meeting & Exhibition (AAPM)** in Austin (USA), in July 2014.

15. Carmona V, García T, Palomo R, **Candela-Juan C**, Richart J, Gimeno J, Lliso F, Granero D, Ballester F, Perez-Calatayud J. *Valencia applicator commissioning using a micro-chamber array*. **Poster** presented at the **56th Annual Meeting & Exhibition (AAPM)** in Austin (USA), in July 2014.

16. **Candela-Juan C.**, Granero D., Vijande J., Ballester F., Perez-Calatayud J., Rivard M. J. *Organ Doses in a Male Phantom Undergoing High-Dose-Rate Brachytherapy Applied to the Prostate.* **Oral presentation** at the **55th Annual Meeting & Exhibition (AAPM)** hold in Indianapolis (USA), from the 4th to 8th August 2013.

17. Granero D., Perez-Calatayud J., Vijande J., Ballester F., **Candela-Juan C**., Rivard M.J. *Limitations and Clinical Implications of the TG-43 Formalism for High-Dose-Rate Skin Brachytherapy.* **Poster** at the **55th Annual Meeting & Exhibition (AAPM)** hold in Indianapolis (USA), from the 4th to 8th August 2013.

18. Vijande J., Granero D., **Candela-Juan C.**, Ballester F., Perez-Calatayud J. *Carlo Dosimetric Study of the CSM40 Low Dose Rate Source.* **Poster** at the **55th Annual Meeting & Exhibition (AAPM)** hold in Indianapolis (USA), from the 4th to 8th August 2013.

19. **Candela-Juan C**., Vijande J., Granero D., Ballester F., Pérez-Calatayud J., Rivard M. J.. *Cálculo MC en braquiterapia de alta tasa.* **Oral presentation** at **XXXIV Bienal de la Real Sociedad Española de Física**, hold in Valencia (Spain), from the 15th to 19th July 2013.

20. Mayo Nogueira P., Verdú Martín G., Rodenas Escriba F., Marín Peinado B., Campayo Esteban J. M., Díez Domingo S., **Candela Juan C.**, Villaescusa Blanca J. I., Hernando González I., Ruiz Manzano P., Melchor Iñiguez M. *Herramienta para la verificación de parámetros geométricos y constancia de calidad de imagen en equipos de radiodiagnóstico*. **Poster** presented at **III Congreso conjunto SEFM-SEPR**, hold in Cáceres (Spain), from the 18th to 21st June 2013.

21. **Candela-Juan C**., Vijande J., Granero D., Ballester F., Pérez-Calatayud J., Rivard M. J. *Cálculo Monte Carlo de dosis equivalente a órganos en un tratamiento de próstata con braquiterapia de alta tasa*. **Oral presentation** presented at **III Congreso conjunto SEFM-SEPR**, hold in Cáceres (Spain), from the 18th to 21st June 2013.

22. Vijande Asenjo J., Granero Cabañero D., **Candela-Juan C**., Pérez-Calatayud J., Ballester Pallarés F. *Caracterización dosimétrica de la fuente CSM40 de Cs-137*. **Poster** presented at **III Congreso conjunto SEFM-SEPR**, hold in Cáceres (Spain), from the 18th to 21st June 2013.

23. Montoro A., Sebastià N., Aparici F., **Candela-Juan C**., Soriano J. M., Pérez-Calatayud J., Gras P., Cervera J., Alonso O., Villaescusa J. I. *Valoración de la radiosensibilidad y correlación entre dosimetría biológica y física en un caso de radiología vascular*. **Oral presentation** presented at **III Congreso conjunto SEFM-SEPR**, hold in Cáceres (Spain), from the 18th to 21st June 2013.

24. **Candela-Juan C.**, Ballester F., Perez-Calatayud J., Rivard M. J. *Organ doses in a male phantom undergoing high-dose rate brachytherapy applied to localized prostate carcinoma*. **Poster** presented at **2nd ESTRO Forum**, hold in Ginebra (Suitzerland), from the 19th to 23rd April 2013.

25. **Candela-Juan C.**, Ros D., Pavía J. *Monte Carlo simulation and optimization of a SPECT system for small animals.* **Poster** presented at **V Conferencia anual del CIBER-BBN,** hold in Zaragoza (Spain), in September 2011.